DEGRADATION BEHAVIOR OF LITHIUM-ION CELLS UNDER OVERCHARGE EXTREMES
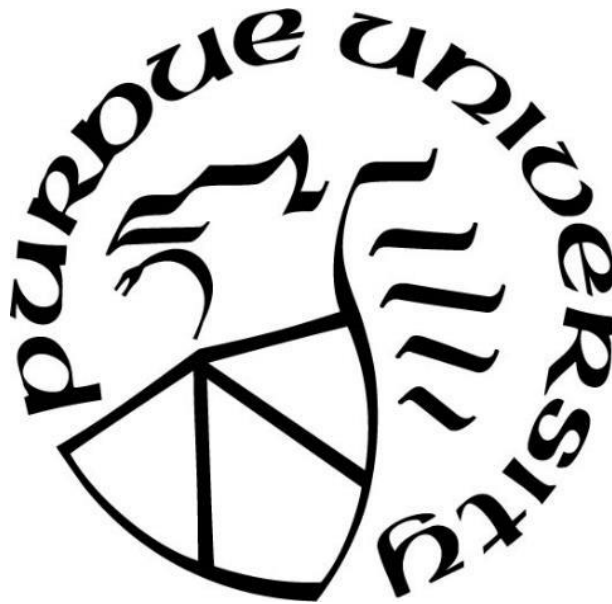
by

Anjul Arun Vyas

A Thesis

Submitted to the Faculty of Purdue University

In Partial Fulfillment of the Requirements for the degree of

Master of Science in Mechanical Engineering

School of Mechanical Engineering

West Lafayette, Indiana

August 2019

THE PURDUE UNIVERSITY GRADUATE SCHOOL
STATEMENT OF COMMITTEE APPROVAL

Dr. Partha P. Mukherjee, Chair

    School of Mechanical Engineering

Dr. Amy Marconnet

    School of Mechanical Engineering

Dr. Jason Ostanek

    School of Engineering Technology

Approved by:

    Dr. Jay P. Gore

        Head of the Graduate Program

To my Family

ACKNOWLEDGMENTS

I would like to extend my sincere gratitude to my committee chair, Dr. Partha P. Mukherjee for trusting in me and guiding me throughout my coursework and research. I would also like to thank my advisory committee members, Dr. Amy Marconnet and Dr. Jason Ostanek for their valuable inputs and willingness to serve in this capacity.

Big Thanks goes to my lab mate and peer mentor Daniel Juarez Robles for being the guiding light throughout this project. I would also like to extend my appreciation to Aashutosh Mistry, Ankit Verma, Conner Fear, Chance Norris and Sobana Rangarajan for their valuable inputs.

I am forever thankful to my parents and my sister for their unconditional love, encouragement and spirited support throughout my life. They will always be the source of inspiration for what I do in my life. Without them I am nothing.

TABLE OF CONTENTS

LIST OF TABLES

.

LIST OF FIGURES

.

ABSTRACT

Author: Vyas, Anjul Arun. MSME
Institution: Purdue University
Degree Received: August 2019
Title: Degradation Behavior of Lithium-ion Cells Under Overcharge Extremes
Committee Chair: Dr. Partha P. Mukherjee

Degradation behavior of commercial lithium-ion pouch cells containing $LiCoO_2$ cathode and graphite anode was investigated for a cycling under continuous overcharge condition. This condition is frequently experienced in electric vehicles in an event of Battery Management System (BMS) failure. Failure of BMS results in an unbalanced module further resulting in overcharging or overdischarging the cells. Commercial cells with 5Ah capacity were continuously cycled at different upper cutoff voltages and 1C-rate to develop a better understanding of the overcharge process. The results show that as the upper cutoff voltage is extended, the cell gains a higher initial capacity. However, the cycle life of the cell diminishes significantly. The extent of overcharge was found to be an important parameter not only for the electrochemical performance but also for cell integrity. Cells overcharged beyond 4.5 V had a significant volume increase and a rapid increase in the capacity fade. The cell starts to swell at this stage and a considerable increase in the temperature and internal resistance of the cells is observed. Thermal imaging of the cell revealed non-uniform temperature distribution and localized degradation sites were identified. Evidence of lithium plating and electrolyte deposits on anode was observed in cells charged beyond 4.4 V, with SEM-EDS verifying their presence. A comparative study of various State of Health (SoH) estimation parameters is presented and the proposed parameter Φ_R based on internal resistance measurement is found to be a good indicator of aggravated degradation in cells.

1. INTRODUCTION

1.1 <u>Energy Storage Systems</u>

Humanity faces the challenge of satiating the ever-increasing energy demand. Currently, society relies heavily on fossil fuels. However, the increasing rise in pollution and climate change have demanded a move away from conventional fossil fuels to find a cleaner and economically viable solution to end energy poverty. This has led to rapid growth in the adaptation of renewable sources of energy for the past decade, however, the shift to renewable energy has its own challenges. Wind energy and solar energy have been the front runners in harnessing energy from renewable sources. Although they produce the cleanest forms of energy, the fluctuations in generating electricity from these sources possess a great challenge in direct integration to the grid. This challenge calls for the need to store energy. Energy storage would compensate for the fluctuations and address the deficit in the supply & demand of required electricity. In peak hours the stored energy can be used to cater the demands whereas in off-peak hours the excess energy being produced can be stored for future usage. Energy storage can be done using various techniques which are mainly categorized as thermal, mechanical and chemical storage. Chemical energy storage devices include batteries also known as accumulators. The aspect which makes batteries unique is that these systems store energy and produce electricity in charge-discharge cycles without any harmful emissions and minimal maintenance requirement [1]. Batteries have found applications at all levels with portable devices at small scale, electric vehicles at a medium scale and grid energy storage at large scale. With the rapidly increasing demand and constantly decreasing cost, batteries are growing as a promising alternative to conventional fossil fuels. The next section will summarize the inception of batteries, the working principle of electrochemical devices, and the classification of batteries.

1.1.1 *Electrochemical Cells*

A chemical reaction can be typically defined as a reaction involving the transformation of one species to another which usually involves breaking and forming of chemical bonds between atoms [2]. However, if a reaction is triggered by the passage of current or produces current in the course of reaction then that reaction is known as an electrochemical reaction. A battery is one such

electrochemical device which converts the chemical energy of a substance to produce current [3]. Electrochemical devices are cleaner, not limited by the Carnot cycle efficiency thus having a higher energy conversion efficiency and hence offer a great advantage over the existing sources of energy.

In 1800, Italian physicist Alessandro Volta was the first person to come up with a working battery known as "Voltaic pile" [4]. It included disks of zinc and copper piled upon each other and separated by a cloth dipped in brine. Volta's model had a large scope of improvement and his work was taken forward by many other scientists. A breakthrough upgrade on Volta's pile was made by the British chemist John F. Daniell. He invented the Daniell cell which consisted of a copper electrode in copper sulfate solution connected to a Zinc electrode in sulfuric acid through a salt bridge. Daniell cell had an operating voltage of 1.1 V and a better life than the Voltaic pile [5]. These cells are known as primary cells and they share a common characteristic that is, once the active materials/electrode material depletes so does the cell life. Advancements in the battery technology were made when the first rechargeable battery was discovered by Gaston Plante. He invented the widely used Lead-acid battery which could be recharged on passing current in the reverse direction. These types of cells are referred to as secondary cells. Hence, depending on the principle of operation the cells are categorized as primary and secondary cells.

1.1.2 *Primary Cells*

These types of cells have a limited amount of reacting compounds/active material and can be consumed only once. The electrochemical reaction is irreversible and hence these batteries are also known as non-rechargeable batteries. They can be discharged just once and hence can just be utilized for use and throw applications. Although inexpensive, lightweight and easy to use, being non-rechargeable remains their major drawback. Daniell cell and voltaic pile are examples of the primary cell.

1.1.3 *Secondary Cells*

Secondary cells were developed to address the drawback of primary cells. The electrochemical reactions occurring in a secondary cell are reversible and hence are called as rechargeable cells. After the energy of the cell is utilized, an external current to overcome the reaction energy is passed

which reverses the reaction and restores the active material to be consumed again. The possibility of these reversible reactions allows power electronics to be recharged which is the fundamental advantage of secondary cells. Lead acid, Ni-MH and Li-ion batteries are examples of rechargeable batteries widely being used in the present. An ideal battery should have high specific energy and high specific power, long life, good tolerance to abuse conditions and economically feasible. Compared to other battery systems, Li-ion batteries satisfy the majority of ideal characteristics and are the frontrunner in energy storage systems rapidly replacing the existing Ni-MH and Lead acid batteries. The next section will summarize the constructions and working of a lithium-ion battery.

1.2 <u>Lithium-Ion Batteries</u>

A lithium-ion cell typically comprises of four main components a cathode (positive electrode), an anode (negative electrode), an electrolyte and a separator. The anode is the electrode which provides electrons to the external circuit by getting oxidized whereas a cathode is the electrode which gains electrons and gets reduced during the electrochemical reaction. Typically, a cathode material must be an efficient oxidizing agent, should remain stable in contact with the electrolyte, low cost, and ease of fabrication. Most commonly used cathode materials are metal oxides such as lithium cobalt oxide (LCO), lithium nickel manganese cobalt oxide (NMC) and phosphates such as lithium iron phosphate (LFP). An anode material should be an efficient reducing agent, high Coulombic output, good conductivity, stable with the electrolyte, easy to manufacture and should have low cost [3]. Most commonly used anode materials include metals, graphite (C), and silicon (Si).

The electrodes are never in direct contact to avoid internal short circuit and are connected by the electrolyte. The electrolyte functions as an ionic conductor and acts as an electronic insulator, i.e., it allows the ions to pass through whereas does not allow the flow of electrons through them to avoid a short circuit [6]. Both aqueous and non-aqueous organic solvents are used as electrolytes. For a Li-ion battery, a mixture of organic solvent with a molten salt is typically used to enhance the battery performance. Some commonly used electrolytes are dimethyl carbonate (DMC), ethyl methyl carbonate (EMC), sulfuric acid, potassium hydroxide, gel, and polymer electrolytes [4].

Separator is a thin porous membrane which as the name suggests is used to separate and avoid direct physical contact of the electrodes. They also prevent the flow of electrons through them but allow the ions to pass through with least amount of resistance and hence a separator is porous in nature. Separators should not react with electrodes, electrolytes and must be stable over a wide range of temperature. Some common separator materials used are polyethylene (PE), polypropylene (PP), and polyethylene terephthalate (PET) [7]. Separator selection is highly dependent on the type of electrolyte and battery chemistry.
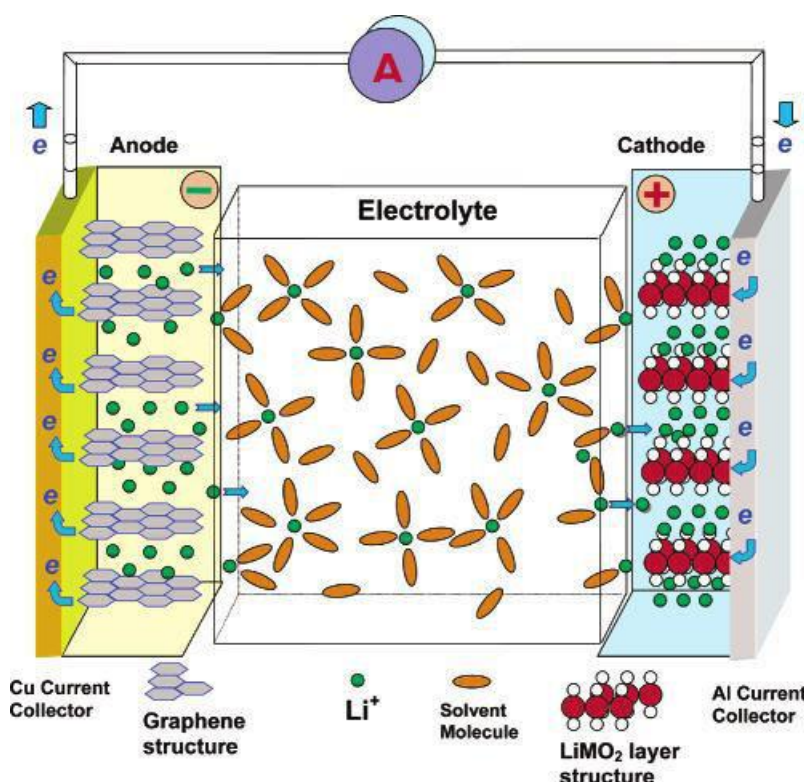
Figure 1.1 Schematic representation of a Li-ion battery during discharge [8].

A schematic of the Li-ion battery has been included to understand the working of a lithium-ion battery. During discharge of a lithium-ion battery, the chemical energy of the system is converted to usable electrical energy. The lithium ion moves from the anode into the cathode. This process of insertion from one electrode to another occurs without significantly changing the structure of electrodes and is known as intercalation. During this process, cathode is the electrode being reduced by gaining electrons whereas, anode is the electrode being oxidized by losing electrons. During charge, external electric energy is supplied to restore the chemical energy of the system.

The lithium ion moves from cathode to anode. During the charging cycle, oxidation takes place at anode and reduction takes place at the cathode. The redox reactions for a typical Li-ion cell has been included below:

Negative Electrode:	$C + xLi^+ + xe^- \leftrightharpoons Li_xC$	Equation 1.1
Positive Electrode:	$LiMO_2 \leftrightharpoons Li_{1-x}MO_2 + x\,Li^+ + xe^-$	Equation 1.2
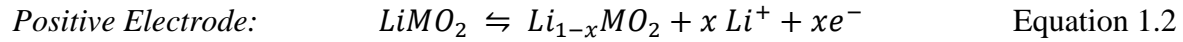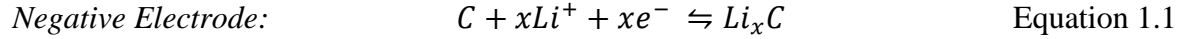
The phenomenon of intercalation and deintercalation is reversible and goes on until the electrodes are degraded. Presently, the majority of research is focused on achieving long cycle life, high energy density, and power density. However, it is equally important to address the safety concerns of Li-ion batteries and understand the degradation mechanism under abuse conditions to make batteries more robust and safer. The next section will summarize the safety concerns related to lithium-ion batteries and discuss a few catastrophic events involving Li-ion batteries in recent years.

1.3   Safety Aspects of Li-Ion Batteries

Although Li-ion batteries come as a boon to facilitate the use of renewable energy sources, safety-related incidents remain a concern. The safety concern is the main obstacle that hinders the large-scale application of Li-ion batteries in electric vehicles and grid energy storage. Although stringent battery safety testing standards are being followed in the industry, accidents involving lithium-ion batteries are still being witnessed. A few such incidents with their probable causes and the type of abuse condition faced have been tabulated in Table 1.1.

Table 1.1 Catastrophic accidents of lithium-ion batteries in the past few years

Description	Type	Probable cause
Battery pack of a Prius caught fire	Thermal abuse	Loose connection led to local overheat [9]
A Chevy Volt which had collided with a pole caught fire also damaging the nearby cars	Mechanical abuse – collision Electrical abuse – External Short circuit	Coolant system was damaged due to the impact and the leaked coolant formed a conductive path for external short-circuit [10].
Battery pack of an auxiliary power unit of a Boeing 787 Dreamliner caught fire.	Electrical abuse – Internal Short circuit	One cell in the battery pack experienced Thermal runaway due to internal short and further triggered Thermal runaway in the adjacent cells of the battery pack [11].
Main battery pack of a Boeing 787 caught fire when the flight was in transit.	Electrical abuse – Internal Short circuit	One of the cells in battery experienced Internal short-circuit followed by excessive heat generation and cell venting. This initiated the cell to cell failure propagation thus resulting in a fire[12].
Samsung Galaxy Note 7 cell caught fire and was banned from carrying in the airplanes	Electrical abuse – Internal Short circuit	Cell pouch deformed from the corners, resulting in electrode tabs touching each other. This led to internal short-circuit eventually resulting in a fire/explosion case [13].
A Tesla Model X caught fire after colliding with an attenuator resulting in a fire.	Mechanical abuse – Crash	Crashing into the barrier deformed the battery pack and resulted in a fire [14]
Tesla Model S caught fire after running over a sharp metallic object.	Mechanical abuse – Penetration	Penetration of the metallic object led to short circuit and fire.
An electric bus manufactured by Shenzen -Wuzhou Dragon automobiles caught fire	Electrical abuse - Overcharge	The battery management system of the battery pack failed to prevent overcharge of the batter resulting in thermal runaway and fire

As visible from the table above, the safety issues in a battery mainly arise under abnormal abuse conditions. To prevent these accidents from occurring it is important to understand the various abuse conditions that lead to these catastrophic events. The next section will briefly discuss the different type of degradation mechanisms, their causes, and consequences.

1.4   **Degradation Mechanisms**

Lithium-ion batteries typically last for 500-1000 charge-discharge cycles. They start degrading with time and the cell's ability to store energy reduces. Degradation of a Li-ion cell may affect the components of the cell individually or combined. Early failure of a cell before its predicted lifetime is mainly a consequence of abnormal abuse conditions. Some of these abuse conditions may lead to an extreme case of fire/explosion. The primary reason for such a catastrophic event is a thermal runaway. Thermal runaway occurs in a case when the abuse condition triggers a chain of reactions which include degradation of battery components one after the other, thus increasing the temperature of the cell to such an extent that it is beyond control and results in a fire or explosion. The abuse conditions which lead to thermal runaway are primarily categorized as:

1.4.1   *Mechanical Abuse*

Mechanical abuse occurs when an externally applied force leads to the destruction of the battery pack. Vehicle collision resulting in crush or penetration are typical examples of mechanical abuse conditions. Mechanical abuse conditions are further categorized as crush and penetration.

1.4.1.1   Crush

Vehicle collision usually results in deformation/crushing of batteries. Deformation may result in tabs touching and leading to external short-circuit. The battery separator could also get damaged (torn-off) thus leading to an internal short circuit. Moreover, the flammable electrolyte may spill out thus resulting in a fire.

1.4.1.2   Penetration

Penetration may also occur during a vehicle collision. The case of a Tesla passing over a sharp object is an example of a penetration abuse condition. It may lead to a fiercer internal short-circuit

resulting in a larger amount of heat generation. Mechanical abuse conditions always lead to electrical abuse finally leading to thermal abuse before going into thermal runaway.

1.4.2 *Thermal Abuse*

Thermal abuse, as the name suggests occurs when the cell undergoes overheating. This could be a consequence of externally heating or inefficient cooling of the battery pack. Usually, thermal abuse is a consequence of mechanical/electrical abuse condition and results in a thermal runaway. Accident 1 included in Table 1.1 was a result of thermal abuse. The metal current connectors which connect the electrodes became loose due to vibration in the vehicle under operation. This loose contact resulted in local overheat on the passage of high current and consequently leading to thermal runaway.

1.4.3 *Electrical Abuse*

Li-ion batteries have a limited range of stability in terms of voltage and temperature [15]. Operating the cell outside the recommended voltage window is a case of electric abuse condition. Electrical abuse conditions are mainly categorized as external short circuit, internal short circuit, overcharge and overdischarge.

1.4.3.1 External Short-Circuit

External short-circuit occurs when the two electrodes are connected by a conductor. As discussed earlier, this could be a consequence of a car collision where cathode and anode tabs may come in contact resulting in a short circuit and cell failure. Water immersion is also a scenario which could lead to an external short circuit. Peak-plateau-drop is a typical characteristic of an external short abuse condition [16, 17]. External short is analogous to a fast discharge process limited by the diffusion speed of lithium ions. The short circuit generates heat and is sometimes accompanied by cell swelling and gas evolution. In extreme case, it may lead to thermal runaway.

1.4.3.2 Internal Short-Circuit

An internal short circuit occurs when anode and cathode come in direct contact with each other. It is an attribute of all the abuse conditions and is the most common feature of a thermal runaway. This can occur in an event of a vehicle collision, penetration, Lithium dendrite growth piercing

through the separator in case of overcharge and copper dissolution in case of an extreme over-discharge of a cell [18, 19].

1.4.3.3 Overdischarge

As mentioned earlier li-ion cells have a stable working voltage window. For a typical LCO/graphite cell it is 2.7-4.2 V, *i.e.*, in this voltage range the cell will work efficiently. If a cell is discharged below the rated voltage (specified by the manufacturer), then the abuse condition is known as overdischarge. Solid electrolyte interface (SEI) is a layer formed over the anode surface during the formation cycle of the cell. Its function is to protect the inner layers of anode from further reacting with the electrolyte Extreme overdischarge may cause the cell to fail whereas, a cell continuously cycled under over-discharge condition results in the capacity fade. During the process of the over-discharge anode is excessively delithiated and once the lithium inventory in the anode extinguishes the lithium present in the SEI starts intercalating into the cathode. This results in SEI decomposition [20]. If the cell is recharged, a new SEI layer is formed which increases the internal resistance of the cell and decreases the capacity retention of electrodes [18, 21]. If the cell is discharged beyond a point that there is no lithium left in SEI and anode for intercalation, the copper ions from the current collector start migrating to the cathode and deposit on the cathode surface [18, 22]. The dissolved copper from copper dendrites, piercing through the separator and can cause an internal short circuit resulting in thermal runaway if an extremely overdischarged battery is recharged [19, 23].

1.4.3.4 Overcharge

Overcharge occurs when the cells are charged above the recommended cell cutoff voltage. For example, the recommended voltage range for an LCO/Graphite cell is 2.7-4.2 V. Charging the cell above the upper cutoff voltage results in overcharge. During overcharge, lithium plating, gas generation, and electrolyte decomposition are some commonly observed phenomena. Overcharge and its effects would be discussed in furthermore detail in the next chapter.

2. LITERATURE REVIEW

2.1 <u>Degradation Mechanisms</u>

In this chapter, an overview of the different aging mechanisms in lithium-ion cells and the associated degradation mechanism have been discussed. Then, it is followed by a discussion on advancements in the safety of lithium-ion batteries and abuse testing developed through the years. The chapter further includes details of overcharge abuse condition, its occurrence and previous works based on overcharge induced degradation. Finally, a discussion on the importance of the research study taken over to address the knowledge gap and enhance the understanding of degradation induced for cycling under continuous overcharge has been presented.

2.1.1 *Aging Induced Degradation Mechanisms*

Lithium-ion batteries have been widely used in the consumer electronics applications owing to their high energy density, high efficiency and long life [24]. These advantages have also made lithium-ion batteries a promising alternative to conventional transportation technologies and grid storage applications. However, catering to the demands of such markets requires more energy and better battery life from Li-ion batteries. The limitations on the battery life of a lithium-ion battery act as a challenge for wide adaptability in the automotive sector [25-28]. To enhance battery life, understanding of the battery aging mechanism becomes a prerequisite. Aging of lithium-ion batteries often results in capacity loss, increase of internal resistance and degradation of the battery components. The capability of lithium-ion batteries to store energy depletes over time and this phenomenon is defined as capacity loss (capacity fade). Capacity loss may be a consequence of long cycling, i.e., using the batteries for a large number of charge and discharge cycles, unsuitable storage conditions, or an uncalled abuse condition.

Battery aging can be broadly classified in two ways: calendar aging and cycle aging [29]. Calendar aging refers to the capacity loss that occurs when the cell is on the shelf and not in use. The conditions in which the battery is stored has a great impact on shelf life. The major parameters that affect the self-discharge of a cell are temperature and state of charge (SoC) [30, 31]. Storing a cell

at higher temperature initiates side reactions, inducing self-discharge which deplete the battery capacity and cycle life. SoC is a representation of the degree of lithiation of an electrode. For example, when the cell is in a completely discharged state, the anode is at 0% SoC and, the cathode is at 100% SoC. The SoC at which the manufactured cells have been stored also impact the shelf life of batteries. If the SoC of a cell is higher, it results in faster capacity fade [32, 33].

Cycle aging refers to capacity fade and degradation of a cell being used continuously. It is dependent on the working conditions under which a battery is being used. Current, temperature and voltage are the major parameters that affect the battery aging phenomenon. Charge-discharge protocol is also a major factor which impacts battery life and the extent of degradation. Higher C-rates result in faster degradation of cells and it is advisable to charge at a slower rate for the initial and final 10% capacity of the cell [34]. Increasing the temperature or voltage of cell significantly decrease the cell life and aggravates the capacity degradation [35].

As mentioned earlier, the aging phenomenon provokes degradation of lithium-ion battery components namely the electrodes, the electrolyte, the separator, and the current collectors. The degradation of the components is attributed to several chemical reactions that occur with long term cycling of lithium-ion batteries [36-42]. The reasons can be classified as loss of active material on the positive electrode, loss of active material on the negative electrode and loss of lithium inventory [43, 44]. Loss of active material on the negative electrode signifies the degradation of the negative electrode. Graphite is widely used as the negative electrode for lithium-ion cells. A passive layer, also known as SEI, is formed due to the reaction of the electrolyte with the anode. The SEI formation consumes active lithium available for the reaction thus reducing the net inventory of lithium. The growth of the SEI layer with cycling results in reduction the lithium inventory, consumption of active anode material, electrolyte decomposition and increase in the cell resistance [45-47]. The SEI layer is metastable in nature and decomposes at a higher temperature at around 90-120 °C. The decomposition of the SEI layer exposes the anode surface and hence the electrolyte reacts with the anode exothermically [40, 48]. Under extreme conditions, such as very low temperature [49, 50] or high charge rates [51], lithium plating may occur. Charging batteries at very low temperatures or faster C-rates, the potential of graphite falls below 0.0 V *vs.* Li/Li$^+$ thus not allowing the lithium to intercalate into graphite and instead it starts depositing on the anode.

This phenomenon is known as lithium plating and again results in loss of lithium inventory resulting in capacity fade [52-54]. This plated lithium can again react with the electrolyte to form a new layer of SEI or can detach from the surface becoming dead lithium.

After prolonged cycling, the growth of SEI as well as Li-plating accounts for capacity loss. The capacity loss that occurs in the initial cycles is dominated by the SEI growth and the capacity under load is observed to have a linear dependency on the charge throughput [55-60]. Many recent studies have reported an aberration from the linear dependence and have observed a non-linear capacity drop after prolonged cycling. Schuster *et al..* report the appearance of non-linear aging after prolonged cycling for NMC/Graphite cell at moderate temperature and charging rates. This point where the change from linear to non-linear degradation is believed to be the point where lithium plating becomes the dominant degradation process. The deterioration in ionic kinetics of anode due to SEI growth and loss of graphite active material are considered as the primary reason for the occurrence of lithium plating [44]. Lithium metal deposition on the anode and between the anode separator interface of long cycled cells have also been reported in the literature thus corroborating the claim of lithium plating becoming the dominant degradation mechanism and results in non-linear capacity decay [61, 62].

Yang et al. conducted a study of long-term aging behavior for NMC/Graphite pouch cells. They observed a similar change of linear to non-linear shift in the capacity decay curve. An anomalous voltage under-shoot in a voltage vs. capacity plot was also reported in their study at high discharge rates of 3C, see Figure 2.1. This behavior is observed when the cell transitions from a linear to non-linear capacity fade. This is a typical indicator of poor electrolyte performance and had been reported in the study of cells at freezing temperatures [49]. The subsequent occurrence of SEI growth along with lithium plating clogs the pores near anode-separator interface and decreases the anode porosity. This reduction in anode porosity leads to the rise of electrolyte resistance resulting in a rapid drop of cell voltage and the voltage to undershoot [63].
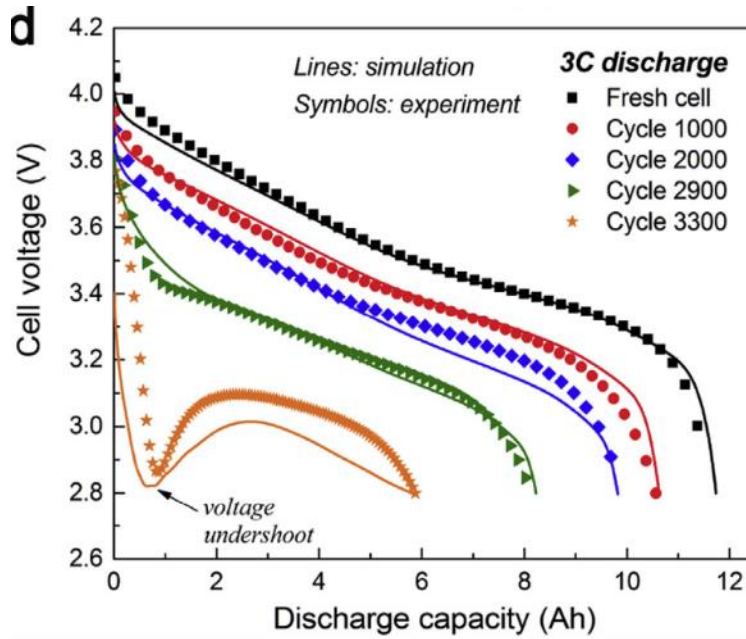
Figure 2.1 Voltage - capacity plot for NMC/graphite pouch cell at 3C discharge rate [63].

The plated lithium layer may grow further and form dendrites like structure, which in the worst-case scenario can pierce through the separator causing an internal short circuit resulting in a catastrophic situation. This event would not only lead to capacity loss instead could result in cell failure. Cell failure accompanied by a hazardous situation is often a consequence of an abuse scenario. A brief introduction to the types of abuse scenarios was presented in the previous chapter. Being aware of all the abuse scenarios necessitates the need to know how the cell's performance degrades under such extreme conditions. Although a lot of safety devices have been incorporated in the modern-day cells, infrequent and fatal accidents still call for a need to further investigate the cell's degradation under abuse conditions. Conducting an abuse response study helps in understanding the degradation mechanism, investigating the cause and effect and, development of safety devices to mitigate them in the future.

2.1.2 *Overcharge Induced Degradation Mechanisms*

Overcharge is often caused due to a faulty charger in portable electronics. As discussed in the previous chapter, the failure of Battery Management System (BMS) to stop charging beyond the upper cutoff voltage is the primary cause for overcharging a cell/battery in electric vehicles [64]. Zhang et al. defined overcharge as a state when electricity is forced through even after it has gained

full capacity [65]. All the lithium-ion cells come with manufacturer's specification. One of the important specifications is the voltage range under which the battery must be operated to get the best performance. If the cell is charged beyond the upper cutoff voltage, then the phenomenon is known as overcharge [66]. During the charge cycle, lithium ions move from cathode to anode. While overcharging an excessive number of lithium ions leave the cathode and intercalate into the anode. Overcharging a battery leads to degradation of cell components depending on the extent of overcharge and can result in a thermal runaway in extreme cases. Overcharge induced thermal runaway is considered harsher than the other abuse conditions as while overcharging the cells gain excessive energy. Thermal runaway can be defined as a series of chain reactions that occur under an abuse scenario resulting in elevated temperature and decomposition of battery components.

Over the years several efforts have been made by the researchers to understand the behavior of lithium-ion batteries under overcharge abuse condition. Some of these studies have been purely experimental [16, 67-70], some purely model-based [71, 72] and a few are a combination of both. Gas and heat generation attributed to the occurrence of various side reactions are the most commonly reported characteristics observed during overcharge [73, 74]. Ohmic heat accounts for the initial part of heat generation. In overcharge, the intercalation sites in anode start filling up and as the anode is completely lithiated, lithium ions start to deposit on the anode. As mentioned in the previous section this phenomenon is known as lithium plating. The ohmic heat generated increases the cell temperature and this increase in temperature facilitates the exothermic reaction of plated lithium with the electrolyte. The heat released due to anodic reactions and over-delithiation of cathode lead to an unstable structure and the results in metal dissolution. The electrolyte also reacts with cathode when the cathode voltage goes beyond the stable voltage of the electrolyte. Gas is generated because of the reaction between electrolyte with both the electrodes. The gas generated usually vents out from a cylindrical cell. However, in a pouch cell, severe swelling due to gas generation can be observed [16]. As the cell is further overcharged, the rate of side reactions accentuates rapidly increasing the amount of gas generated. With the increase in gas generation, the internal pressure of the cell rises and ruptures the cell. This rupturing of the cell exposes the lithium metal to atmosphere further resulting in an exothermic reaction of lithium with moisture present in the air and combustion of the flammable gases. An excessive amount of heat generation accelerates the rise in cell temperature thus initiating thermal runaway. Meanwhile, the parallel

growth of lithium dendrites may pierce through the separator causing an internal short circuit. A combination of heat generated through the internal short circuit and side reactions can also lead to thermal runaway. A qualitative schematic of all the degradation processes for an NMC/graphite cell leading to thermal runaway has been depicted in Figure 2.2. Thermal runaway in battery modules is even more catastrophic. Lopez et al. studied the cell to cell propagation of thermal runaway in a module using experimental [75] and modeling techniques [76].
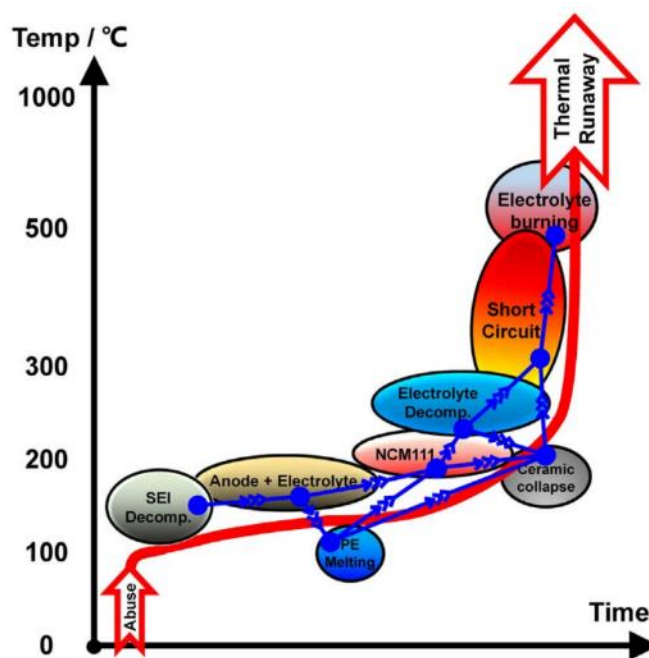
Figure 2.2 Qualitative representation of the chain reactions during a thermal runaway [73].

The extent of degradation in overcharge depends on various factors such as C-rate, temperature, pressure, SoC, type, size, and chemistry of the cell. Ouyang et al. conducted a study to understand the overcharge induced capacity fade in a commercial pouch cell (NMC+LMO / graphite). They overcharged the cells to different SoC to study the degradation process. It was observed that no significant capacity fade occurs till 120% SoC and the internal resistance starts rising as the cell is overcharged. Volume expansion and loss of active material were also observed for cells charged above 14% SoC. Thermal runaway was observed when the internal pressure created due to gas generation ruptures the pouch cell resulting in a series of exothermic reactions [66].

Leising et al.. studied the effect of C-rates for overcharge of commercial prismatic LCO/graphite cells. They observed that at low C-rates swelling, temperature and internal resistance increased at a lower rate as compared to the cells charged at higher C-rates [77]. It was also identified that cathode is the major source of heat generation thus confirming that overcharge is cathode dominated process which was consistent with DSC studies conducted by Zhang et al.. [16, 78]. Studies have also been done to compare the stability of different electrode materials under overcharge condition. It was found that with graphite as anode material, LCO was more stable cathode material as compared to LMO [79]. Similarly, in the work done by Larsson et al.., lithium-ion cells with LFP based cathode show more stability as compared to cobalt-rich cathode materials [80]. Takahashi et al.. studied the effect of external pressure on cells by restricting them with two plates under the overcharge condition. They observed that overcharge mechanism is influenced by C-rate, heat dissipation and the presence of restricting plate. It was concluded that the restrained cells were less prone to explosion [81]. A similar study conducted by Ren et al.. suggests that restraining plates do not significantly affect the electrical behavior of the cell. However, it improves the overcharge performance of the battery and delays the occurrence of thermal runaway [67]. Zhao et al.. studied the effect of externally applied compression on lithium-ion battery degradation under high temperature. They concluded that the application of external pressure reduced the delamination of electrode materials due to gas generation at high temperatures [82]. Similarly, Hofmann et al.. modified NMC/graphite pouch cells by connecting them to a small application vacuum pump. They were able to avoid fire/explosion for a cell going into a thermal runaway by venting the gases released during the overcharge test [83].

The work done by Ohsaki et al.. on LCO/graphite prismatic cell proposed a comprehensive reaction mechanism that occurs during overcharge. A representation of the same has been included in Figure 2.3. In region 1, the cell voltage keeps increasing as the cathode is delithiating. The excess lithium starts depositing on the anode, whereas the cell temperature and gas evolution is minor. In region II, the cell has reached 100% SOC and now cathode resistance increases thus increasing the ohmic heat. The increase in ohmic heat leads to a rapid rise in cell temperature rises rapidly facilitating the reaction between the electrolyte and de-lithiated cathode. This reaction being exothermic in nature produces more heat and leads to gas generation. In region IV, the cell temperature reaches the separator shutdown temperature which stops the transport of lithium ions.

As a result, the cell temperature falls due to a steep fall of current. However, at higher C-rates the ohmic heat produced in region II and II and is high enough to facilitate the exothermic reaction of plated lithium with the electrolyte which finally culminates in a thermal runaway [69].
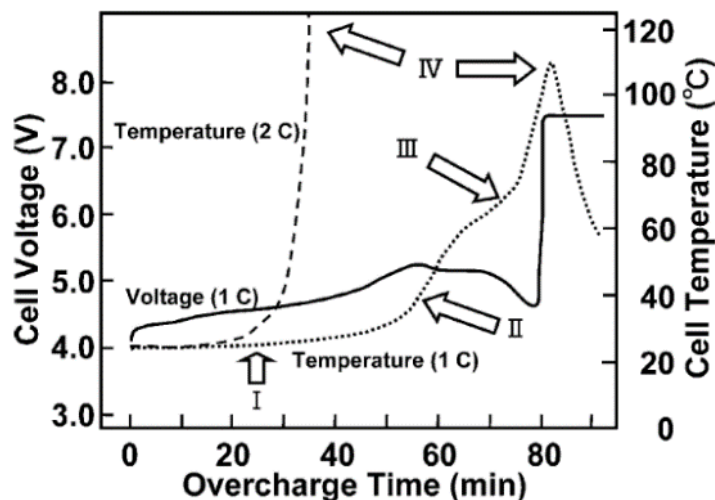
Figure 2.3 Overcharge reaction mechanism of a Li-ion cell [69].

Gas evolution results in degradation of batteries and hence it becomes necessary to understand the reactions leading to gas generation. Gas generation is believed to displace the electrolyte and block the ionic path for transport of lithium ions thus making a region of electrode inactive and resulting in capacity fade[70]. Gas generation occurs during overcharge and is also observed for deep cycled cells. Carbon dioxide (CO_2), carbon monoxide(CO), hydrogen(H_2), methane (CH_4), ethylene (C_2H_4), and ethane (C_2H_6) were found to be the major components of gas evolution during the overcharge test of lithium-ion cells [69, 84, 85]. To find out the which gases are released at the cathode and anode Metzger et al.. isolated the cathode and anode in two separate cells. The study concluded that CO_2 and CO are produced at cathode whereas, H_2, CH_4, C_2H_4 were formed at the anode [86]. A mechanism for gas evolution has been proposed by Jung et al. where they suggest that the evolution of CO_2, CO occurs because of the reaction between oxygen and electrolyte on the cathode side of the cell. [87].

Electrolyte decomposition during overcharge is another key aspect we need to study to get a better understanding of gas evolution and cell degradation. As specified earlier, electrolyte also has a

stable voltage limit. If the electrode voltage exceeds this safe value, the electrolyte starts to decompose initiating in aggravated degradation of the cell [88-94]. The electrochemical voltage for lithium-ion batteries exceeds the stability voltage of aqueous electrolytes and hence a mixture of carbonates are the preferred choice of electrolytes [95, 96]. Some commonly used electrolytes include dimethyl carbonate (DMC), diethyl carbonate (DEC), and ethylene carbonate (EC) [97, 98]. The flammable nature of the carbonates poses a safety concern in the wake of thermal runaway. Several research efforts have been made to understand the electrolyte degradation mechanism. Gas chromatography-mass spectroscopy has been implemented on electrochemically and thermally degraded electrolytes [99] [100-103]. Gachot et al.. proposed a degradation scheme to understand the decomposition of electrolyte for coin cells kept at 55 ^{o}C and cycled until a cutoff capacity [104]. A similar study was also conducted by Horsthemke et al. where different commercial cells were cycled until a predetermined end of life criteria [105]. Another study conducted by Gachot et al.. studied the effect of temperature on decomposition of the electrolyte. This study also included in-situ gas collection and predicted the reaction mechanism for the degradation of the carbonates [106]. Understanding the reaction mechanism behind the decomposition of electrolyte helps in deciding the safety additives to be used in a cell to prevent any hazardous situation. Research is being done on the development of flame retardants and non-flammable electrolytes to mitigate the flammability of vented electrolyte [107].

Overcharge is a serious concern for single cells and becomes extremely severe for large scale applications of lithium-ion batteries. Despite the availability of several studies of aging-induced degradation and overcharge-induced degradation, there still exists a knowledge gap of what would happen if a cell is cycled under overcharge condition. It is important to understand how the increase in the voltage window affects the capacity retention, cycle life, and degradation of the cell.

The objective of this research study is to understand the degradation behavior of lithium-ion pouch cells for cycling under overcharge extremes. This study aims to provide an in-depth understanding of such degradation mechanisms and be a guide in safety developments of battery systems.

3. METHODOLOGY

3.1 Experimental Setup

Conducting experiments on lithium-ion batteries is a time-consuming process and hence the proper design of experiments is of paramount importance. Battery testers are used to test lithium-ion batteries. All the cells were cycled using an Arbin BT-2000 system at room temperature. A commercial 5Ah Wanma pouch cell has been used in this study, which has Lithium Cobalt Oxide (LCO) and graphite as its cathode and anode respectively. A picture of the cell and a schematic showing construction of a cell has been depicted in Figure 3.1 and Figure 3.2. The next section elaborates on all the tests conducted in this study.

Figure 3.1 5 Ah LCO/graphite Wanma® pouch cell.
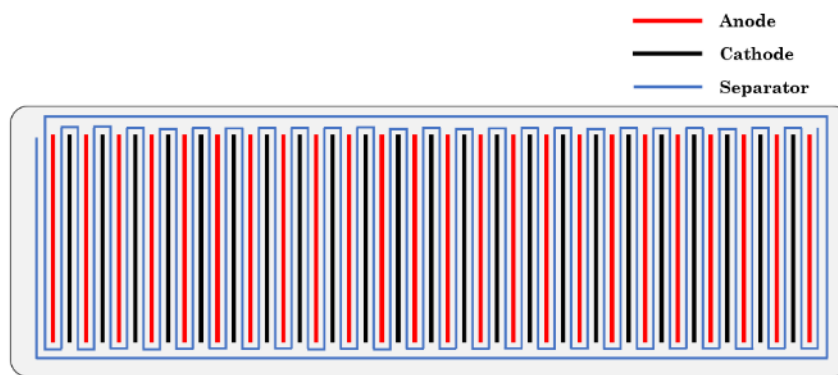
Figure 3.2 Schematic of the bottom view from the Wanma® pouch cell.

3.2 Electrochemical Test

Electrochemical testing of lithium-ion batteries includes developing a protocol which specifies the steps to be performed in the test. Figure 3.3 displays a representative flow chart of the steps employed in the protocol used for all the cycling under continuous overcharge tests. Importance of each step included in the protocol will be discussed in the next section.
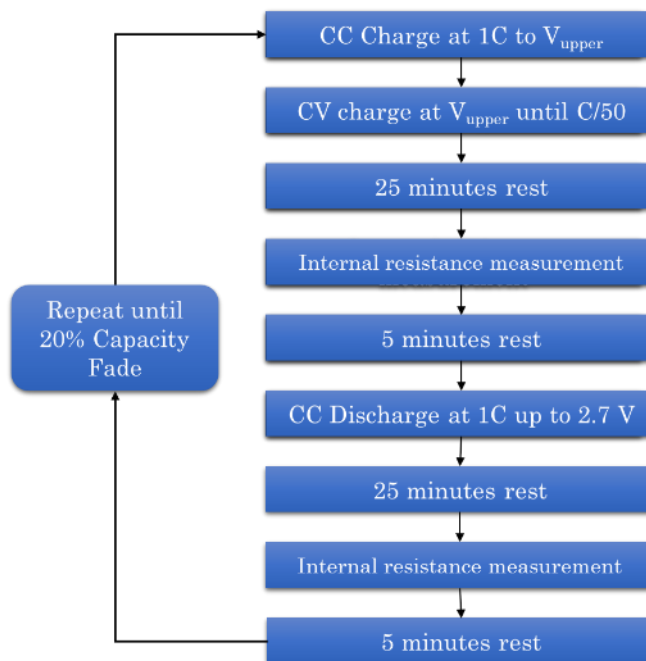
Figure 3.3 A schematic representation of cycling under overcharge protocol.

3.2.1 *Conditioning Test*

While testing a cell, it is important to know its initial state to obtain reliable results. Hence, each cell should be initially tested under the stable voltage window as per manufacturer's specifications. This initial charge-discharge cycle of a cell is defined as a conditioning test. Conditioning test gives us a measure of the initial charge and discharge capacity of the cell. Typically, the initial capacity obtained should be very close to the nominal capacity specified in the datasheet. If the initial capacity is significantly lower, then that cell should be discarded. Including the condition, this step helps to gauge if a cell should be used for testing. All the cells were initially subjected to a conditioning test where the cell was initially discharged to the lower cut-off voltage of 2.7 V followed by a rest of 30 minutes. The initial capacities of all the cells were characterized by cycling

them one time at 1/10 C (constant current charge up to 4.2 V at 1/10 C and then constant voltage charge at 4.2 V until the current goes lower than 0.1 A, finally followed by a constant current discharge to 2.7 V at 1/10 C).

3.2.2 *Internal Resistance*

The resistance of a battery depends on various factors such as chemistry, temperature, age and size of the battery. Monitoring the resistance provides valuable information and can also be used as an indicator for the end of life. Internal resistance was measured after each charge and discharge cycle using an in-built function in the Arbin system. Resting the cell for 25 minutes after each charge and discharge cycle, a series of current pulses were passed through the cell to get an average reading of the internal resistance of the cell. A total of 10 pulses are used at an interval of 100 milliseconds to obtain the cell resistance.

3.2.3 *Cycling Test*

There are many ways in which a battery can be charged. A constant current charging, constant voltage, constant power or a combination of these charging protocols could be employed for testing of cells. The manufacturer of the battery usually provides a standard protocol to be used for optimum performance and extended life of the battery. In this study, all the cells were subjected to a combination of CCCV (Constant Current - Constant Voltage) charging protocol. Initially, the cell is charged at a constant current up to a maximum voltage specified while designing the protocol. The upper cutoff voltage was varied from 4.2 V to 4.8 V for different cells. All the cells were charged a 1C-rate. C-rate is a measure of how much time a cell takes to charge or discharge. In this study, the nominal capacity of the battery is 5 Ah, hence at 1C the system would provide 5 A current and charge the battery in 1 hour. After performing the conditioning test, the cell was put into cycling tests using an Arbin BT-2000 system at room temperature. In each cycle, the cell was charged at 1C using a CC charge to the specified upper cutoff voltage, followed by a CV at the upper cutoff voltage until the current dropped to 1/50 C (0.1 A). CV step is included to ensure the cell gains maximum capacity. Further, the cell is rested for 25 minutes followed by an internal resistance measurement and again resting the cell for 5 minutes. Then, the cell is discharged at 1C-rate using a constant current discharge to a lower cut-off voltage of 2.7 V followed by a rest of 25 minutes, internal resistance measurement and 5 minutes of additional rest before moving to the

next cycle. The charge and discharge capacity were reset at each cycle and the cycling was repeated until the cell capacity fades to 80% of the nominal capacity (5 Ah). All the parameters were recorded at an interval of one second for the complete duration of the test. The 20% capacity loss was set as the stopping criteria of tests because it is considered as the end of life for primary applications of Li-ion batteries.

3.3   Thermal Measurements

Temperature is a key parameter which affects the performance of batteries and hence it is important to study the evolution of temperature while performing tests on lithium-ion batteries. Cell skin temperature for all the cells subjected to cycling under continuous overcharge tests was recorded using a T-type thermocouple (Omega). The thermocouple was attached on the surface of the battery and connected to the battery tester. Temperature data acquired at an interval of 1 second was used to study the temperature evolution and find out the heat generation in the cells during the charge and discharge cycles. Temperature evolution of the cell was also captured using a FLIR A 325 thermal imaging camera (Figure 3.4). A video of the first and last cycle was recorded which helped in visualizing the temperature distribution over a cell and identifying localized sites where degradation initiates.

Figure 3.4 FLIR A325 thermal camera used to extract thermal images of the cell.

3.4 Physical Analysis

3.4.1 *Thickness Measurement*

As discussed in the previous chapter, cell swelling is a characteristic of the overcharge test for pouch cells. The tests performed in this study involve cycling a cell in an overcharge window and hence significant cell swelling was observed. To study the effect of upper cutoff voltage on cell swelling, the thickness of the cell was measured using an in-house fabricated fixture. The top and side view of the fixture has been shown in Figure 3.5. The cell was placed between the two parallel acrylic plates followed by tightening of the 4 bolts in the corner. The bolts were tightened until the cell remained fixed at its position and overtightening was avoided. Then a Vernier caliper was used to measure the inner distance between the two plates. This was repeated for all the cells before proceeding for cell autopsy.
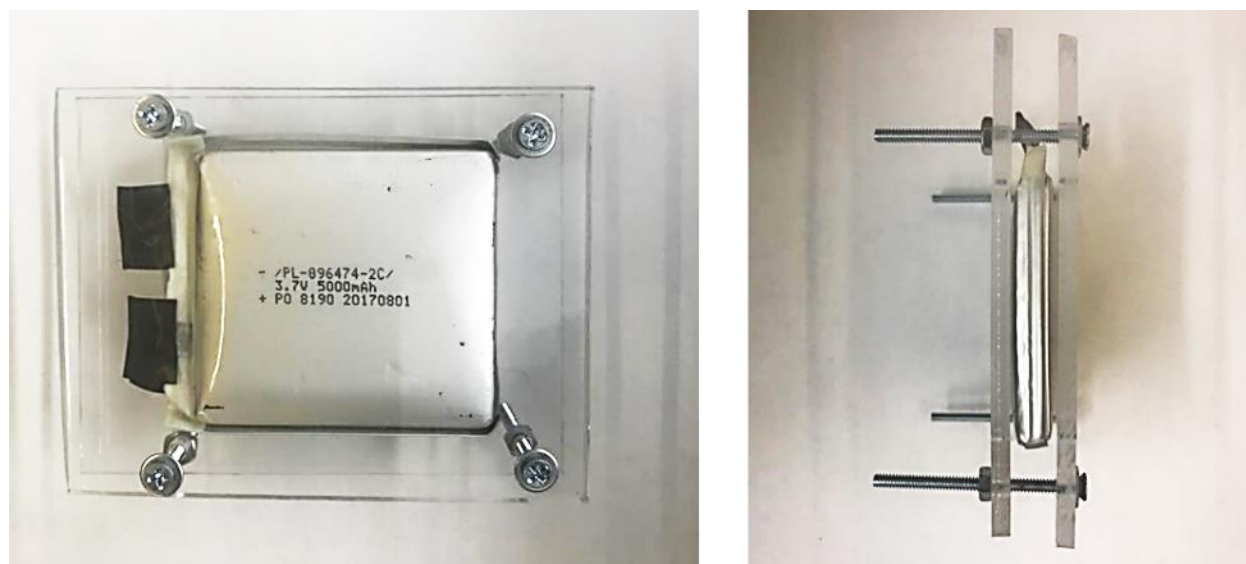
Figure 3.5 Front and side view of the fixture used for thickness measurement of the cell.

3.4.2 *Post-Mortem Analysis*

Physical analysis of the tested cells helps in analyzing the effect of test parameters on the cell components. For example, in the last section, the effect of the overcharge test on the thickness of the cell was quantified. Post-mortem analysis is a robust and widely-adapted tool used to gain further insights into the failure analysis of a cell. Opening these cells helps in visualizing and

characterizing the changes that occurred in the cell components during the test and compare them with that of a fresh cell. A step by step procedure followed for disassembling the pouch cell will be discussed here.

Lithium is very reactive in nature and therefore disassembly of the cell can't be done in the surrounding air. Overcharged cells have more energy than fresh cells and hence opening these cells poses more risk of fire or explosion. An MBRAUN argon-filled glove box is used to carry out the cell autopsy minimizing the risk of a hazard (Figure 3.6). All the tools required to carry out the cell autopsy are shown in Figure 3.7.
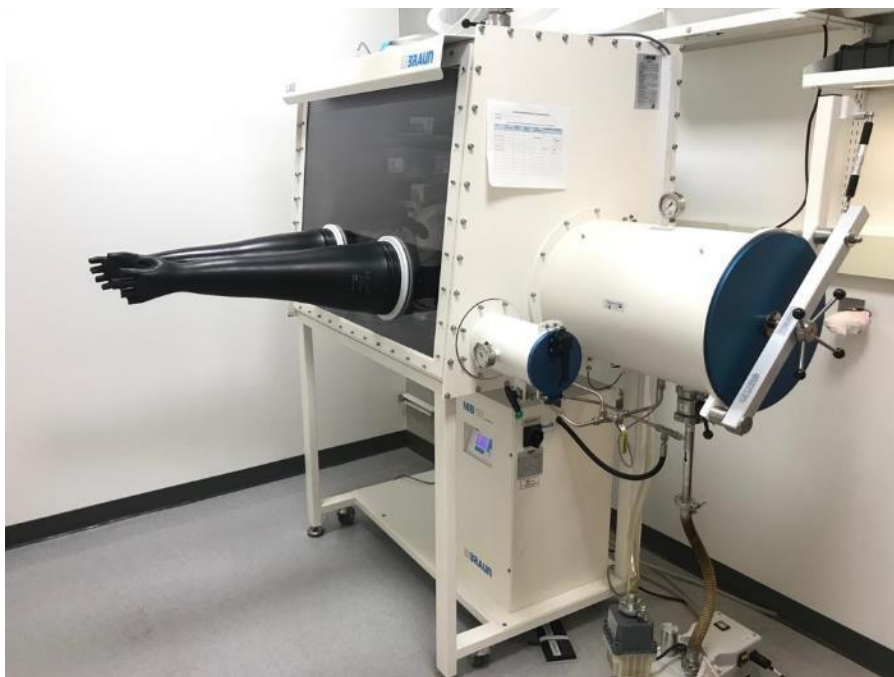
Figure 3.6 M-Braun Glove box used to conduct the cell autopsy.
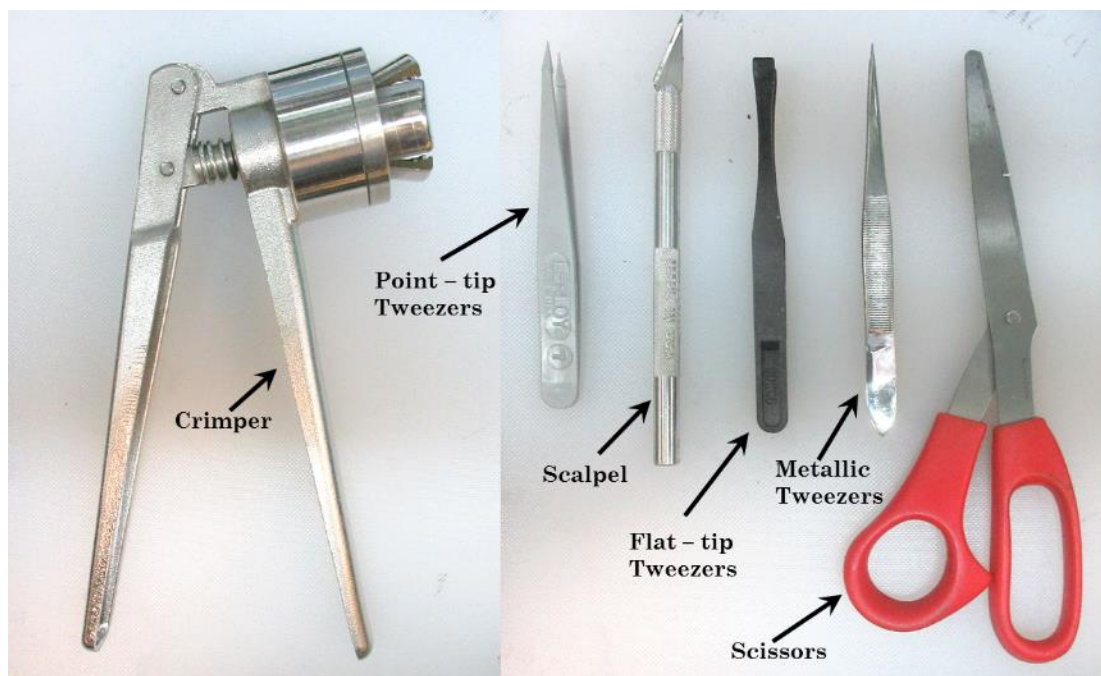
Figure 3.7 Tools used to conduct the destructive physical analysis of the cell.

1. Insulation of tabs: The first step should be to isolate both the tabs of the pouch cells. This is an extra precaution that needs to be taken in order to avoid any case of an external short circuit. The tabs are isolated using electrical insulation tape. A picture of the same has been shown below in Figure 3.8.
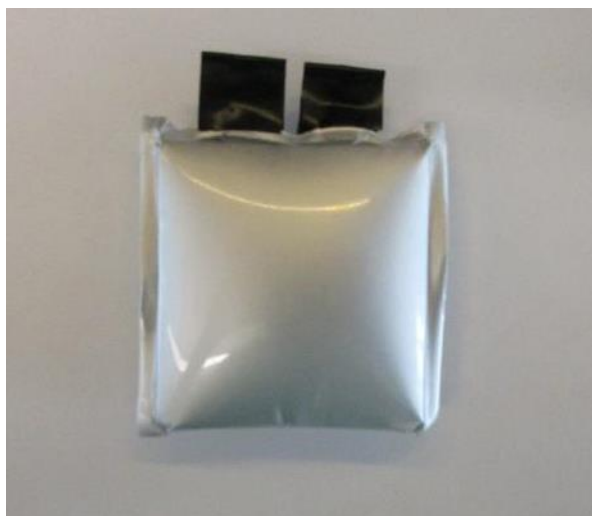
Figure 3.8 Wanma pouch cell cycled under continuous overcharge condition with isolated tabs.

2. Preparation of materials: Sealing bags are used to store the electrodes, separators and other components of the cell. A total of 5 sealing bags, one for each electrode, one for the separator, one for the electrolyte and one for storing the other cell components such as pouch and tabs are labeled based on the things they will house. A glass vial, vial septum, and a vial cap are used to collect the electrolyte of the cell.

3. Transfer of materials in the glove box: Glovebox provides the inert gas atmosphere required to open and construct lithium-ion cells. All the materials prepared to collect the cell components along with the cell and a camera are inserted in the glovebox antechamber. The antechamber is then cycled for a minimum of 3 times to maintain the optimum level of oxygen and moisture. The glove box used for dismantling the cells has been shown in Figure 3.6. A maximum level of 0.5 ppm oxygen and H_2O contamination is acceptable for the proper functioning of the glove box. After cycling, it should be made sure that the pressure gauge indicates 0 pressure thus confirming that antechamber is not in a vacuum and can be accessed from the inside. The antechamber can be opened from inside to access the transferred materials.

4. Disassembly of the pouch and tabs: After transferring the cell inside the glove box, a plastic board is used to disassemble the cell. This is used to avoid contact of tabs with the metallic floor of the glove box. The process starts with piercing the pouch using a stainless-steel scalpel. This initial cut is made near one of the tabs as shown in Figure 3.9. Extra care should be taken while using the scalpel to avoid any kind of short circuit and hence it is recommended to keep one of the tabs insulated. The cutting process should be done very slowly and with extra care. Once the cut along the width of the cell is complete, a pair of point-tip plastic tweezers were used to pull up the pouch from the center as shown in Figure 3.10. Following this, the scalpel was used to cut along the length from the center of the cell as shown in Figure 3.11. After the cut along the length has also been completed, the pouch is pulled off from the cell as shown in Figure 3.12. after opening the pouch, the pouch remains connected to the cells through the metallic nickel tabs. A pair of scissors is used to cut the tabs and separate the pouch and tabs from the cell. Again, extra precaution should be taken while cutting the tabs to avoid short circuit.

Figure 3.9 Cell disassembly. Initial cut near the tab of the pouch cell.
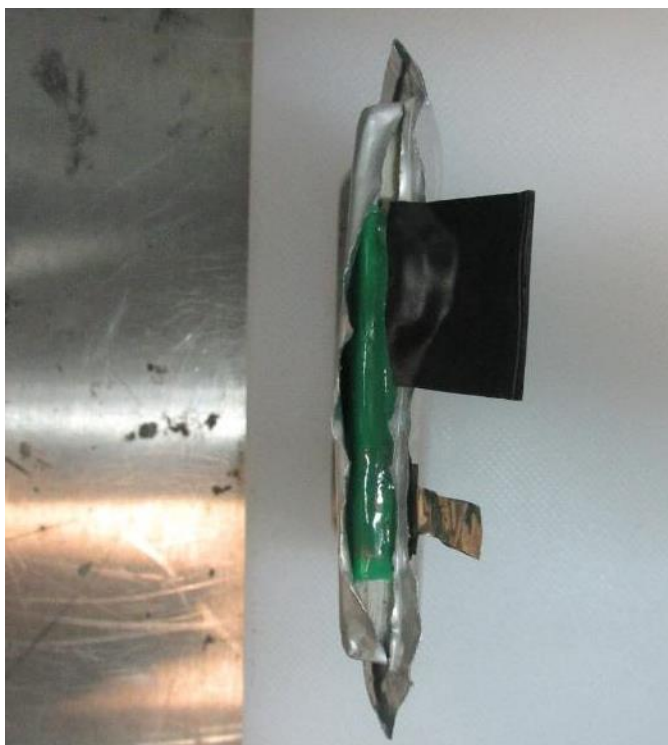
Figure 3.10 Cell disassembly. Complete cut along the width of the pouch.

Figure 3.11 Cell Disassembly. Initial cut along the length of the pouch.

Figure 3.12 Cell Disassembly. Complete cut along the length of the pouch.

5. Electrolyte collection: The process of electrolyte collection is shown in Figure 3.13. The electrolyte is collected by pouring a few drops of isopropyl alcohol (IPA) over the disassembled pouch. The contents are then carefully poured into the glass vial without spilling any of it. The glass vial is then closed with a septum and cap. As IPA is volatile in nature it is important to seal the collected electrolyte. A manual crimper is used to seal the glass vial. The collected electrolyte is further analyzed to study the decomposition of electrolyte using gas chromatography and mass spectroscopy.

Figure 3.13 Cell Disassembly. IPA poured on the pouch to collect electrolyte.

6. Disassembly of tapes on separator: A total of 4 conductive tapes were removed to start unwinding the separator. Tapes are removed by using a pair of flat-tip tweezers. Images of the same are shown in figure Figure 3.14 - Figure 3.18.

Figure 3.14 Cell Disassembly. Cell before removing the conductive tapes on the separator.
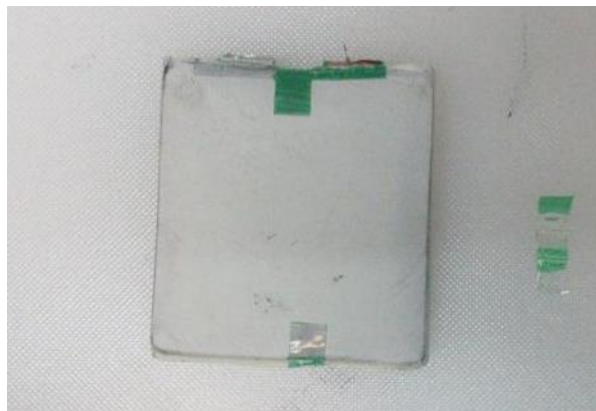
Figure 3.15 Cell Disassembly. Cell after removing the bottom conductive tape on the separator.

Figure 3.16 Cell Disassembly. Cell after removing the conductive tape along the width of the cell.
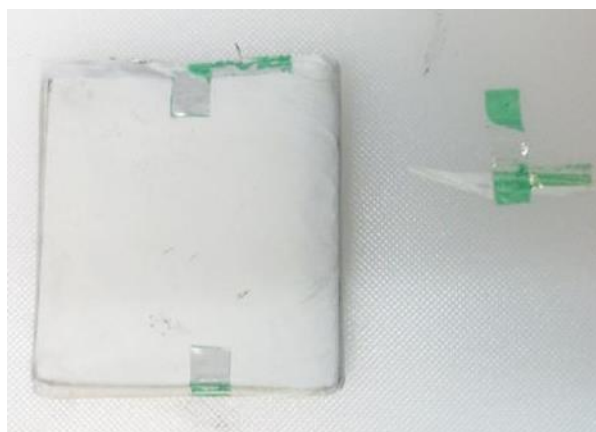
Figure 3.17 Cell Disassembly. Cell after removing the top conductive tapes on the separator.

7. Disassembly of separator and electrodes: Once all the tapes are removed, the separator can be unwound to access the electrodes. Two separate pair of plastic tweezers were used to extract cathode and anode. Extra care must be taken while separating the electrodes because the electrodes or the active material on the separator may get in contact with other electrode resulting in a short circuit. An image of unwinding the separator and extraction of electrodes has been shown below (Figure 3.18).

Figure 3.18 Cell Disassembly. Unwinding the separator and extraction of electrodes.

8. Storage of cell components: All the cell components extracted must be stored in their respective sealing bags. The bags should be put in another container for extra precaution. Samples for carrying out material characterization can be taken from the stored electrodes.

3.4.3 *Scanning Electron Microscopy and Energy Dispersive X-ray Spectroscopy*

A Hitachi S4800 Field Emission Scanning Electron Microscope (SEM) with a provision for EDS was used to study the morphology of electrodes. Electrodes taken out after dismantling the aged cells were used in the SEM. Samples were extracted by cutting small pieces of electrodes inside an argon-filled glove box. The extracted samples were stuck to a 4-inch stage using double-sided conductive tape. A 30 kV acceleration voltage and 10 µA current were used to get the SEM images at different magnifications. EDS analysis was also done on the same equipment for the SEM images obtained to get the chemical composition of the electrodes. The extent of degradation was analyzed using SEM and EDS results.

3.5 Composition Analysis

3.5.1 *Gas Chromatography-Mass Spectroscopy (GC-MS)*

The electrolyte collected while opening the cell was analyzed for its components using an Agilent 5975C MSD equipment. The chromatographic separation was performed using a DB-5MS column (30 M x 0.250 mm x 0.25µm film). Helium was used as the gas carrier with a constant flow rate of 0.8 ml/min. Electron impact and chemical ionization were obtained in the mass range of 45-500 amu. A syringe was used to extract samples from the glass vials. The injector temperature was 250 $^{\circ}$C and the split ratio of 1:20 was used with 1 µl of the sample being injected. The results obtained were analyzed using a NIST library.

4. RESULTS AND DISCUSSION

4.1 <u>Electrochemical Results</u>

This section initially presents the test procedure deployed for conducting experiments and the definition of capacity fade used for this study. This is followed by discussing the results for capacity fade, voltage evolution and internal resistance evolution for cells charged up to different upper cutoff voltage. Finally, a comparison of various state of health parameters has been done and a new way to qualitatively know the state of health has been proposed.

4.1.1 *Test Procedure*

Electrochemical tests are done using various protocols and under different conditions. A CCCV charge and a CC discharge protocol have been utilized in this study. A typical protocol used for cycling the cell under continuous overcharge for a voltage range of 2.7 V to 4.8 V has been presented in Figure 4.1. In each cycle, the cell was charged at 1C rate using a CC charge to the specified upper cutoff voltage (4.8 V in this case), followed by a CV at the upper cutoff voltage until the current dropped to 0.1 A. The CV step is included to ensure the cell gains maximum capacity. Further, the cell is rested for 25 minutes followed an internal resistance measurement and again resting the cell for 5 minutes. Then the cell is discharged at 1C using a constant current discharge to a lower cut-off voltage of 2.7 V (for all cells) followed by a rest of 25 minutes, internal resistance measurement and 5 minutes of additional rest before moving to the next cycle. The charge and discharge capacity were reset at each cycle and the cycling was repeated until the cell capacity fades to 80% of the nominal capacity. All the cells were tested at room temperature and were only subjected to overcharge abuse condition. Voltage, current, resistance, temperature, and capacity were recorded for each cycle and further used to analyze the results.
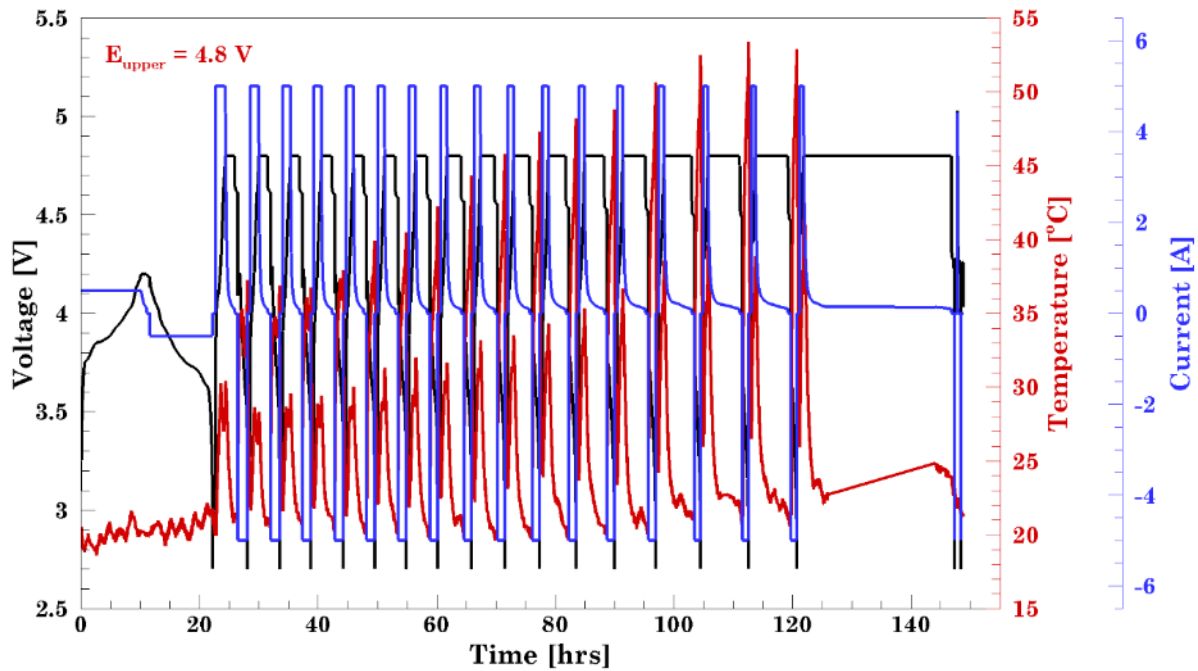
Figure 4.1 Voltage, current, temperature variables *vs.* time for cycling under overcharge protocol for a cell charged up to 4.8V.

4.1.2 *Effect of Upper Cutoff Voltage on Capacity Fade*

Secondary batteries including lithium-ion cells offer the advantage of reusing them for several cycles. However, even they have a finite life and start to degrade after long term use. Aging of the cell occurs due to loss of active material and lithium inventory and results in capacity fade. The nominal capacity of a cell is defined as the amount of energy a cell can retain while it's charged as per the manufacturer's specifications. The cell is said to have experienced a capacity fade when the ability to store energy decreases. For example, a cell with 2 Ah nominal capacity has experienced a 50% capacity fade if the cell is able to retain only 1 Ah of capacity under the same charging and discharging conditions.

Safe voltage window for a cell depends on the chemistry and is again provided by the manufacturer. Charging the cell beyond its upper cutoff limit results in overcharge. A fresh Wanma cell was overcharged at C/5-rate to characterize the typical overcharge behavior and to decide the upper cutoff voltages to be used for cycling under continuous overcharge condition. From Figure

4.2, it can be seen that the cell starts to fail as the voltage rises to 5 V. In order to avoid failure of the cell in the first cycle, upper cutoff voltages up to 4.8 V were chosen for this study. Figure 4.2 shows the upper cutoff voltages chosen and indicates the safe voltage window and the overcharge region.
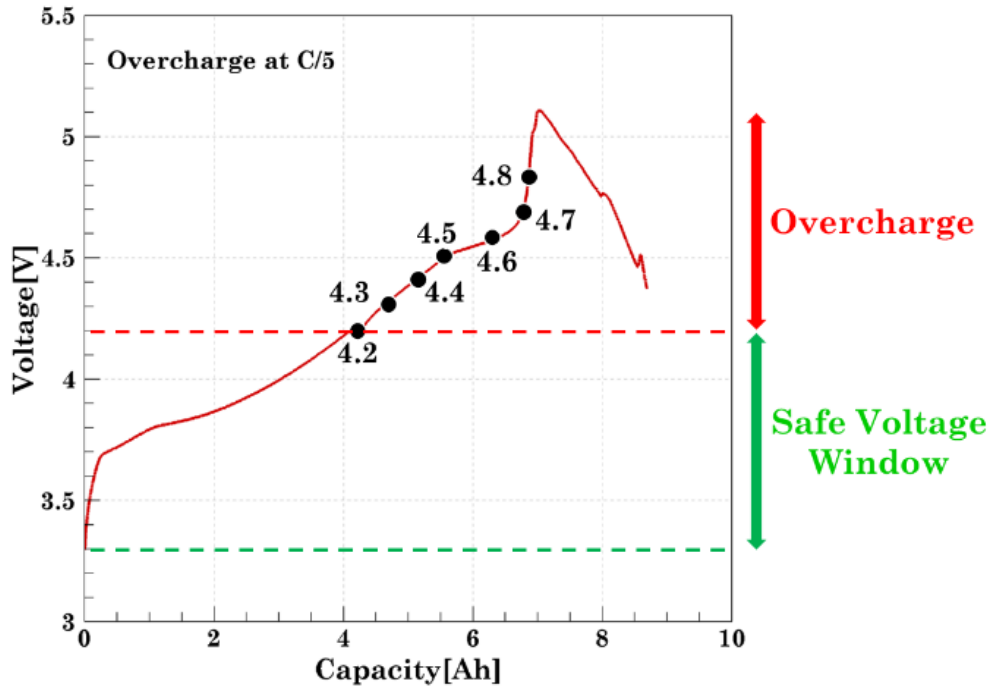
Figure 4.2 Voltage evolution plot for a 5 Ah pouch cell overcharged at C/5-rate.

After deciding the upper cutoff voltages, overcharge tests were performed by varying the upper cutoff voltages and allowing the cells to cycle until 20% capacity had been lost (4 Ah). A 20% capacity fade with respect to the nominal charge capacity is set as the stopping condition for all the tests in this study as for primary applications, 20% capacity loss is considered being the end of cycle life. Figure 4.3 shows the capacity retention of two cells cycled between 2.7 – 4.2 V and 2.7 – 4.5 V. It can be seen that the initial capacity of the cell cycled between 2.7 - 4.5 V is higher than that of cell charged between 2.7 - 4.2 V. Due to the different capacities observed for each cell in the first cycle, the initial capacity cannot be taken as a reference for capacity fade. Hence the nominal capacity of the cell (5 Ah) is taken as the reference to observe capacity fade. The charge capacity of 4 Ah represents 20% capacity loss and is the stopping criteria for all the tests. The

additional capacity obtained above 5 Ah is defined as the overcharge capacity as shown in Figure 4.3.
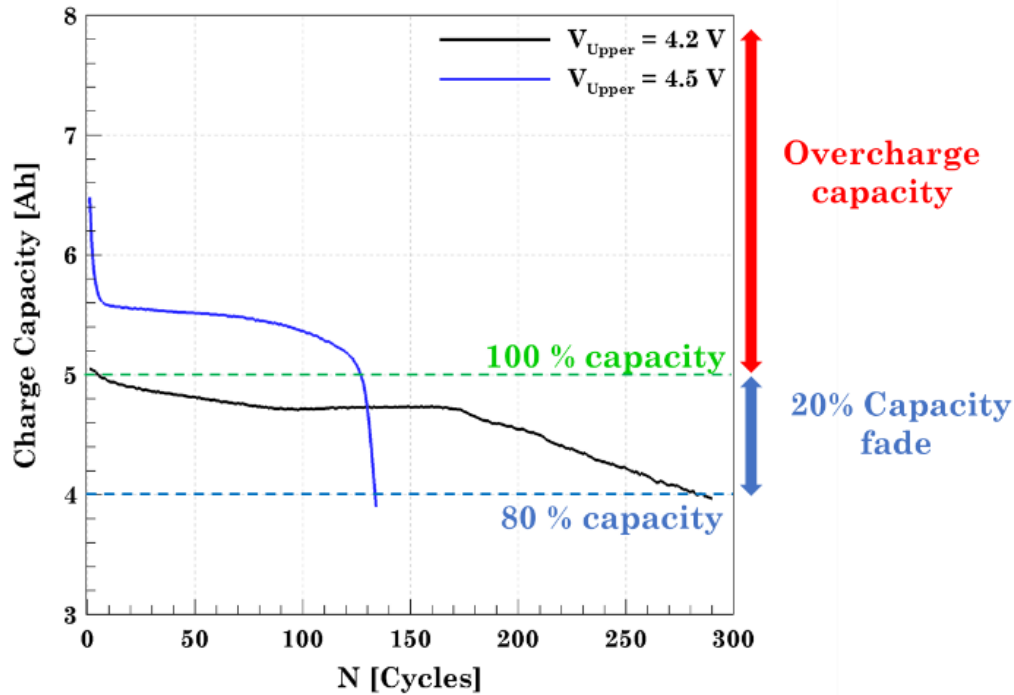
Figure 4.3 Charge capacity (1C-rate) of a 5 Ah Wanma cells at two different voltages representing the 20% capacity fade with respect to the nominal charge capacity.

In order to understand the dependence of capacity fade on the upper cutoff voltage, a capacity vs. number of cycles plot was made for all the voltages (Figure 4.4 and Figure 4.5). Along with the evolution of charge and discharge capacity, the coulombic efficiency of the cell was also graphed on the same plot. Coulombic efficiency is defined as the efficiency by which the electrons are transferred into batteries and is given by the ratio of discharge capacity over the charge capacity. It is an indicator of how much energy can be extracted from the battery with respect to the energy stored in the battery. Low coulombic efficiency is an indicator that the cell has started degrading as a result of capacity loss. It also indicates that less amount of discharge capacity is obtained as compared to the charge capacity, thus indicating an increase in the net loss of energy.

$$\eta_{Coulombic} = \frac{Discharge\ Capacity}{Charge\ Capacity} \times 100\%$$

A total of seven cells were cycled at 1C-rate for different upper cutoff voltages. Figure 4.4(a) shows capacity evolution for cell 1 which was cycled in the safe voltage window of 2.7 – 4.2 V. The cell achieved an initial capacity of 5.05 Ah in the first cycle and took 285 cycles to fade to 80% of its capacity. Figure 4.4(b) shows capacity evolution for cell 2 which was cycled in the overcharge voltage window of 2.7 – 4.3 V. As expected the cell achieved a higher initial capacity of 5.46 Ah in the first cycle as compared to cell-1. However, the cell decayed at a faster rate and took 209 cycles to fade to 80% of its capacity.

Figure 4.4(c) shows capacity evolution for cell 3 which was cycled in the overcharge voltage window of 2.7 – 4.4 V. This cell achieved an even higher initial capacity of 5.84 Ah in the first cycle as compared to the previous cells. The cell took 198 cycles to fade to 80% of its capacity.
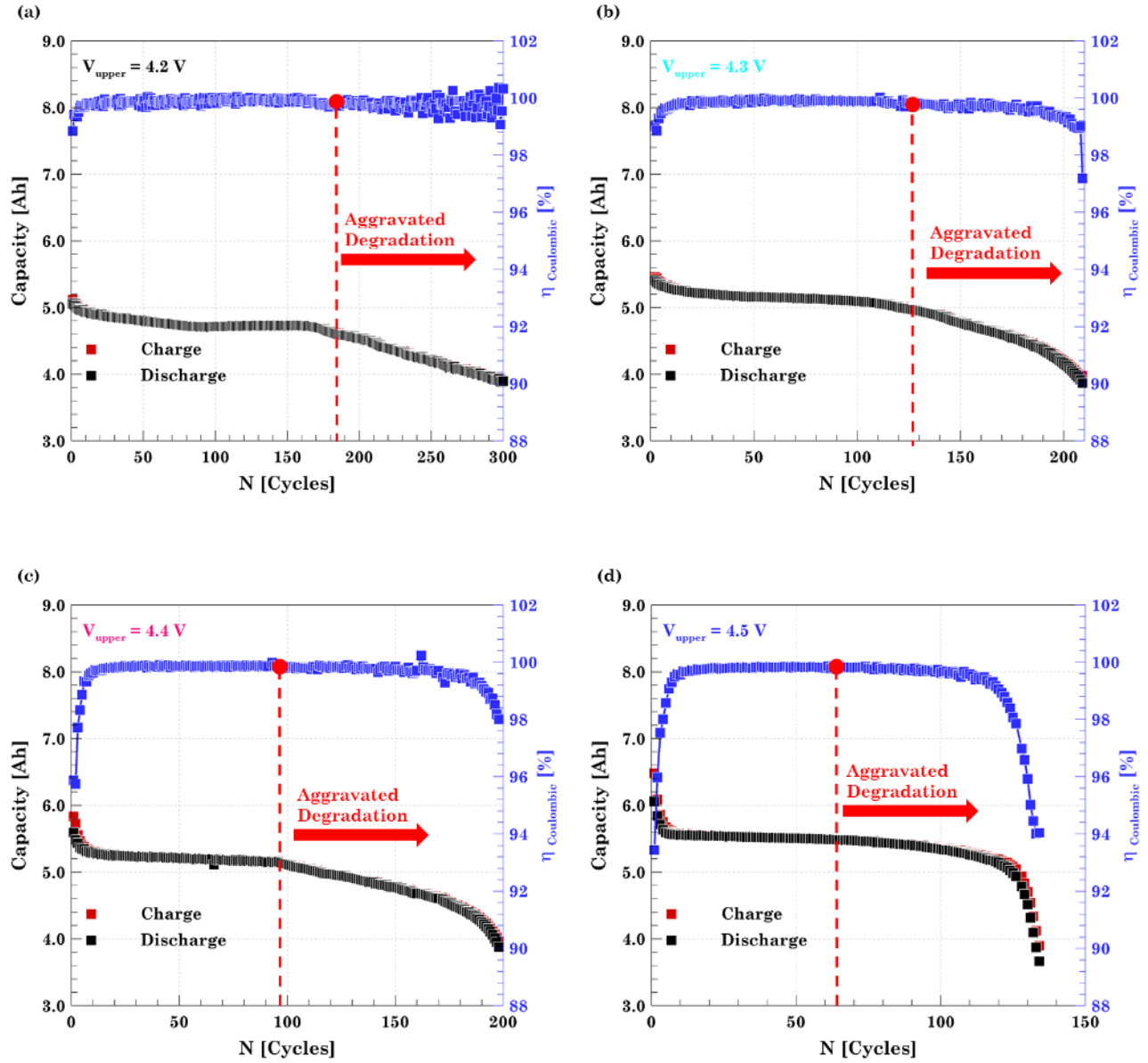
Figure 4.4 Capacity fade: Charge (1C), discharge (1C) capacity and coulombic efficiency curves for voltage range (a) 2.7 - 4.2 V, (b) 2,7 – 4.3 V, (c) 2.7 - 4.4 V, (d) 2.7 – 4.5 V.

Figure 4.4(d) shows capacity evolution for cell 4 which was cycled in the overcharge voltage window of 2.7 – 4.5 V. This cell achieved an even higher initial capacity of 6.48 Ah in the first cycle as compared to the previous cells. The cell took 135 cycles to fade to 80% of its capacity.
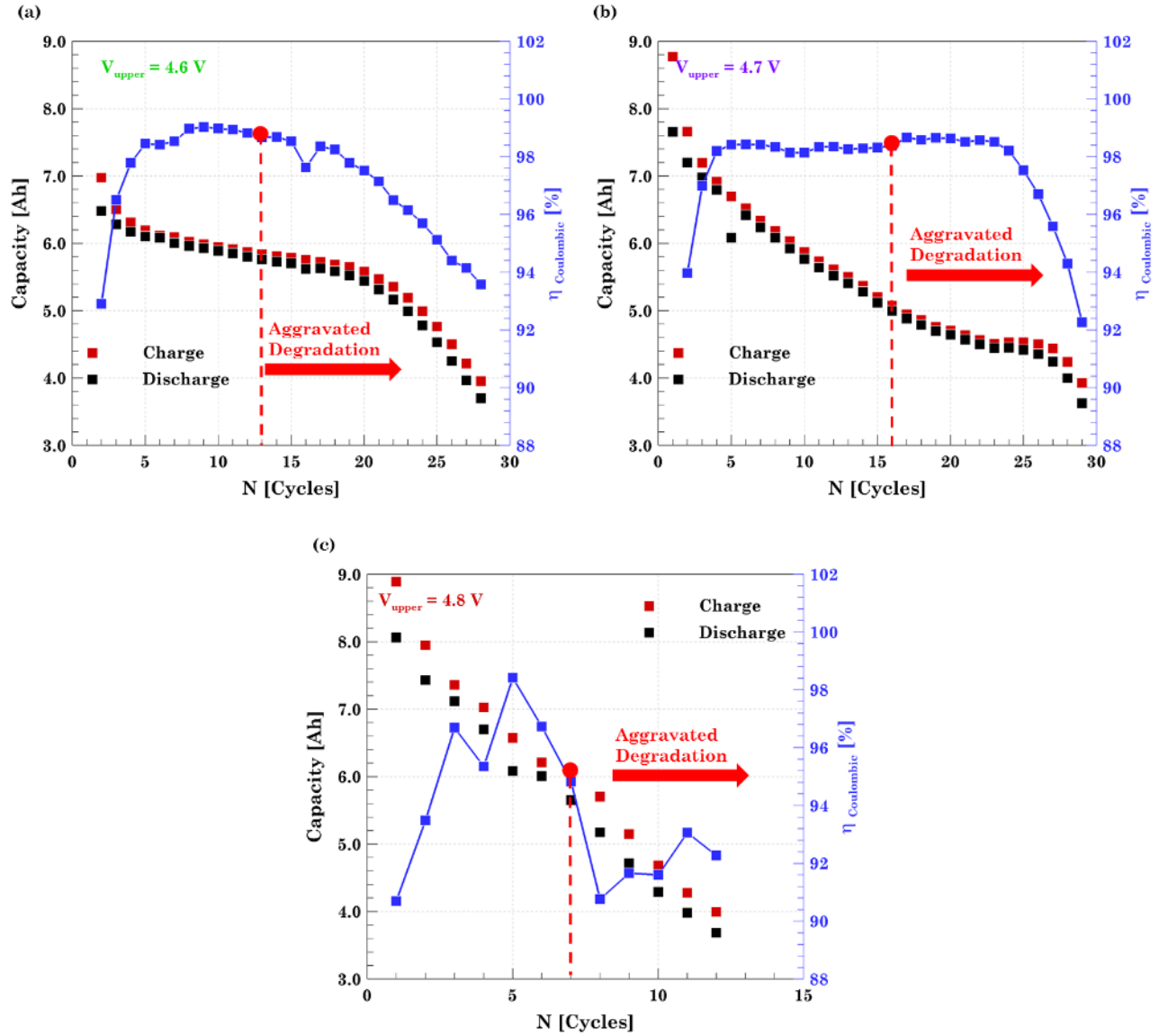
Figure 4.5 Capacity Fade: Charge (1C), discharge (1C) capacity and coulombic efficiency curves for voltage range (a) 2.7 - 4.6 V, (b) 2,7 – 4.7 V, (c) 2.7 - 4.8 V.

Figure 4.5(a, b, c) show capacity evolution for cells 5, 6 and 7 cycled up to 4.6, 4.7 and 4.8 V respectively. Cell 5, 6 and 7 achieved initial capacities of 6.97, 8.77 and 8.99 Ah in the first cycle respectively. The cells 5 and 6 took 29 cycles to fade to 80% of their capacity whereas the cell 7 reached the 80% capacity fade limit in just 15 cycles.
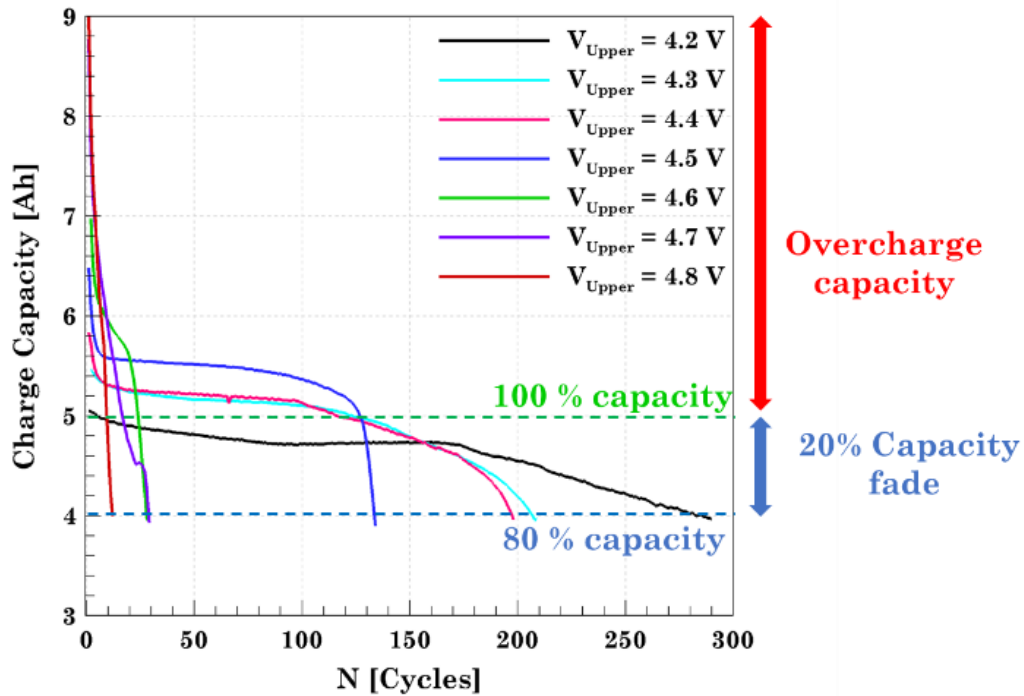
Figure 4.6 Comparison of Capacity fade behavior for all the cells cycled up to different cutoff voltages of 4.2, 4.3, 4.4, 4.5, 4.6, 4.7 and 4.8 V and till 20% capacity fade.

Figure 4.6 includes the capacity fade behavior of all the 7 cells cycled up to different cutoff voltages. A significant change in the capacity behavior of cells charged up to different upper cutoff voltage is observed. It can be inferred that as the voltage window is expanded by increasing the upper cutoff voltage, the initial capacity of the cell increases. The cell attains maximum capacity when cycled from 2.7 - 4.8 V and least when it is cycled from 2.7 – 4.2 V. It should also be noted that as the upper cutoff voltage increases, the cell decay increases rapidly. The cell cycled under the safe voltage window of 2.7 - 4.2 V faded to 80% capacity in 290 cycles whereas the cell cycled in the voltage window of 2.7 – 4.8 faded to 80% capacity in 15 cycles. So, there exists a trade-off between the initial capacity obtained and the cycle life of the cell. By expanding the voltage window, i.e., by increasing the extent of overcharge, a higher initial capacity can be obtained whereas the cell cycle life is compromised.

The coulombic efficiency of all the cells starts decreasing as the capacity approaches the 20% fade limit. In extreme cases such as the cells charged up to 4.7 and 4.8 V, the coulombic efficiency

starts decreasing a faster rate as the cells start failing. The decrease in coulombic efficiency signifies that the energy extracted from the cell with respect to the amount of energy being supplied keeps decreasing. The loss of energy indicates degradation which is a consequence of energy lost to the side reactions occurring in a lithium-ion cell.

An indicator of aggravated degradation has been shown in all the plots of Figure 4.4 and Figure 4.5. This point indicates the cycle at which the cell starts failing at a faster rate, i.e., the cell starts losing its capacity. Various parameters including coulombic efficiency, capacity, and internal resistance have been explored to predict the onset of failure. As discussed earlier, the decrease in coulombic efficiency can be used as an indication for a faster degradation rate of the cell. Similarly, a decrease in capacity and increase in resistance are clear indicators of cell degradation.

As the capacity of the cell evolves with cycling the change in capacity signifies a change in cell behavior. Investigating these changes can help in elucidating the conditions under which these cell starts to fail and hence provide a better understanding of cell degradation. Although the point at which cell starts failing faster can be inferred from the capacity fade plot, a qualitative way to predict the onset of rapid degradation needs to be explored. In order to do the same, a differential analysis of capacity and coulombic efficiency with respect to the number of cycles was done. A third order polynomial and a sixth order polynomial were found to be the best fit for the charge capacity data and the coulombic efficiency data respectively. The graph in Figure 4.7 shows dQ/dN and $d\eta/dN$ analysis for all the cycled cells. The peaks obtained in the dQ/dN serves as an indicator for cell degradation and that a change has occurred in the cell. Similarly, the point at which the $d\eta/dN$ crosses zero indicates a change in the trend of coulombic efficiency. Usually, the coulombic efficiency increases in the first few cycles and remains constant until the cell starts to fail. Hence, a significant change in the trend of coulombic efficiency could act as an indicator of some change in the cell. There are several points in the $d\eta/dN$ curve at which the curve crosses zero. Some of these peaks may occur due to over or underfitting of the data. However, most of these points are observed in all the cells and hence can be considered as an indicator of major change occurring in the cell. Some of the major points have been marked in the differential analysis plots which can
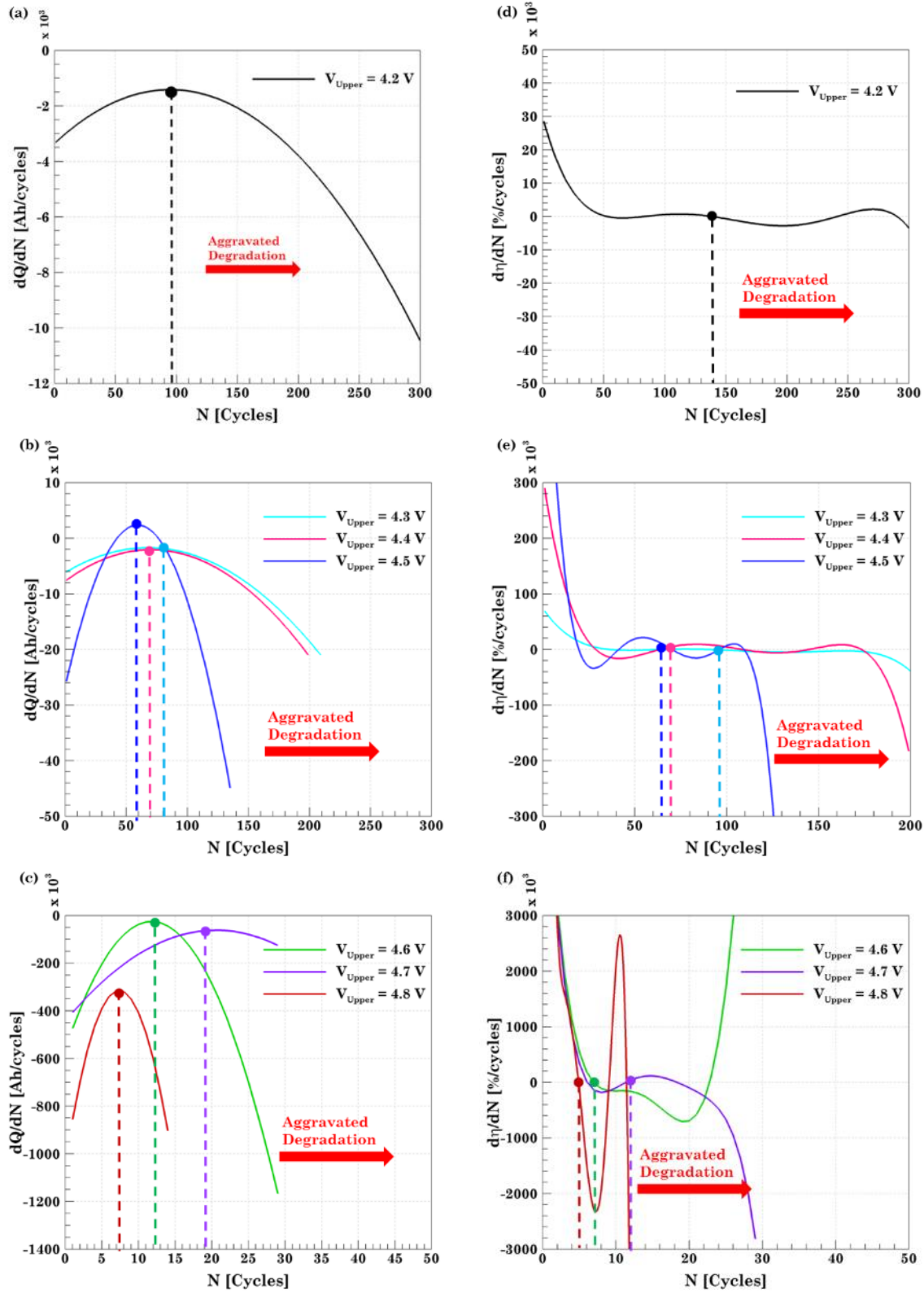
Figure 4.7 Development of dQ/dN curves for the overcharged cells at different cutoff voltages (a) 4.2 V (b) 4.3V, 4.4V, 4.5V (c) 4.6 V, 4.7 V, 4.8 V. (d-f) are corresponding dη/dN curves. Aggravated degradation is represented by the vertical line indicating the cycle number.

serve as the indicator for aggravated degradation. A general trend visible in both the plots for dQ/dN and dη/dN is that as the upper cutoff voltage is increased the number of cycles for initiation of cell degradation decrease. For example, the prediction for the onset of failure for cell cycled up to 4.2 V is 98 cycles and 139 cycles as per the dQ/dN and dη/dN respectively. Whereas, for the cell cycled up to 4.8 V the prediction for the onset of failure is 7 cycles and 5 cycles as per the dQ/dN and dη/dN respectively. Internal resistance was also used as an indicator for the prediction of aggravated degradation and will be discussed in the next section. Moreover, the credibility of the predictions made by various parameters will be discussed in the next section.

4.1.3   *Effect of Upper Cutoff Voltage on Internal Resistance*

Resistance is described as the ability of a component to hinder the flow of current through it. Each component of the cell contributes to some resistance and a combination of all the resistances act in a working lithium-ion cell. In order to study the evolution of resistance with cycling, the internal resistance of the cell was measured after each charge and discharge cycle. The cell was rested for a duration of 25 minutes to allow it to reach an equilibrium state. A series of pulses were passed using the Arbin Battery Tester and the internal resistance of the cell was recorded. The data recorded for the cells charged up to 4.2, 4.3, 4.4 and 4.5 V has been presented in Figure 4.8(a-d). Similarly, the data for cell charged up to 4.6, 4.7, and 4.8 V has been shown in Figure 4.9(a-c). Charge resistance has been defined as the resistance after the charge cycle and discharge resistance as the resistance after the discharge cycle. The resistance contribution of each component can be deciphered using Electrochemical Impedance Spectroscopy (EIS) however, this has not been included and is beyond the scope of this study.

Two major inferences can be made by observing the data presented in Figure 4.8 and Figure 4.9. Firstly, it can be observed that the with cycling the internal resistance of the cell increases indicating that the cell has started degrading. The resistance for all the cells was recorded until they lost 20% of their nominal capacity. Another notable inference is that as the upper cutoff voltage of the cell is increased, the magnitude of resistance increases and at a faster rate. Moreover, the resistance of the cell charged up to a higher voltage increases in a lesser number of cycles. For example, both the charge and discharge resistance of the cell cycled from 2.7 to 4.2 V is

approximately 36 milli-ohms after 285 cycles. However, for a cell cycled between 2.7 and 4.7 V, the resistance of the cell increases to 60 milli-ohms in just 28 cycles. This indicates that the cell charged up to a higher cutoff voltage degrades faster and further strengths our understanding about the increase of resistance leading to capacity fade of cells. The rise in the internal resistance of the cell is mainly attributed to the growth of the SEI layer with cycling [108]. This is observed in figure 4.8 for the cells charged up to 4.5 V. However, the abrupt increase in resistance in lesser number of cycles is observed for the cells charged up to higher voltages (4.6, 4.7, and 4.8 V). This is an indication that some other phenomenon was responsible for the rapid degradation of the cells and will be investigated in the next sections.
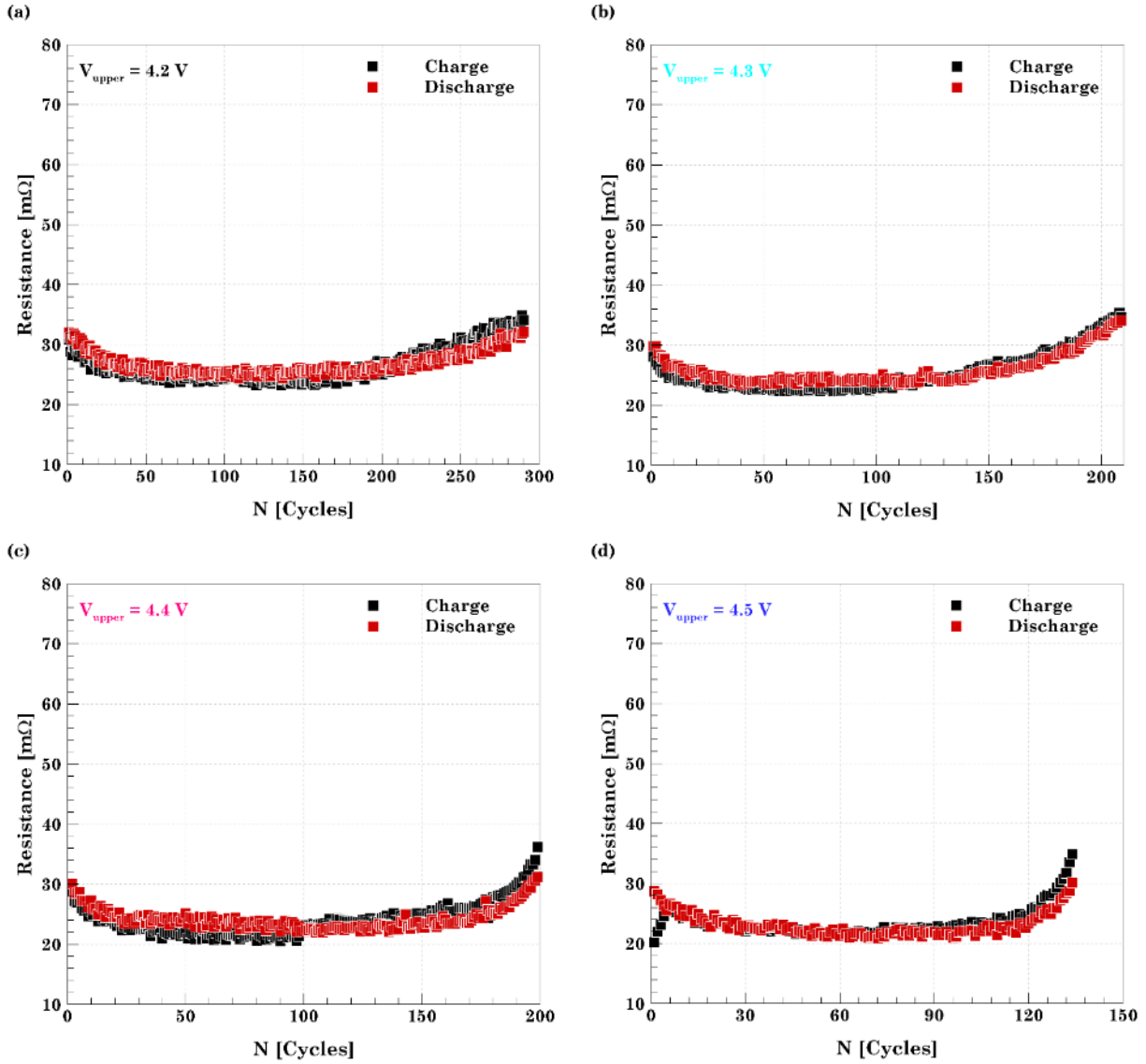
Figure 4.8 Internal resistance evolution for cells cycled at different voltage range (a) 2.7 – 4.2 V, (b) 2.7 – 4.3 V, (c) 2.7 – 4.4 V, and (d) 2.7 – 4.5 V.
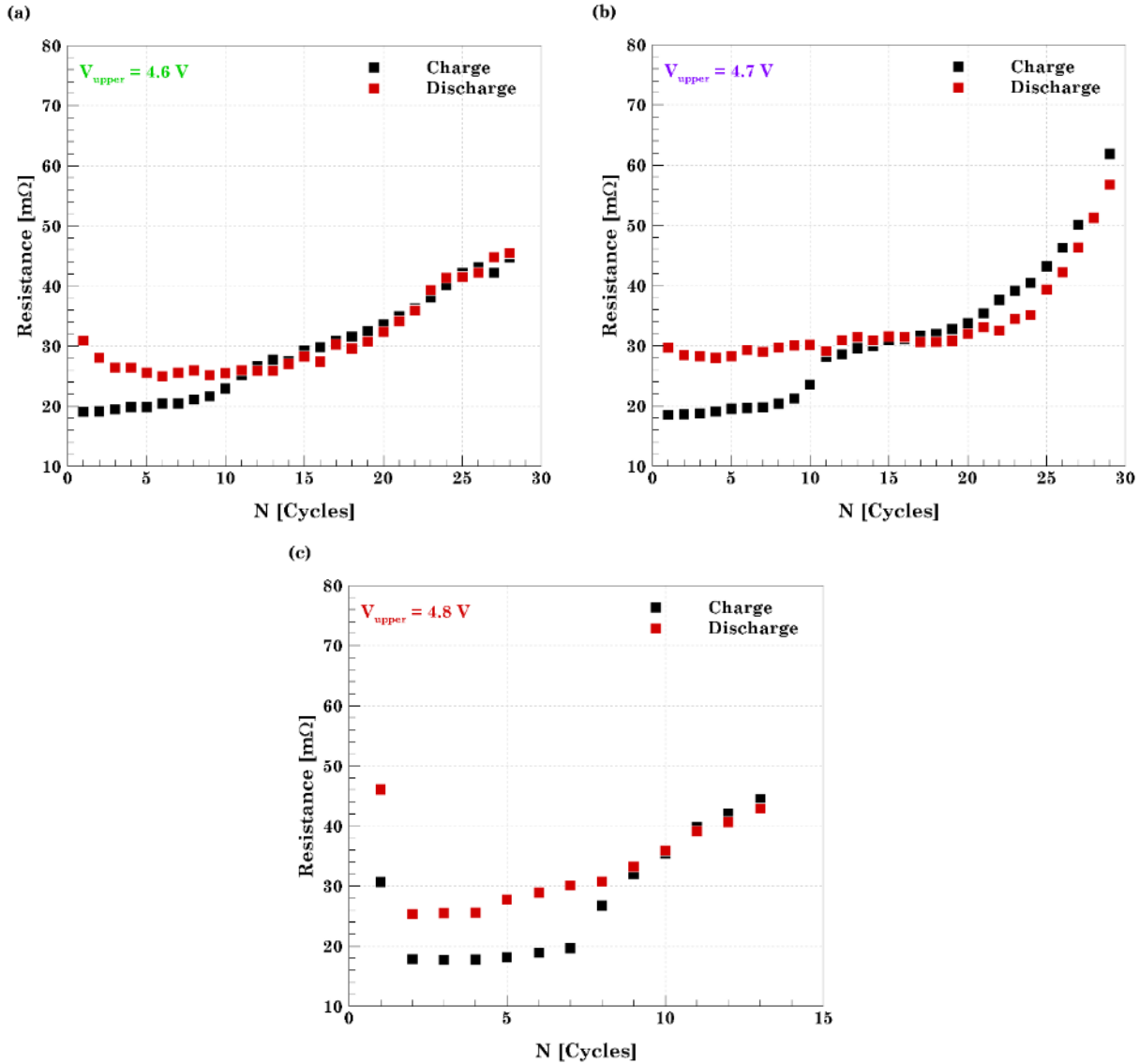
Figure 4.9 Internal resistance evolution for cells cycled at different voltage range (a) 2.7 – 4.6 V, (b) 2.7 – 4.7 V, and (c) 2.7 – 4.8 V.

Internal resistance has been explored as one of the parameters to monitor battery State of Health (SoH). The state of Health refers to the condition of the battery. It is important to have knowledge of SoH in order to predict the occurrence of any severe battery failures and avoid hazardous events [109]. In the previous sections, dQ/dN, and dη/dN analysis were explored as an indicator to predict the inception of aggravated degradation of the battery. In this section, internal resistance has also been explored as a predictor of rapid failure of the battery. It is intriguing to notice that in all the plots presented in Figure 4.10 and Figure 4.11 the cells start with a stage where the magnitude of

discharge resistance is higher than the charge resistance. The discharge resistance remains higher for the majority of the initial cycles but after a point, the charge resistance becomes larger than the discharge resistance. Owing to this characteristic trend a non-dimensional parameter Φ_R has been defined and proposed as an indicator of aggravated degradation.
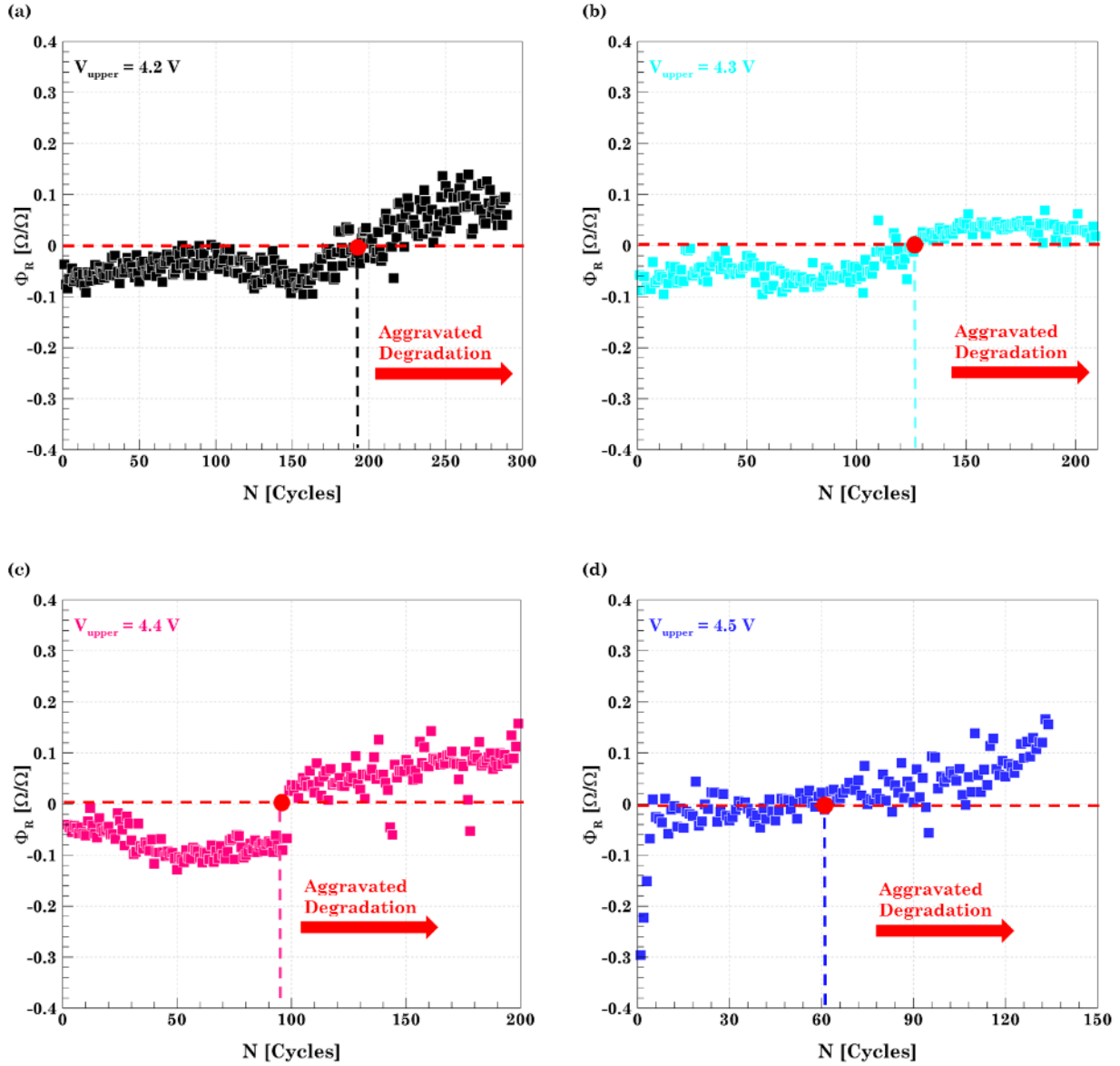
Figure 4.10 Plots of Φ_R for cells cycled at different voltage range (a) $2.7 - 4.2$ V, (b) $2.7 - 4.3$ V, (c) $2.7 - 4.4$ V, and (d) $2.7 - 4.5$ V to predict the onset of aggravated degradation represented by the vertical line indicating the cycle number at which degradation rate increases.

Φ_R is defined as the ratio of the difference between the charge and discharge resistance over discharge resistance.

$$\Phi_R = \frac{Charge\ resistance - Discharge\ resistance}{Discharge\ resistance} = \frac{R_c - R_d}{R_d}$$

This nondimensional quantity Φ_R is plotted against the number of cycles as shown in Figure 4.10. A horizontal red line at $\Phi_R = 0$ has been marked on all the plots indicating the change in
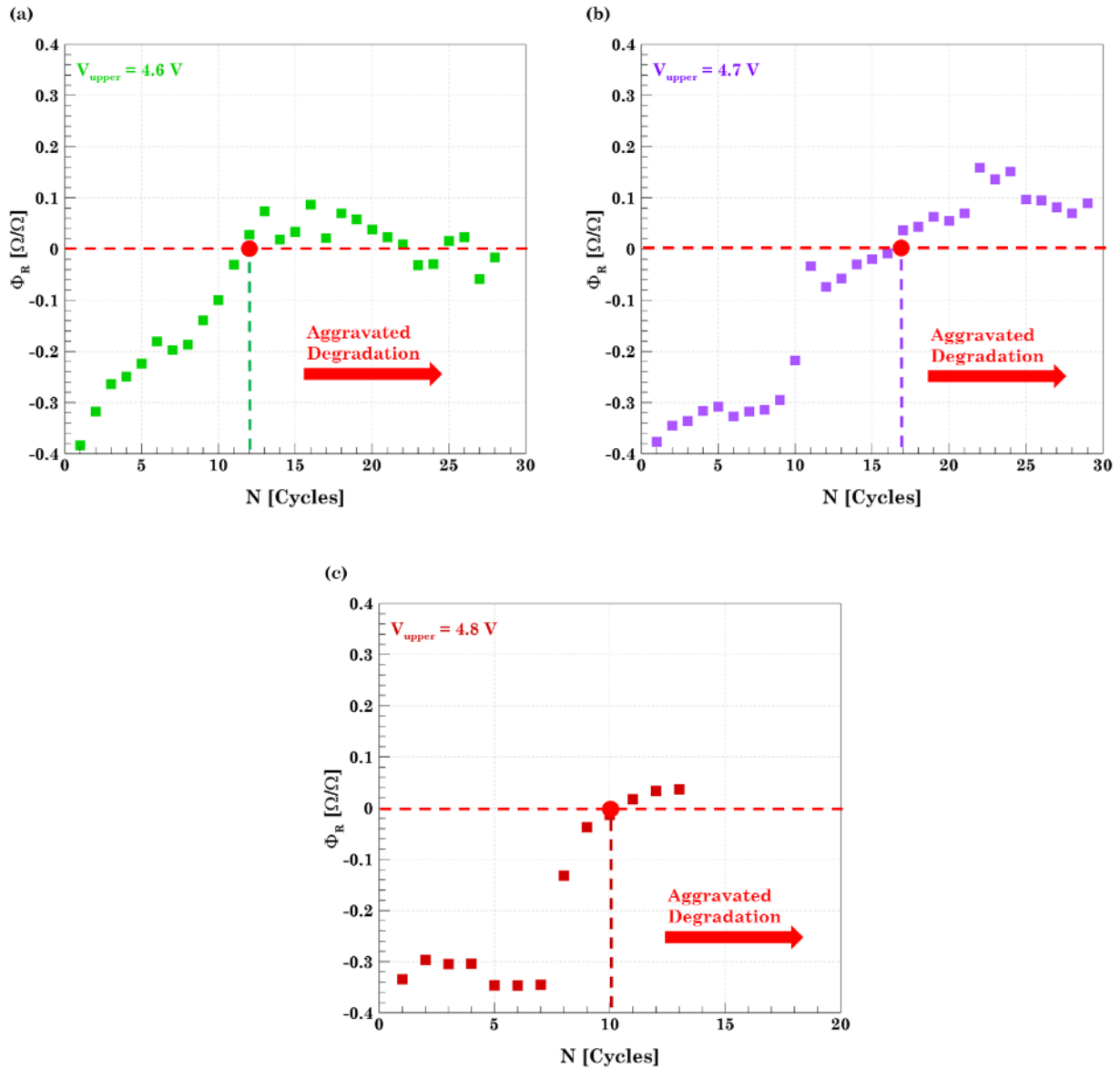
Figure 4.11 Plots of Φ_R for cells cycled at different voltage range (a) $2.7 - 4.6$ V, (b) $2.7 - 4.7$ V, (c) $2.7 - 4.8$ V to predict the onset of aggravated degradation represented by the vertical line indicating the cycle number at which degradation rate increases.

the trend of resistance. Further, the cycles corresponding to the point at which Φ_R crosses the zero mark has been identified as the indicator of aggravated degradation. This point exactly corresponds to the state of the cell when the charge resistance surpasses the discharge resistance. From the predictions made, it is evident that the cell charged up to a higher voltage fails at a faster rate which is in agreement with the results presented for the capacity fade.

To compare the accuracy of all the SoH indicators analyzed in this study, a comparative study with the actual point at which the cell starts to fail faster has been presented in Figure 4.12. The actual point is obtained by analyzing the capacity fade results. It can be observed that Φ_R is the best predictor as compared to the other parameters. The incorrect predictions made by dQ/dN and dη/dN for cells charged to lower voltages of 4.2 V, 4.3 V, and 4.4 V can be accounted to poor curve fitting. Moreover, the capacity vs. cycles curve at a lower voltage is relatively flat making it difficult to predict the exact point of failure. For the cells cycled to higher voltages including 4.5 V, 4.6 V, 4.7 V, and 4.8 V all three parameters are very close to the actual point of failure. In conclusion, all the indicators discussed can at least alert us about any possible future failures which can be taken as a measure to conduct a complete inspection of the battery. Moreover, Φ_R was found to be the best predictor of aggravated degradation and can be utilized for SoH monitoring in lithium-ion batteries.
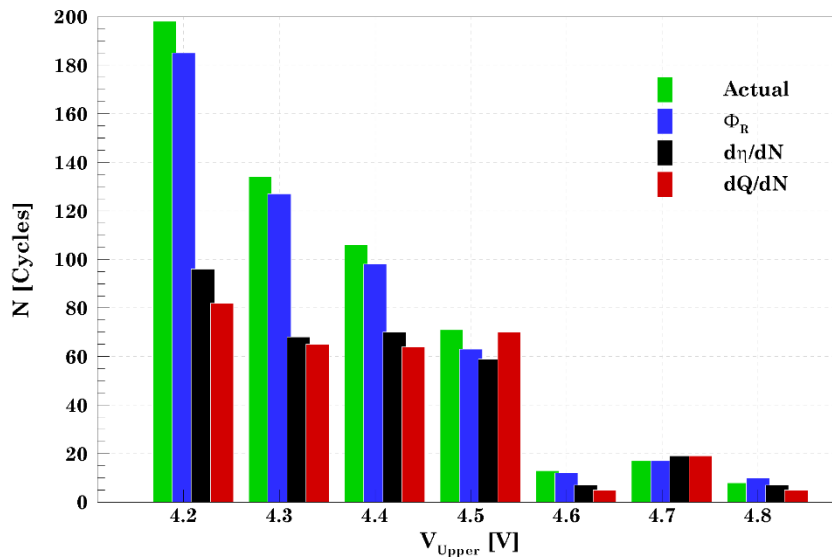
Figure 4.12 Cycle number predicted by each SoH parameter representing the onset of aggravated degradation

4.1.4 *Voltage Spectra*

In the above sections, it was observed that the number of cycles to retain capacity decreases with an increase in upper cutoff voltage. A sudden drop in the cycle life was observed at 4.6 V and in order to further investigate the same, voltage vs. capacity of each cell was acquired. Figure 4.13(a-d) shows the voltage evolution with SoC for cells cycled up to 4.2 V, 4.3 V, 4.4 V, and 4.5 V.

Figure 4.13 Capacity fade for Wanma® cells at different cycling voltage window: (a) 2.7 - 4.2 V, (b) 2.7 - 4.3 V, (c) 2.7 – 4.4 V and, (d) 2.7 – 4.5 V. Voltage profiles for 0%, 5%, 10%, 15%, and 20% capacity fade are depicted.

Voltage profile was obtained at five cycles corresponding to 0% capacity fade (initial cycle), 5% capacity fade, 10% capacity fade, 15% capacity fade and 20% capacity fade (last cycle). It can be seen that as the upper cutoff voltage increase the capacity obtained at the first cycle increases. The cell cycled in range 2.7 – 4.8 V achieved 1.6 times (160 % SoC) more than the nominal capacity of 5 Ah.
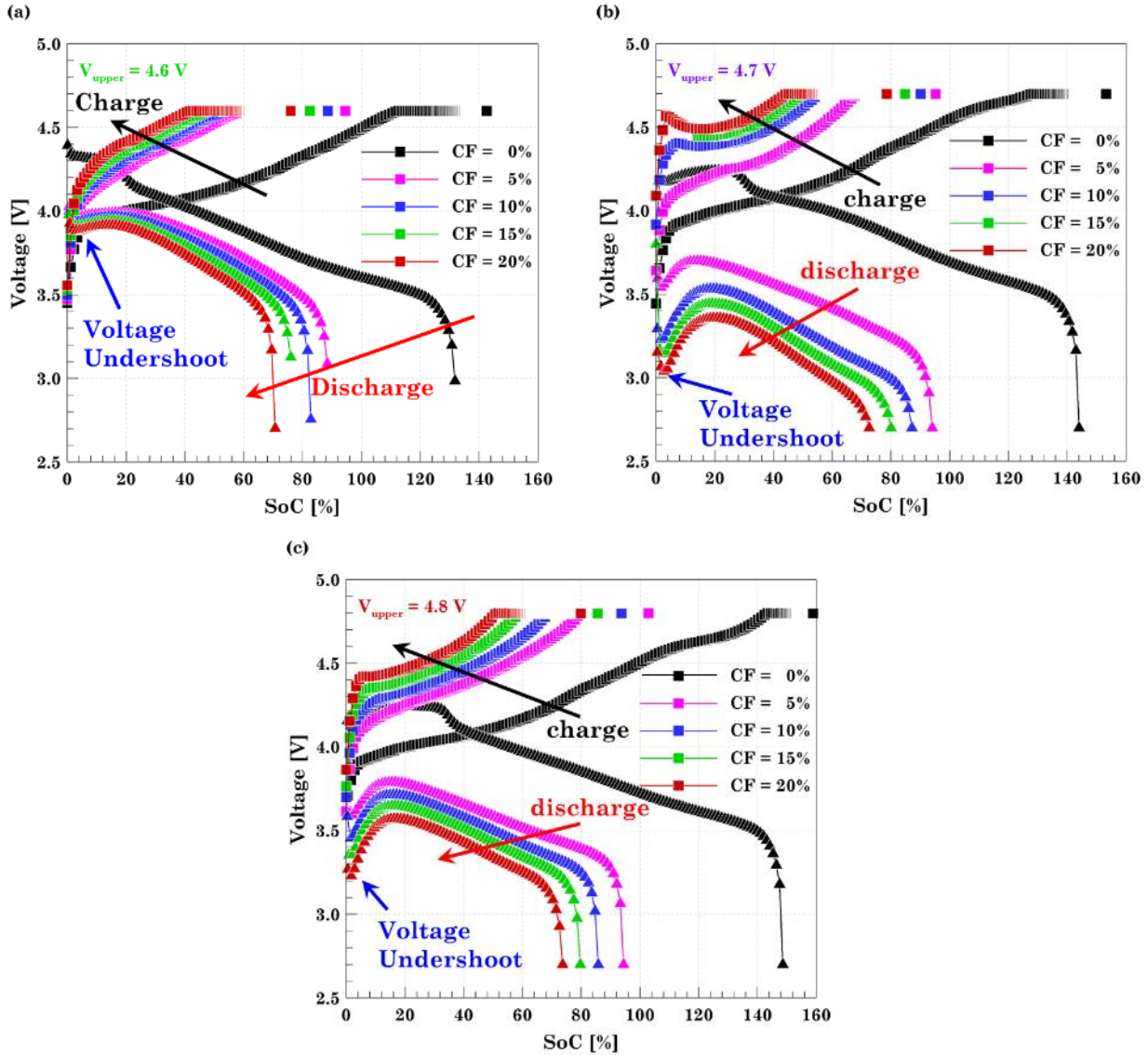
Figure 4.14 Capacity fade noticed for the 5 Ah Wanma® cell at different cycling voltage window (a) 2.7 - 4.6 V, (b) 2.7 - 4.7 V and, (c) 2.7 – 4.8 V. Voltage profiles for 0%, 5%, 10%, 15%, and 20% Capacity fade are depicted

The four cells cycled up to 4.2 V, 4.3 V, 4.4 V, and 4,5 V are similar to a typical voltage capacity curve of lithium-ion batteries. However, an aberration is observed when the upper cutoff voltage is increased beyond 4.5 V. A unique feature of "voltage undershoot" is observed for all the plots shown in Figure 4.14. In the discharge curve for cells charged up to 4.6, 4.7 and 4.8 V, the voltage decreases to a low value (local minima) and suddenly starts to increase. The occurrence of this voltage undershoot is considered a typical indicator of poor electrolyte performance and occurs when the cells transitions from linear to non-linear aging resulting in lithium plating. It is known that as the cell is cycled for a very long time the SEI growth leads to capacity fade. Hence, the subsequent occurrence of SEI growth along with lithium plating clogs the pores near anode-separator interface and decreases the anode porosity. This reduction in anode porosity leads to the rise of electrolyte resistance resulting in a rapid drop of cell voltage and the voltage to undershoot [49, 63].

To elucidate the overcharge behavior of the cell and further investigate the changes occurring during the overcharge reaction of a cell, a differential voltage capacity (dV/dQ) analysis was performed. The dV/dQ study physically signifies the change of resistance per unit time. Hence, it is an indicator of changes occurring in the internal resistance of the cell at each cycle. The data for constant current charge and discharge was acquired and a 7th order polynomial was found to be the best fitting curve for the experimental data. An equation expressing voltage in terms of capacity was obtained and the derivative dV/dQ was calculated. The obtained expression for dV/dQ was then plotted against the capacity to analyze the cell performance. Figure 4.15(a-d) and Figure 4.16 (a-c) show the dV/dQ analysis for all the cycled cells at different voltages. Several peaks can be observed in all the dV/dQ plot. All these peaks represent a phase change occurring in the system. A similar approach of acquiring the data at 0, 5 10, 15 and 20 % capacity fade was followed to obtain the dV/dQ plots for the charge cycles of all the cells. One similar trend observed in all the plots is that at the capacity decreases, the peaks shift towards left. This is considered a typical characteristic of aging of cells [110]. dV/dQ plots shed light on how the resistance of the cell varies in a cycle. It can be observed that the phase transitions occur early with an increase in the upper cutoff voltage. Further, the distance between the occurrence of the peaks also reduces denoting that the changes are occurring at a faster rate. It is always beneficial to analyze the dV/dQ data for a full cell with dV/dQ data for its individual electrodes in the form of half cells. As the cells tested

were commercial, the data for the exact composition of electrolyte was unknown thus limiting the study of dV/dQ analysis.
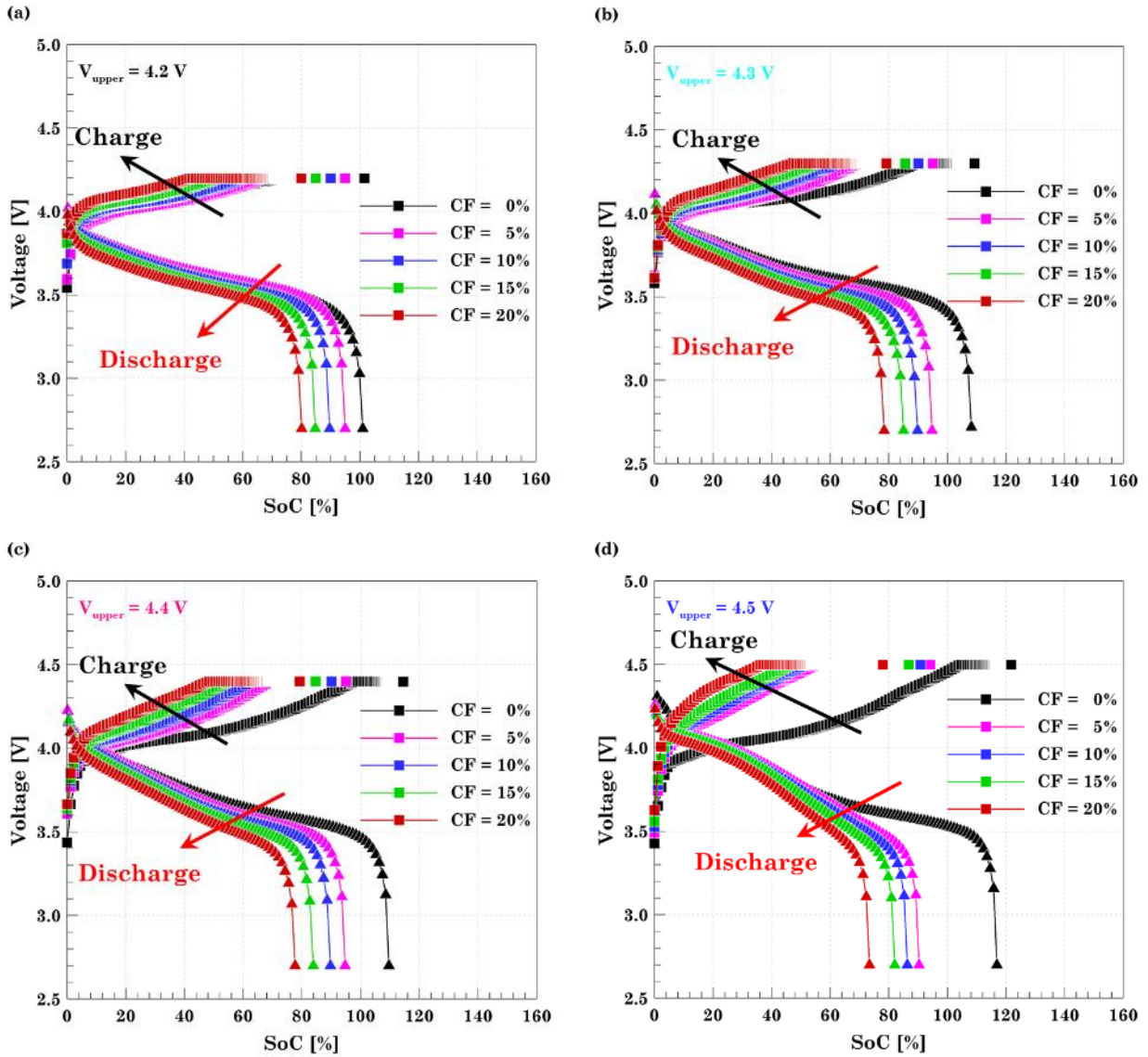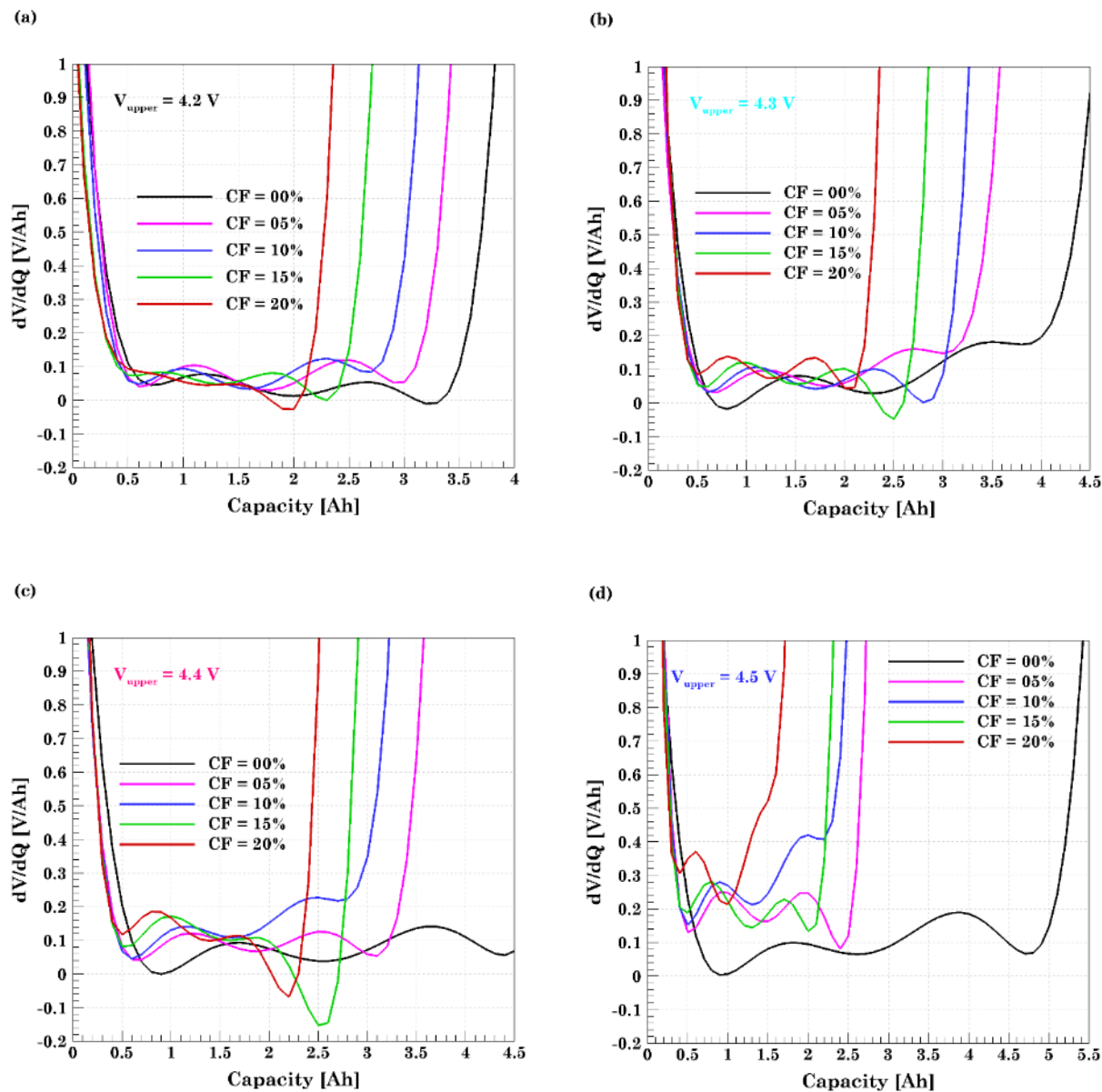

Figure 4.15 dV/dQ curves obtained from charge EMF curves at different cycling voltage window (a) 2.7 - 4.2 V, (b) 2.7 - 4.3 V, (c) 2.7 - 4.4 V and, (d) 2.7 – 4.5 V. Profiles for 0%, 5%, 10%, 15%, and 20% capacity fade are depicted
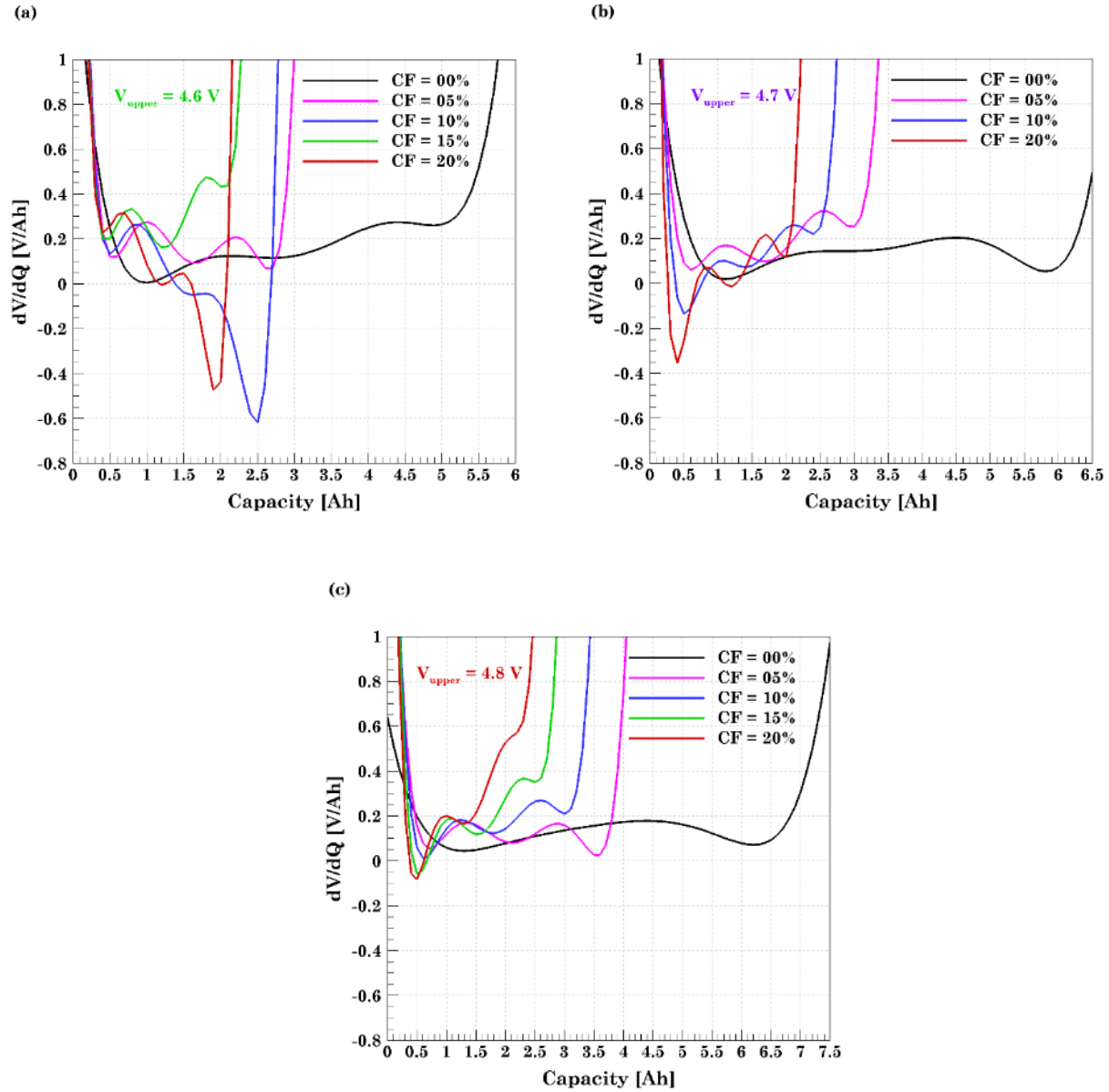
Figure 4.16 dV/dQ curves obtained from charge EMF curves at different cycling voltage window (a) 2.7 - 4.5 V, (b) 2.7 - 4.6 V and, (c) 2.7 – 4.8 V. Profiles for 0%, 5%, 10%, 15%, and 20% Capacity fade are depicted

Considering the voltage undershoot as an indicator of lithium plating and electrolyte deterioration the electrodes and electrolyte extracted from these cells were analyzed. The results obtained would be discussed in the upcoming sections. The temperature evolution of the cell will be discussed in the next section.

4.2   <u>Effect of Upper Cutoff Voltage on Temperature Evolution</u>

As discussed earlier, all abuse conditions finally lead to thermal abuse and in extreme conditions, it may translate into a thermal runaway situation. It is well known that the temperature of the cell and surroundings have an impact on the performance of the cells. Hence it is important to investigate the temperature evolution of the cell for cycling under continuous overcharge conditions. The evolution of temperature was done using a thermocouple and a thermal camera.

4.2.1   *Cell Temperature*

A T-type thermocouple was attached to the cell surface to acquire the temperature data. The data for temperature was recorded for the whole test duration at an interval of one second. To analyze the effect of overcharging on the temperature of the cell, temperature data acquired was plotted against the SoC at 0%, 5%, 10%, 15%, and 20% capacity fade as shown in Figure 4.17 and Figure 4.18. It can be inferred from all the plots that the temperature of the cell increases with an increase in the capacity fade. It further implies that the temperature also increases with the number of cycles. It should also be noted that the cell temperature increase during each cycle is related to Joule heating. For the charge cycle, the temperature first increases and reaches a maximum until the end of the constant current charge and then starts decreasing in the constant voltage phase. The temperature decrease in the CV phase occurs due to a drop in the ohmic heat (i^2R) generated in the cell which occurs a consequence of a decrease in the charging current. Another notable observation is that the temperature during the discharge cycle is greater than that of the charge cycle. This can be explained using the internal resistance plots shown in Figure 4.8 and 4.9. The discharge resistance was found to be greater than the charge resistance and hence the ohmic heat generated is greater for the discharge cycle. Ohmic heat is one of the major contributors to increase the cell temperature. However, side reactions such as SEI decomposition, electrolyte decomposition, and Li-plating can lead to a rapid rise of temperature and aggravated degradation.

It can be observed that as the cell degradation increased, the maximum temperature reached during the charge and discharge cycle also increased. For example, the cell cycled in the range 2.7-4.5 V attained a higher temperature of 41 ºC at end of discharge after 20 % capacity fade as compared to a temperature of 34 ºC at the end of discharge of the initial cycle. Hence, it can be inferred that side reactions are also contributing to the increase in cell temperature.

Figure 4.17 Temperature evolution for the 5 Ah Wanma® cell at different cycling voltage window (a) 2.7 - 4.2 V, (b) 2.7 - 4.3 V, (c) 2.7 - 4.3 V and, (d) 2.7 – 4.8 V. Temperature profiles for 0%, 5%, 10%, 15%, and 20% Capacity fade are depicted.

For the cells charge up to 4.7 V and 4.8 V, the maximum temperature observed was approximately 55 °C. However, for cells cycled up to relatively lower cut off voltages, maximum temperature observed was approximately 40 °C. Hence, using a higher value of upper cutoff voltage for cycling, the maximum temperature attained during cycling increases. A significant change in maximum temperature is observed between cell 4 and cell 5. A similar trend was observed for the voltage capacity results presented in the previous section. Voltage undershoots indicating Li-plating and

electrolyte deterioration was observed when the upper cutoff voltage for cycling was increased from 4.5 to 4.6 V. The effect of this phenomenon is also observed in the temperature curves, therefore, indicating aggravated degradation. In conclusion, it can be inferred that the temperature increases with the loss of capacity and is higher at higher cycling voltages.
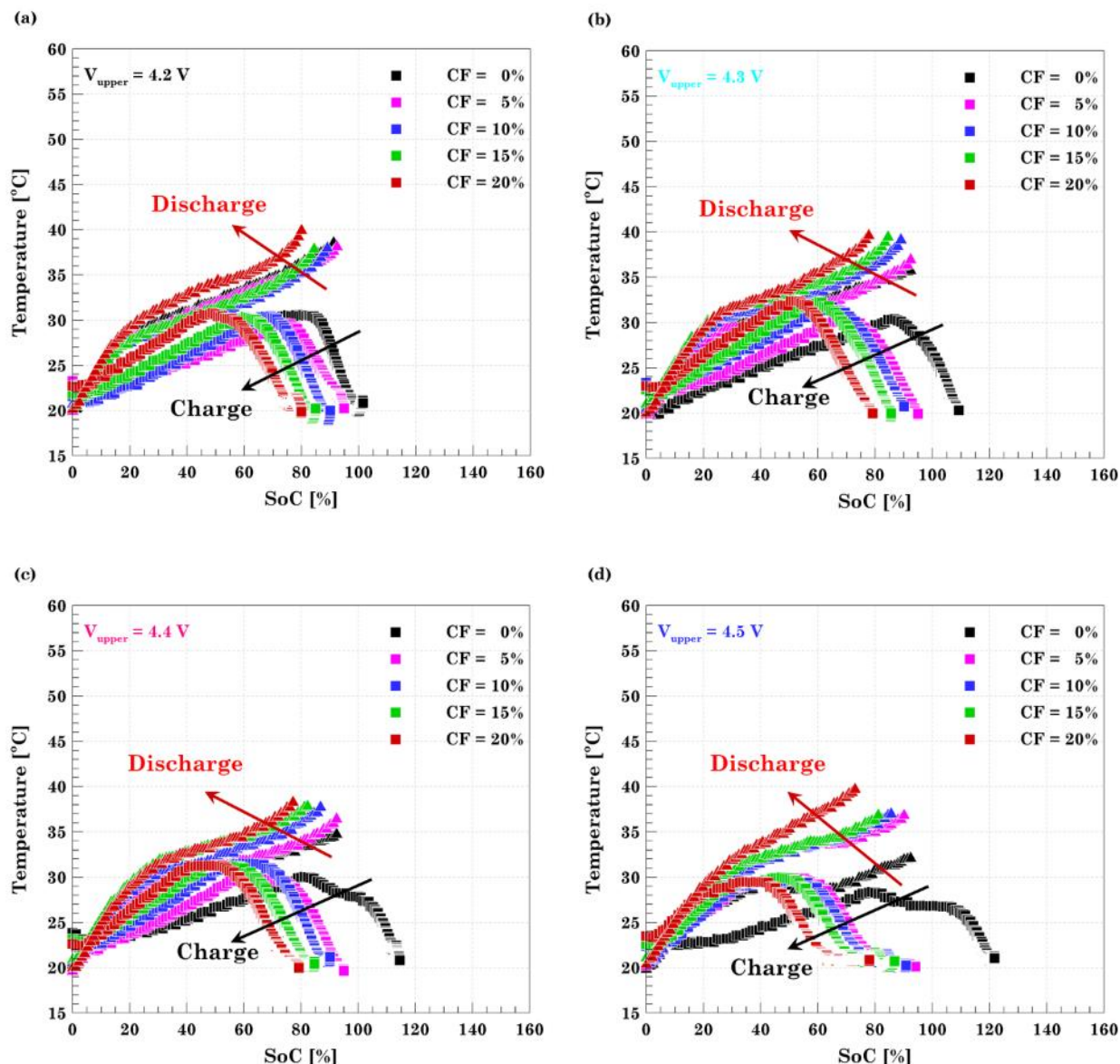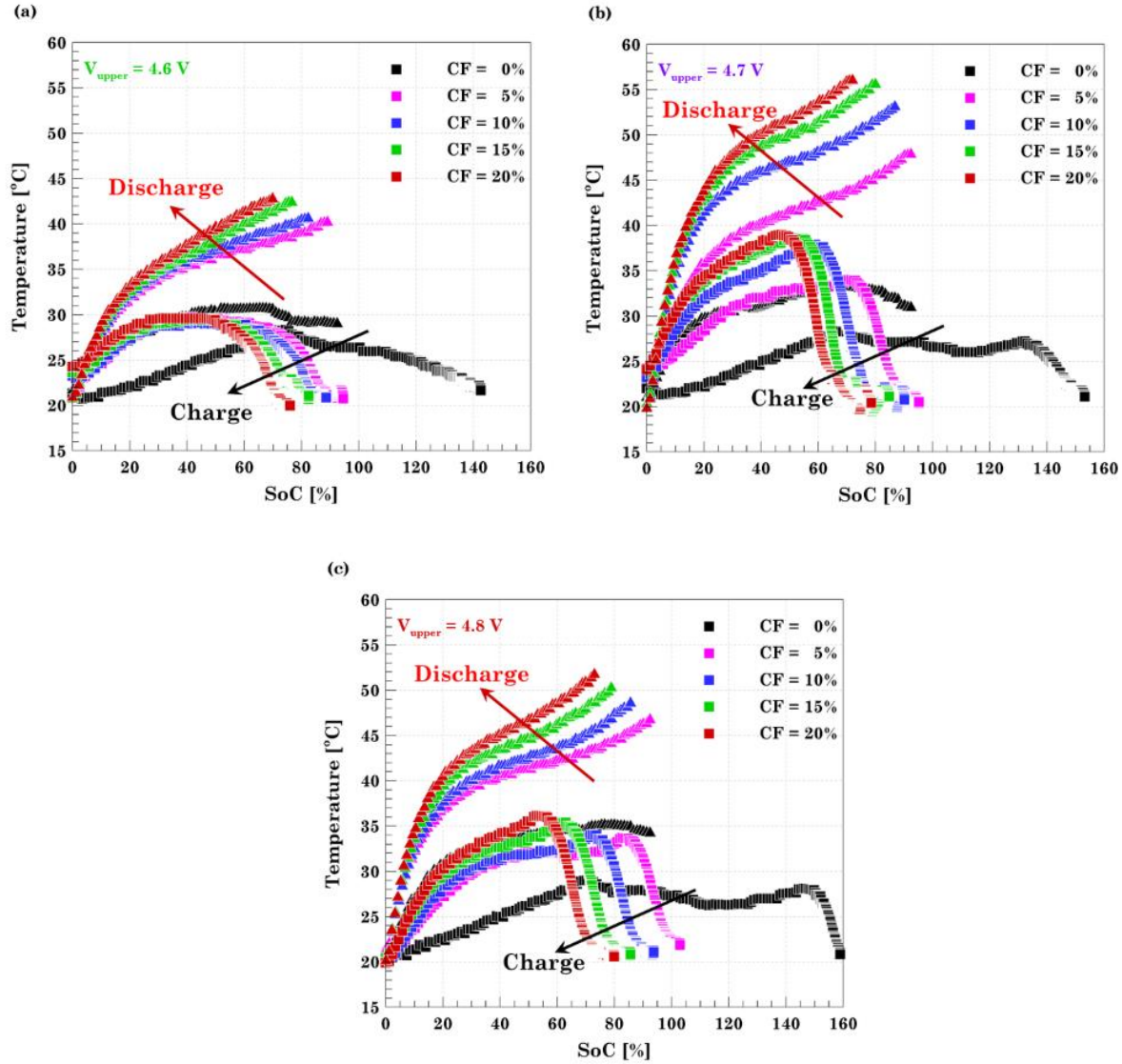

Figure 4.18 Temperature evolution for the 5 Ah Wanma® cell at different cycling voltage window (a) 2.7 - 4.6 V, (b) 2.7 - 4.7 V and, (c) 2.7 – 4.8 V. Temperature profiles for 0%, 5%, 10%, 15%, and 20% capacity fade are depicted.

4.2.2   *Thermal Imaging*

The temperature recorded using a thermocouple provides an overview of how the temperature evolves with capacity fade. However, no inferences can be made about the temperature distribution over the cell surface. Thermal imaging empowers the user to visualize the temperature distribution over a cell under any condition. Videos of the first and last cycles for all the cells were captured using a FLIR A325 thermal imaging camera.
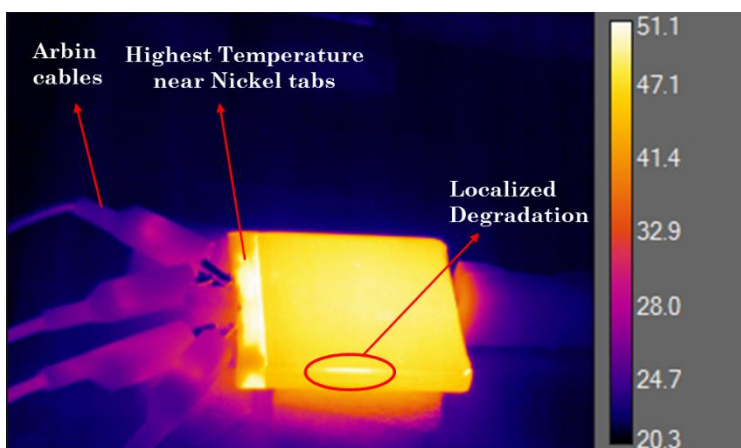
Figure 4.19 Thermal image of a cell cycled in 2.7 - 4.8 V range depicting sites of localized degradation and highest temperature near nickel tabs.

Snapshots of cell temperature distribution extracted from the videos at the end of the CC charge and discharge cycle after the cell had faded to 80% of its capacity have been presented in Figure 4.20 and Figure 4.21. It is clearly visible that irrespective of the upper cutoff voltage, the temperature during the discharge cycle is greater than the corresponding change cycle. Moreover, the temperature of the cell increases with an increase in the extent of the overcharge. The temperature of the cell cycled from 2.7 to 4.7 V was as high as 56 $^\circ$C at the end of discharge. However, the temperature of the cell cycled in the nominal voltage window reached a maximum of 39 $^\circ$C.

It is very intriguing to see that the temperature distribution across the cell surface is not uniform. The highest temperature is observed near the tabs as the current flows through them. Different temperature contours can be observed on the cell surface indicating that the temperature distribution is non-uniform. The non-uniform temperature distribution is a consequence of non-

uniform lithiation across electrodes. This claim would be further strengthened in the next section where the electrodes extracted are analyzed. Regions with a relatively higher temperature than the average surface temperature were also observed. These sites indicate the occurrence of localized degradation in the cell as shown in Figure 4.19.
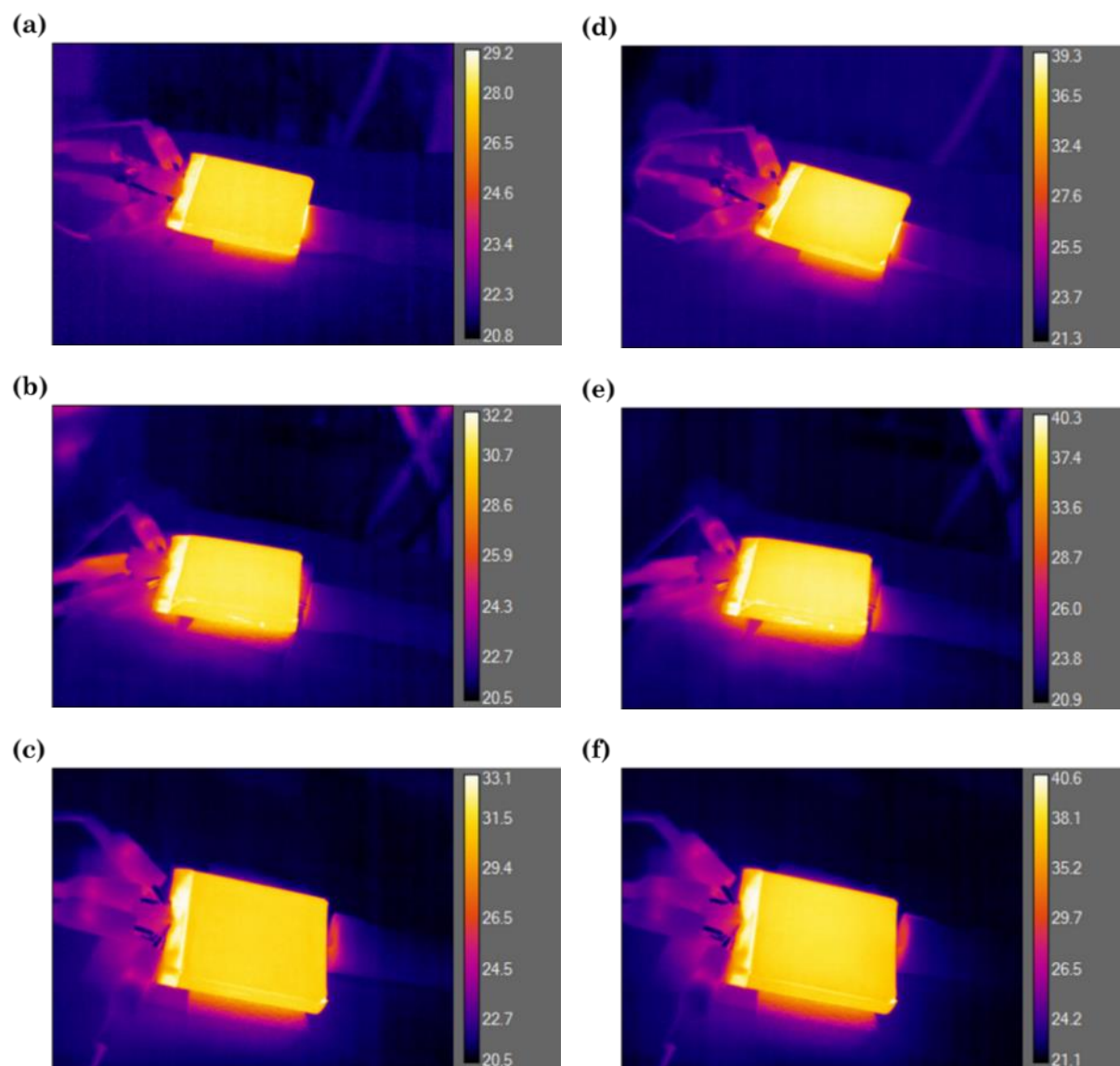
Figure 4.20 Thermal images captured for the last cycle at the end of charge for different cycling voltage window (a) 2.7 - 4.2 V, (b) 2.7 - 4.3 V and, (c) 2.7 – 4.4 V. (d)-(f) are corresponding thermal images at the end of discharge.
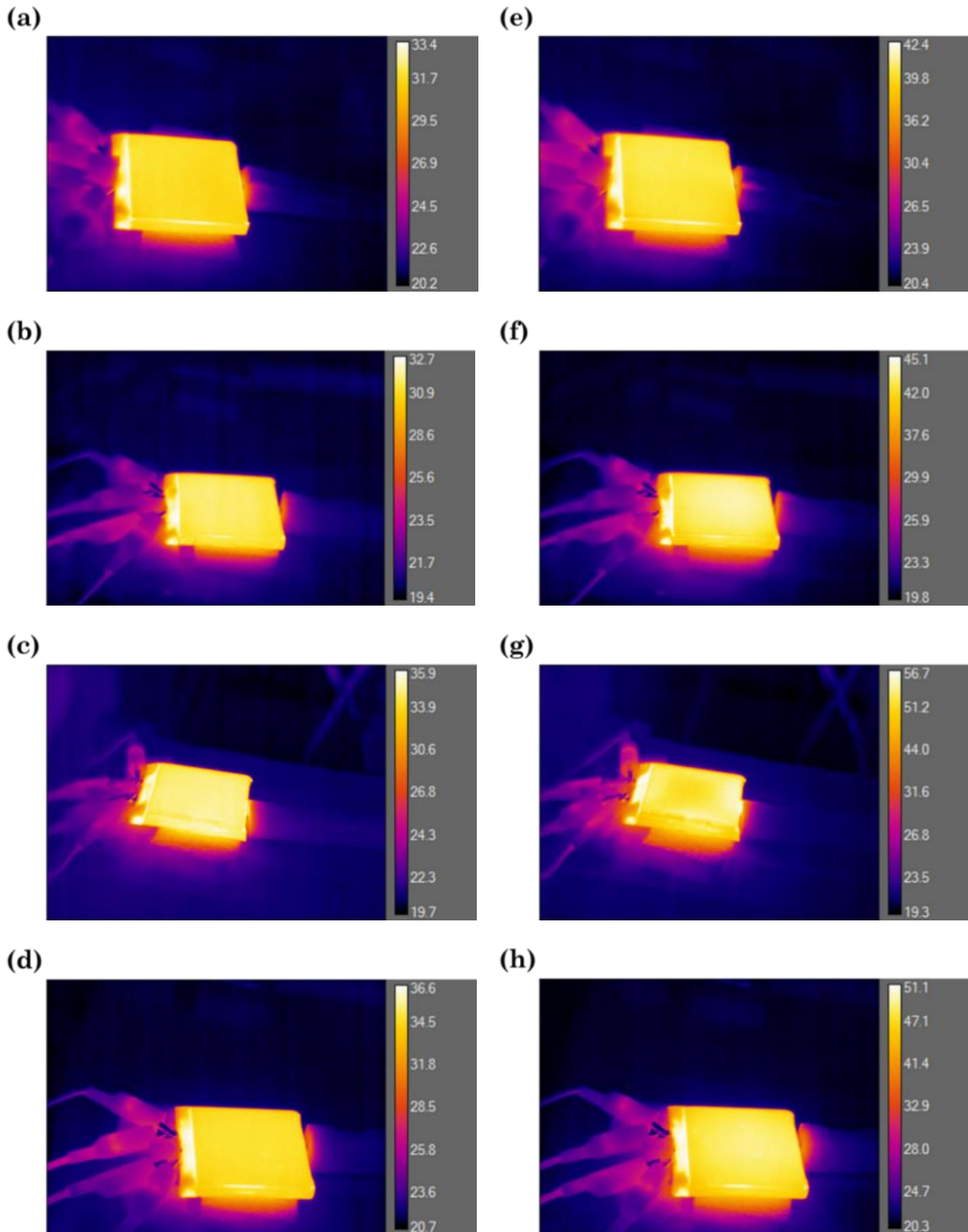
Figure 4.21 Thermal images captured for the last cycle at the end of charge for different cycling voltage window (a) 2.7 - 4.5 V, (b) 2.7 - 4.6 V , (c) 2.7 - 4.7 V and, (d) 2.7 – 4.4 V. (e)-(h) are corresponding thermal images at the end of discharge.

A rise in the area of this localized degradation would be observed if the cell degradation is severe and heat generated through side reactions becomes dominant. The heat generated by the initial set of side reactions would facilitate the occurrence of many other side reactions resulting in a large amount of heat generation. The temperature of the cell may rise up to $300 - 500\ ^{\circ}C$ and may result in thermal runaway. However, the maximum temperature attained in this study was $56\ ^{\circ}C$ which signifies that Ohmic heat was the major contributor to the rise in temperature. If the cells were allowed to cycle beyond 20% capacity fade, the cells would have reached a higher temperature. In conclusion, the results obtained through the thermal imaging are in agreement with the temperature evolution recorded using the thermocouple. Moreover, the thermal images provide valuable insights into the temperature distribution over the cell surface and help in identifying the localized sites where the degradation initiates.

4.3   Destructive Physical Analysis

Having done a detailed analysis of the electrochemical and thermal results, doing a physical analysis of the cell components was conducted to widen the understanding of cell degradation. A physical study of the cell also acts as a confirmation to the electrochemical results presented above. This section initially discusses a thickness measurement study to quantify the volume increase of the cell, followed by a visual analysis of the electrodes. Later, Scanning Electron Microscopy (SEM) and Electron Dispersive Spectroscopy (EDS) results for selected samples from each cell have been presented.

4.3.1   *Physical Analysis*

Cell swelling is a well-known characteristic of overcharge in a pouch cell. Electrode degradation and gas evolution are the two major reasons for the swelling of cells. An effort has been made to see the volume expansion in a cell by quantifying the increase in cell thickness. A fresh cell was taken as the reference for comparison. A fixture to measure the thickness was fabricated in-house. The fixture has two parallel acrylic plates fastened at the ends with 4 sets of nuts and bolts. The cell was placed between the two plates and was tightened using the screws until the cell stopped moving and remained fixed in that position. A Vernier caliper was used to measure the inner distance between the plates. A total of 12 readings were taken (3 on each side) and a plot of thickness variation with upper cutoff voltage is shown in Figure 4.22.
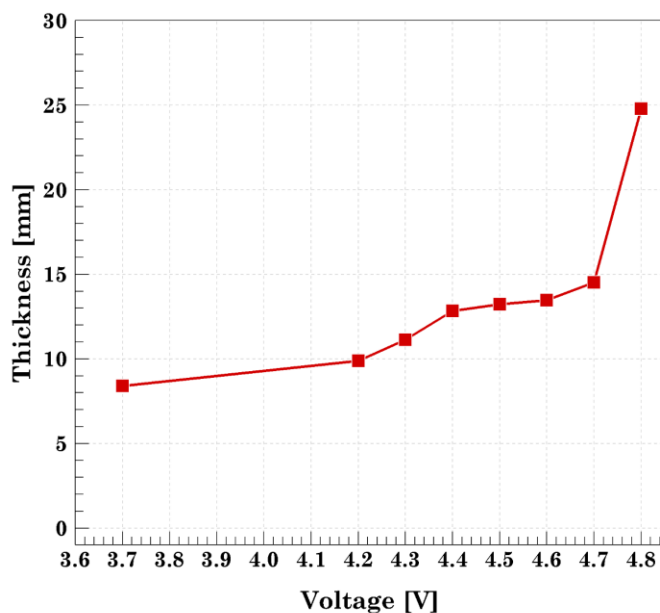
Figure 4.22 Thickness evolution indicating cell swelling with an increase in upper cutoff voltage.

The thickness of a fresh cell (3.7 V) was measured to be around 8.5 mm. As the upper cutoff voltage kept increasing there was a gradual increase in the thickness of the cell. A slight increase in the cell thickness was also observed for the cell cycled under the safe voltage window. The cell cycled between 2.7 V and 4.8 V experienced a 300% increase in cell thickness (Figure 4.23). At higher voltages, larger amounts of electrolyte reduced at the cathode. Moreover, the Li-plating on anode also reacts with electrolyte resulting in a larger amount of gas generation. Therefore, it can be inferred that gas generation increases with an increase in the extent of the overcharge.

Figure 4.23 Comparison of a fresh cell with a cell cycled in voltage range 2.7 – 4.8 V. The cycled cell under the overcharge condition shows a significant increase in cell swelling.

Physical analysis of a cell also includes analyzing the condition of the cell components. Battery autopsy is a widely used tool to visualize the physical changes that occur in a cell. Postmortem inspection of the cells is a very important aspect to gain valuable insights on cell failure modes and to corroborate the claims made by analyzing the electrochemical results. The procedure to open the cells has been elaborated in the third chapter. All the cells were opened in the discharged state. After opening all the cells, images of electrodes were acquired and compared. Figure 4.24 shows the cathode retrieved from all the cells.
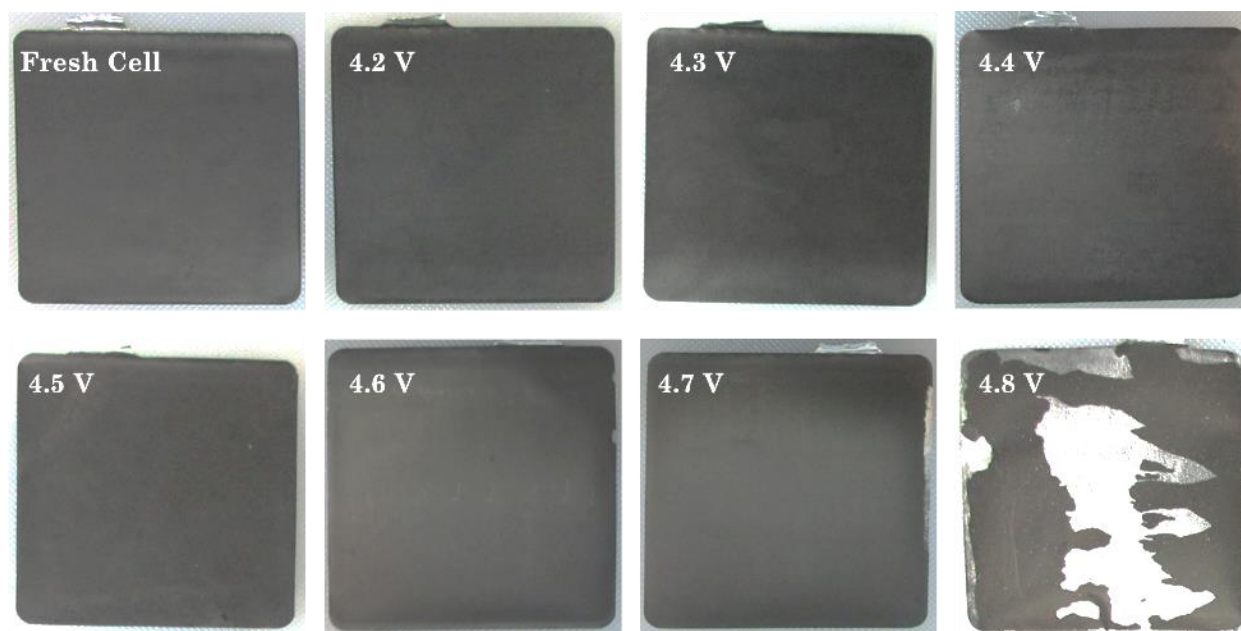
Figure 4.24 Cathodes retrieved after cell autopsy of overcharged cells. The upper cutoff voltage used for cycling of the cells has been indicated on each image.

By looking at the figure 4.24, no visual degradation is observed for the cells cycled up to 4.5 V. However, for the cells cycled to higher voltages, delamination of active material can be observed. The cathode of cell cycled to 4.8 V shows the highest amount of delamination. The cathode material from the electrode is heavily transferred to the separator. While performing the cell autopsy it was also observed that the extraction of the cathode from the separator got more difficult for a highly overcharged cell. This behavior is expected as during overcharge, excessive lithium ion moves from cathode to anode. Over-delithiation of cathode leads to destabilization of cathode structure and particle cracking. Moreover, the cobalt present in cathode also gets transferred to the separator and anode.
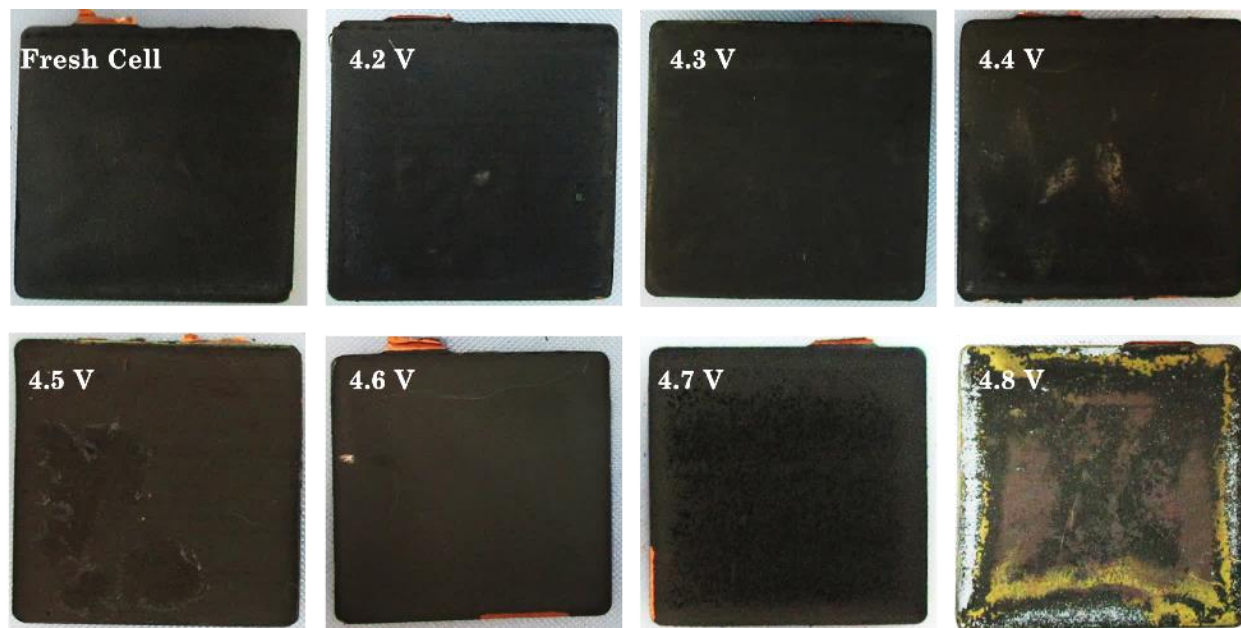
Figure 4.25 Anodes retrieved after cell autopsy of overcharged cells. The upper cutoff voltage used for cycling of the cells has been indicated on each image.

Similarly, images of anode extracted from all the cells have been presented in Figure 4.25. The change in degradation of the anode is visually more significant as compared to the cathode. As the voltage window is extended, the extent of degradation also increased. Having a closer look at the anode of cell cycled up to 4.8 V, traces of lithium deposit can be observed at the edges. Moreover, different degree of delithiation is also observed thus strengthening the results of non-uniform temperature distribution over the cell. A small trace of lithium plating and charring is observed in cells overcharged to 4.6 V and 4.7 V respectively. The occurrence of lithium plating on cells charged beyond 4.6 V also corroborates the inference of voltage under-shoot observed in voltage-capacity curve being an indicator of lithium plating.

4.3.2 *Morphology Analysis*

Battery autopsy helps in visualizing the physical changes that occur in a cell. However, it does not provide insights on morphology changes that occur in a lithium-ion battery. It is important to analyze the changes occurring at the particle level to get a better understanding of failure modes and degradation mechanism of a lithium-ion battery. Several material characterization techniques are utilized to study the morphological changes. Scanning electron microscopy (SEM) and electron dispersive spectroscopy (EDS) are widely accepted techniques used to visualize the electrodes at

the particle level and to determine the chemical composition. Samples were extracted from electrodes of each cell and a Hitachi S-4800 SEM-EDS equipment was used to characterize the electrodes. The SEM images were acquired at 5kX magnification and have been presented in Figure 4.26 and Figure 4.27.

Figure 4.26 SEM images of Cathode surfaces at 5kX magnification for different cycling voltage window. (a) Fresh cell, (b) 2.7 – 4.2 V, (c) 2.7 - 4.3 V and, (d) 2.7 – 4.4 V. LCO and binder can be clearly differentiated.

Visualizing the electrodes at such a high magnification aids in differentiating the active particle from the binder. A demarcation of LCO particle and binder material has been shown in the fresh cell image. As the upper cutoff voltage is increased the cathode structure destabilizes. The same was observed in Figure 4.24 where the cell charged in 2.7-4.8 V resulted in delamination of the electrode. A similar trend is noticed in the SEM images where cracks are observed in the active

material signifying destabilization of LCO cathode material. This is observed for cells charged above 4.5 V. The cracking of cathode particles is attributed to the development of mechanical stress. As the overcharge voltage is increased, excessive delithiation of cathode destabilizes the structural stability and hence seeing the particle cracking is justified.

Figure 4.27 SEM images of Cathode surfaces at 5kX magnification for different cycling voltage window. (a) 2.7 – 4.5, (b) 2.7 – 4.6 V, (c) 2.7 - 4.7 V and, (d) 2.7 – 4.8 V. Particle cracking starts occurring at high cutoff voltages.

The SEM images at 5kX magnification for anode at different upper cutoff voltages are shown in Figure 4.28 and Figure 4.29. SEM image of a fresh electrode is also included and is taken as a reference to analyze the extent of degradation. The image of a pristine graphite electrode clearly depicts the shape of the graphite particles. Considering the condition of this electrode as a
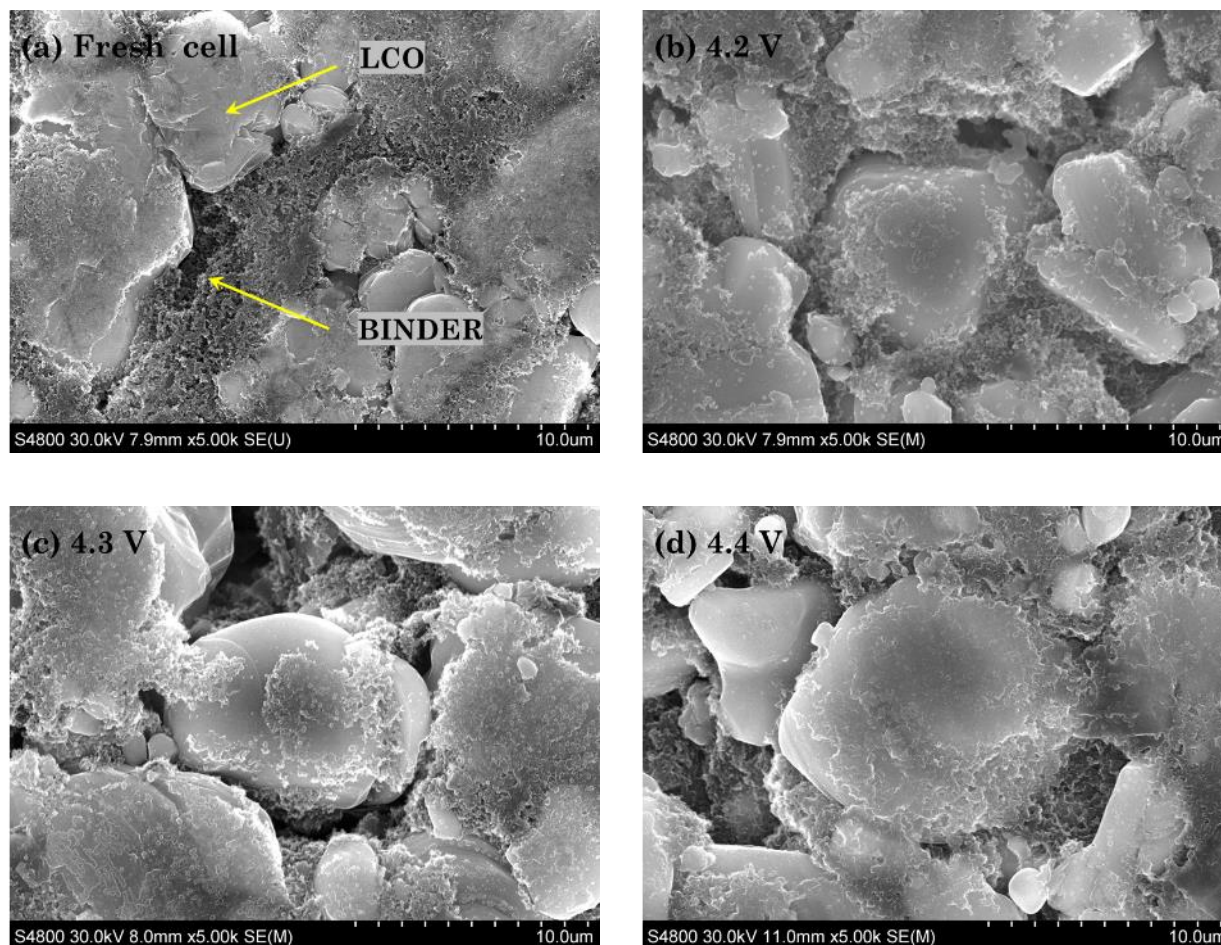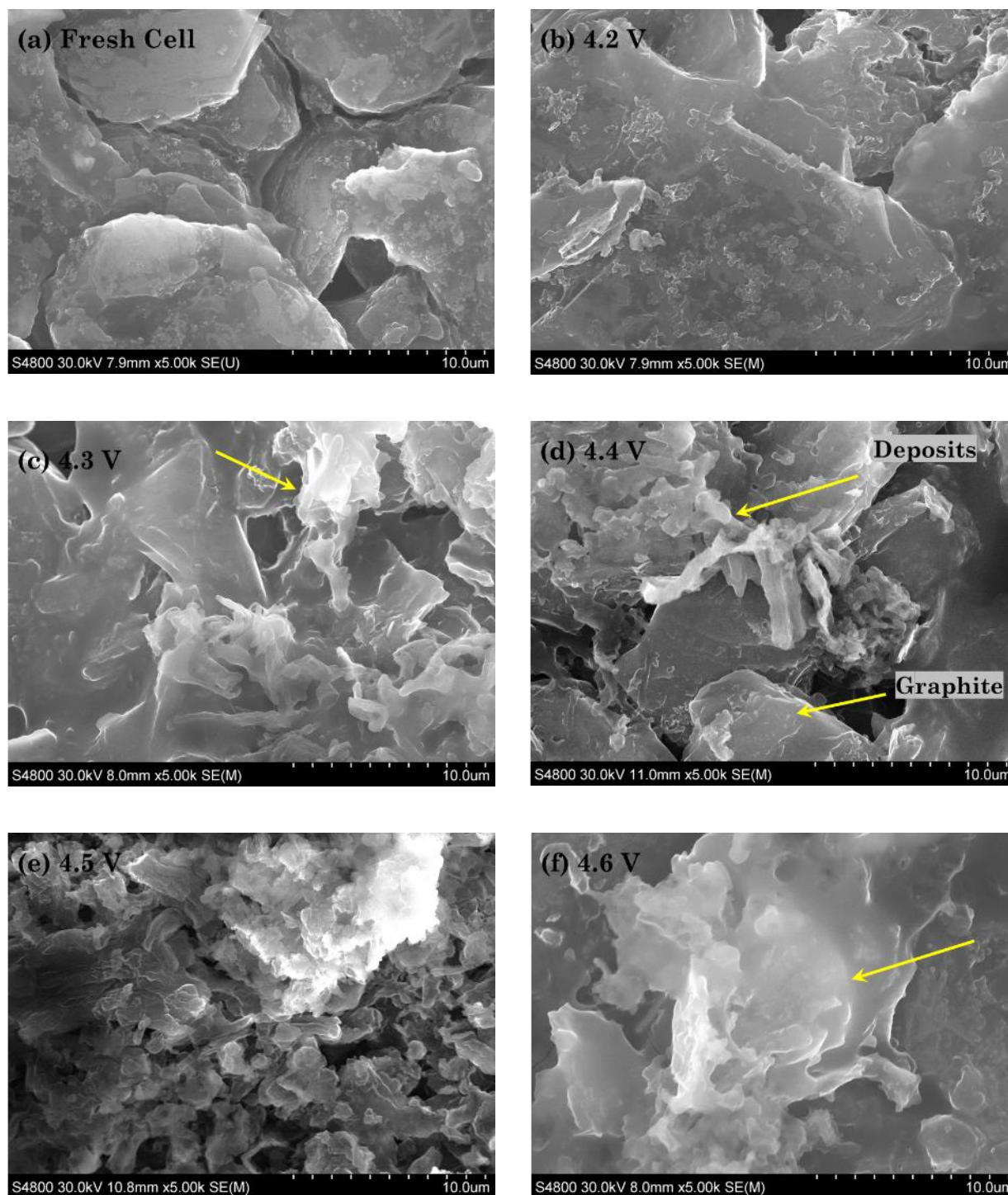
Figure 4.28 SEM images of Anode surfaces at 5kX magnification for different cycling voltage window. (a) Fresh cell, (b) 2.7 – 4.2 V, (c) 2.7 - 4.3 V, (d) 2.7 – 4.4 V, (e) 2.7 – 4.5 V, (f) 2.7 – 4.6 V. Electrolyte deposits, graphite particle and lithium plating have been indicated.
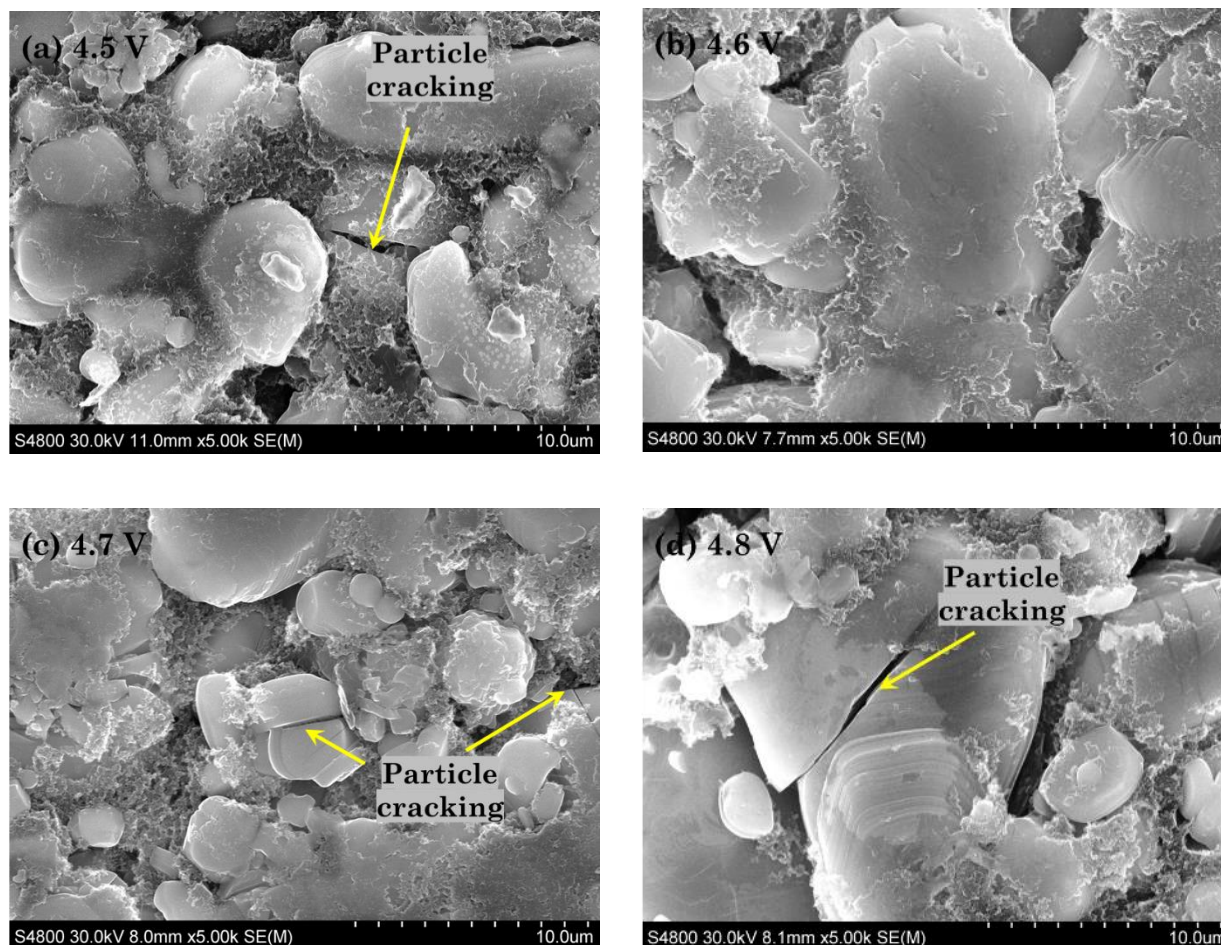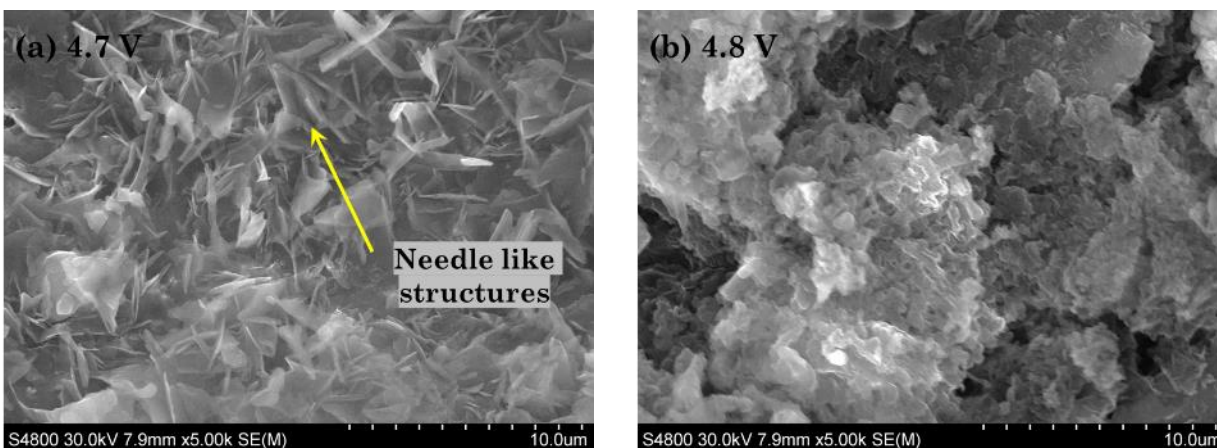
Figure 4.29 SEM images of Anode surfaces at 5kX magnification for different cycling voltage window. (a) 2.7 – 4.7 V, (b) 2.7 – 4.8 V. Needle like structures start appearing as the extent of overcharge increases.

reference, cell degradation is clearly visible as the value of upper cutoff voltage for cycling is increased. Figure 4.28 (a-b) shows a part of the electrode covered with deposits. These deposits can be clearly differentiated from the graphite particles. The area covered by theses deposits increased for the cells cycled at higher voltages of 4.5 - 4.8V. EDS analysis of these electrodes revealed a significant increase in the amount of oxygen.

The arrows marked show evidence of lithium plating on electrodes. An intriguing feature of "needle-like structures" is observed for the cell cycled from 2.7 V to 4.7 V. Similar observations have been made by other research groups in the community and it is found that the presence of these needle-like structure indicates that the formation of lithium dendrites [68, 111-114]. The formation of lithium dendrites also explains the charring effect observed during the destructive physical analysis of the cell electrodes for the cell charged to 4.7 V.

EDS results were also obtained for all the SEM images presented above. Unfortunately, the device used to carry out EDS has a low energy resolution and does not detect lithium and hydrogen elements. The results obtained from EDS analysis have been presented in Table 4.1 and Table 4.2. Moreover, a representative EDS map spectrum for a cathode and anode have been included in Figure 4.30. EDS analysis of cathode shows a rise in carbon, fluorine and phosphorous content as the voltage window is extended, thus indicating the deposits from electrolyte decomposition. The cobalt content also decreased with an increase in the upper cutoff voltage signifying dissolution of

cobalt as expected during the overcharge process. Anode results also indicate a small increase in the cobalt content on the anode with an increase in overcharge voltage thus confirming the occurrence of cobalt dissolution. With increasing voltage, a significant increase in oxygen content along with a significant decrease in carbon content is observed in the EDS analysis of anode. This presence of oxygen denotes the occurrence of lithium plating. The fluorine and phosphorous content also significantly rise once the voltage window is extended beyond 4.5 V.

Table 4.1 EDS analysis of the anode at different overcharge voltages

Upper Cutoff Voltage (V)	C (wt %)	O (wt %)	F (wt %)	Al (wt %)	P (wt %)	Cu (wt %)	Co (wt %)
4.2	76.4	18.3	2.7	1.4	0.5	0.5	0.2
4.3	58	35	5	0.8	0.7	0.4	0.1
4.4	28.3	45.4	3.1	8	0.8	12.2	2.2
4.5	29.3	50.6	5.1	5.7	1.9	4.5	2.9
4.6	45.2	40.8	8.6	3.2	1.3	0.7	0.1
4.7	37.2	53.7	3.8	1.4	2.8	0.8	0.4
4.8	28.4	49	15.5	3.1	2.6	0.9	0.6

Table 4.2 EDS analysis of the cathode at different overcharge voltages

Upper Cutoff Voltage (V)	Co (wt %)	C (wt %)	O (wt %)	F (wt %)	Al (wt %)	P (wt %)	Cu (wt %)
4.2	37.5	31.3	18.8	6.8	5.3	0.3	0
4.3	33.1	32.9	19.8	7.3	6.1	0.7	0.1
4.4	36	33.6	19.7	7.8	2.2	0.7	0
4.5	36.1	32.8	19.8	8.2	2.3	0.8	0
4.6	38.8	31.5	14.7	9.6	5.2	0.2	0.1
4.7	36.3	34.8	19.1	5.3	4.3	0.2	0.1
4.8	36.4	35.1	19.6	6	2.7	0.1	0.1
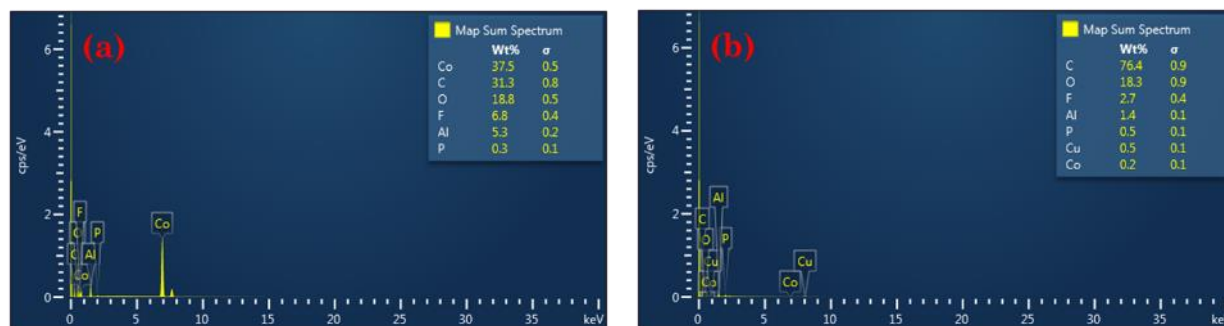
Figure 4.30 Images of sample EDS Spectrum obtained for cell cycled in the nominal voltage window (a) Cathode, (b) Anode.
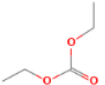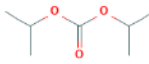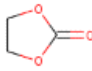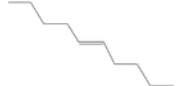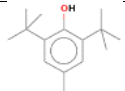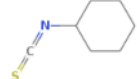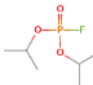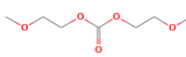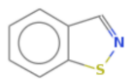
The increase in fluorine and phosphorous content signify the reaction of plated lithium with electrolyte thus resulting in electrolyte decomposition and gas evolution. Thickness measurement analysis also revealed a rise in cell thickness and observing cell swelling for the cells cycled up to 4.6, 4.7 and 4.8 V. In conclusion, the SEM and EDS results further strengthen the claim that voltage undershoot is an indicator of significant Li-plating and electrolyte decomposition.

4.4   Electrolyte Composition Analysis

The electrolyte of the cells was collected while performing cell autopsy. The results for the composition of electrolyte obtained using gas chromatography-mass spectroscopy. The electron impact ionization spectrums were obtained using an Agilent 5975C MSD equipment and the results were analyzed using the in-built NIST library. Figure 4.31, Figure 4.32, and Figure 4.33 features the chromatograms corresponding to electrolytes of cells cycled up to different upper cutoff voltage. Some common components The chromatograms obtained reveal several peaks, each corresponding to a specific compound. The presence of diethyl carbonate, ethylene carbonate and butylated hydroxytoluene (BHT) was detected in all the cells. Therefore, these components are an integral part of the initial electrolyte composition. BHT is a widely used additive to improve the cycling performance of the cells[115]. Presence of diisopropyl carbonate was also observed in all the aged cells. A previous study by Kamui *et al.*. also found the presence of dipropyl carbonate for an overcharged and overdischarged cell[85]. From electrolyte solution analysis presence of isofluorphate was observed, therefore, suggesting that LiPF$_6$ salt also degrades with overcharge.

Table 4.3 presents the list of compounds detected after analyzing the GC/MS spectrums for all the cells. Although the study of electrolyte composition was carried to observe the change in decomposition compounds with an increase in the cycling upper cutoff voltage, the lack of mass spectra data available in the NIST libraries led to not identifying several peaks in the ionization spectrum. However, with an increase in the upper cutoff voltage, the intensity of the peaks decreased. This was expected because, as the cell voltage increases beyond the safe operating voltage of 4.5 V for the electrolyte, the electrolyte reacts with the cathode causing gas generation. This was also evident from the volume expansion study where the cells started expanding as the cycling voltage was increase above 4.5 V. The increase in the amount of gas generation is a result of aggravated decomposition of the electrolyte compounds thus justifying the reduction in number and intensity of the peaks.

Table 4.3 Compounds detected in the electrolyte recovered from the cells subjected to cycling under continuous overcharge. The crosses indicate the identification of the compounds.

Structure	Name	V_{upper}						
		4.2 V	4.3 V	4.4 V	4.5 V	4.6 V	4.7 V	4.8 V
	Diethyl Carbonate	X	X	X	X	X	X	X
	Di-isopropyl carbonate	X	X	X	X	X		
	Ethylene Carbonate	X	X	X	X	X	X	X
	5-Decene	X	X	X	X	X	X	X
	Butylatedhydroxy toluene (BHT)	X	X	X	X	X	X	X
	Cyclohexyl, isotiocyanate	X	X	X	X	X	X	X
	isoflurophate	X		X				
	Ethanol,2 methoxy carbonate					X	X	X
	1,2-Benzisothiazole						X	X
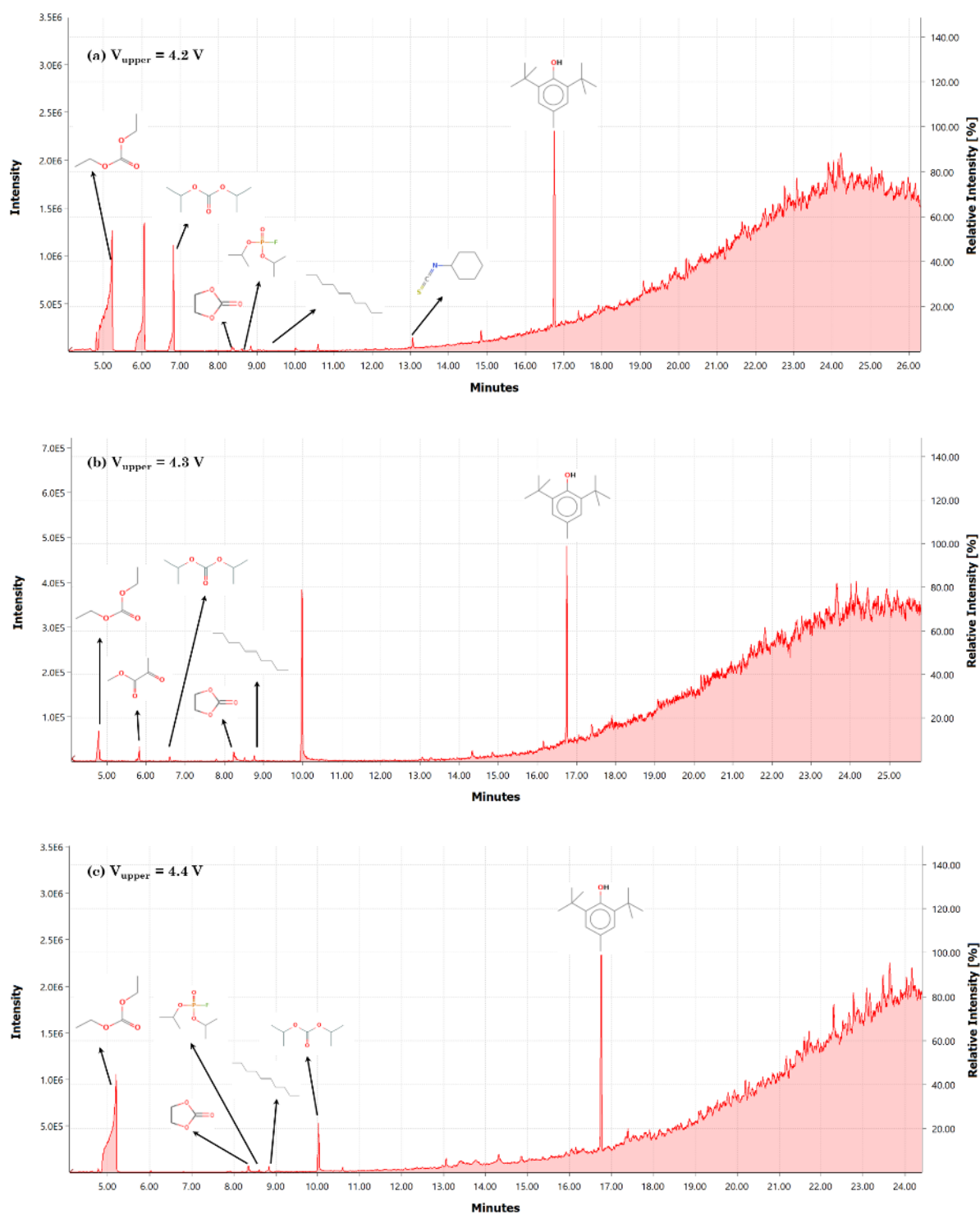
Figure 4.31 GC/MS Chromatograms of electrolyte for the cell cycled between different voltage window (a) 2.7 – 4.2 V, (b) 2.7 - 4.3 V, (c) 2.7 -4.4 V
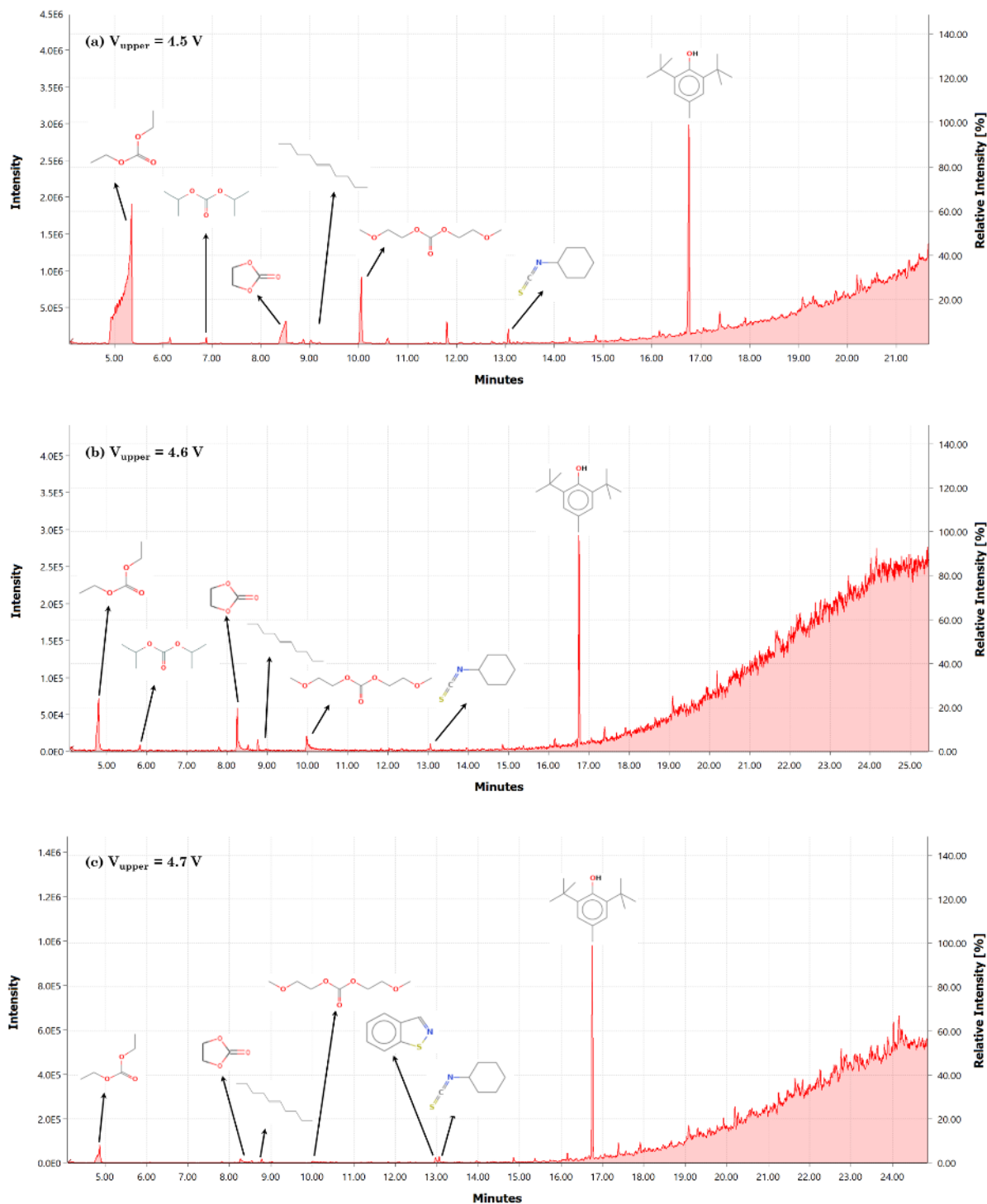
Figure 4.32 GC/MS Chromatograms of electrolyte for the cell cycled between different voltage window (a) 2.7 – 4.5 V, (b) 2.7 - 4.6 V, (c) 2.7 -4.7 V
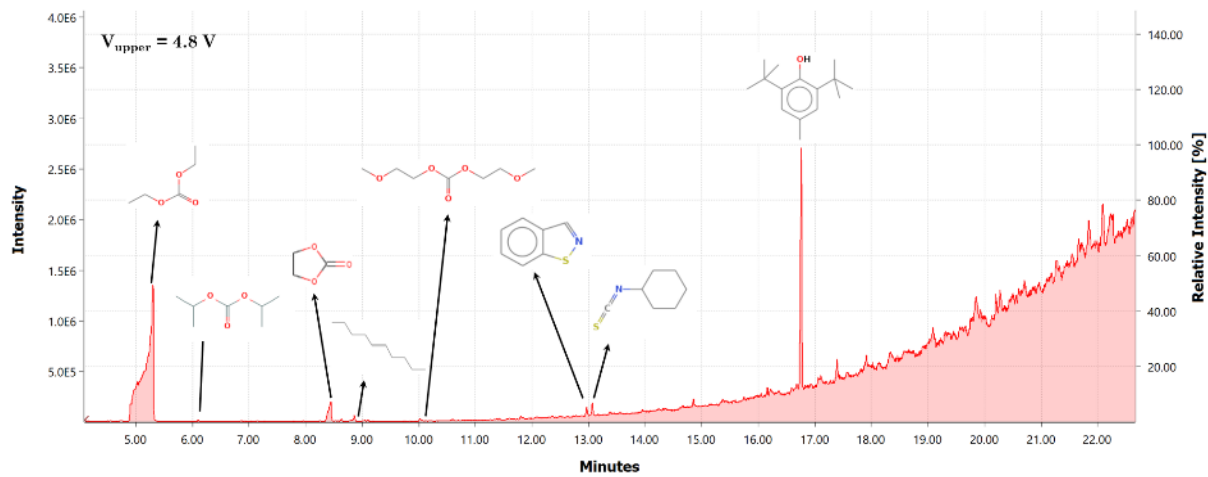
Figure 4.33 GC/MS Chromatograms of electrolyte for the cell cycled between 2.7 – 4.2 V.

5.   CONCLUSIONS AND FUTURE WORK

5.1   <u>Conclusions</u>

Aging-induced degradation mechanisms and overcharge induced degradation mechanisms of lithium-ion batteries have been investigated separately in the previous works. In this study, a combined effect of both cycling and overcharge has been investigated for medium power lithium-ion pouch cells using experimental techniques. The cells were subjected to cycling under continuous overcharge conditions wherein the upper cutoff voltage for the cells was varied (4.2 through 4.8 V) until the capacity faded 20% with respect to the nominal capacity. The upper cutoff voltage during cycling was found to play a key role in determining the rate and extent of degradation. The electrochemical analysis showed that with an increase in the upper cutoff voltage, cells gain higher initial capacities. However, the cycle life of the cell was compromised resulting in a faster and an aggravated degradation. Coulombic efficiency of the cell also decreased at a faster rate with increasing upper cutoff voltage.

As expected, the cell internal resistance, for the 2.7 - 4.2 V baseline case, increased with aging. On further analysis, it was observed that as the upper cutoff voltage for cycling is increased, the magnitude of cell resistance increases at a faster rate in a lesser number of cycles. This indicates that the cell charged up to a higher cutoff voltage degrades faster and the increase of resistance contributes to capacity fade of cells. The gradual rise in internal resistance is attributed to the growth of SEI which is seen for the cells charged up to 4.5 V. However, an abrupt increase of cell resistance and a decay of the cell lifetime was observed for the cells charged beyond 4.5 V. Electrolyte decomposition along with the presence of lithium plating on graphite and fracture on the LCO active material are the main reason for the increment.

Destructive physical analysis and in-depth characterization of the electrodes show evidence of significant amount lithium plating on anodes for cells charged beyond 4.4 V. These results corroborate that the voltage undershoot feature observed in the voltage-capacity curve is an indicator of lithium plating. Delamination of active material and particle cracking was also observed in cathodes of cells charged up to 4.6, 4.7 and 4.8 V representing destabilization of the

cathode structure. Previous studies have shown lithium plating is more likely to happen under low temperature and/or high C-rates. This study proves the fact that a high SoC, directly associated with high cutoff voltages, can also lead to lithium plating.

Cell swelling due to gas generation is a characteristic of overcharge abuse condition. Thickness measurements of the cell show that as the cycling window is extended, the cell thickness also increases. The volume expansion is directly associated with the gases generated due to electrolyte decomposition and its reaction with cathode. This phenomenon is more evident in the cells overcharged beyond 4.5 V corroborating that electrolyte decomposes beyond its safe voltage window of 4.5 V. Along with cycling the gases accumulate increasing the distance between the electrodes and separator and consequently increasing the transport resistance in the electrolyte.

The thermal results exhibited that the temperature of the cell increased with increase in the upper cutoff voltage. Thermal images of the cell revealed a nonuniform temperature distribution over the cell. Moreover, localized sites with high temperature representing the onset of degradation were identified. The cell cycled up to 4.7 and 4.8 V experienced a maximum temperature of 55 $^{\circ}$C. Although the temperature rise is significant as compared to the cell cycled in the nominal voltage window, it is very unlikely that the cell goes into thermal runaway. However, it should be reminded that the cells were cycled only until 20% capacity loss was observed. Conducting the tests until the cells fail may result in higher temperature and lead to thermal runaway.

Electrochemical differential analysis including dQ/dN, dη/dN analysis, and internal resistance were implemented to predict the SoH of the cell. A new dimensionless indicator, Φ_R, based on the internal resistance at the fully charged and fully discharged condition was introduced. The new SoH indicator can predict the onset of aggravated degradation of the cell by simply tracking back the point where its value becomes zero. The proposed method to predict the SoH, using the internal resistance measurements, can be easily integrated into a working battery module and could be utilized as a way to predict battery failures and avoid any hazardous event.

5.2   <u>Future Work</u>

There are very few works that study the degradation mechanism induced by cycling under an abuse condition and hence this work will serve as a beginning point for the researchers to further explore this idea. The current work proposes a comprehensive methodology to study the behavior of a single cell subjected to cycling under a fixed overcharge condition. In order to emulate the overcharge condition of a single cell in a module, a new study with a variable and increasing upper cutoff voltage should be necessary.

All the cells were tested at the 1C rate and room temperature focusing only on the effect of voltage. The effect of temperature and C-rates at different cutoff voltages can be investigated. The study was only limited to LCO/graphite pouch cell. Moreover, a study using different types of protocols should be done to get a better understanding of degradation in each condition. Identical tests can be conducted on cylindrical, and prismatic cells to differentiate the characteristics of degradation in different forms of cells. Moreover, conducting these tests for different cathode and anode materials would elucidate the effect on different cell chemistries. Electrochemical Impedance Spectroscopy (EIS) could be utilized to get a better understanding of resistance change. EIS would help in deciphering the cell component responsible for the increase in internal resistance.

The presented methodology can be extended to other degradation phenomena such as overdischarge. The effects of cycling a cell below and after the reverse potential could be studied. Unlike the overcharge condition, overdischarge has its own degradation modes such as the dissolution of the copper substrate, SEI decomposition and copper bridge formation on the separator. Furthermore, the degradation behavior associated with a combination of an overdischarge and overcharge condition for the non-monitored and unbalanced modules can be explored.

REFERENCES

1.   Badwal, S.P.S., et al., *Emerging electrochemical energy conversion and storage technologies.* Frontiers in chemistry, 2014. **2**: p. 79-79.

2.   McNaught, A.D., et al., *IUPAC compendium of chemical terminology.* 2006, International Union of Pure and Applied Chemistry: Cambridge, UK.

3.   Linden, D. and T.B. Reddy, *Handbook of batteries.* 2002, New York, N.Y.: McGraw-Hill.

4.   Buchmann, I., *Batteries in a Portable World : a Handbook on Rechargeable Batteries for Non-Engineers.* 2016, Richmond, British Columbia: Cadex Electronics Inc.

5.   Pistoia, G., *Lithium-ion batteries : advances and applications.* 2014.

6.   Huggins, R.A., *Primary, Non-rechargeable Batteries.* 2016.

7.   Orendorff, C.J., *The Role of Separators in Lithium-Ion Cell Safety.* The Electrochemical Society Interface, 2012. **21**(2): p. 61-65.

8.   Dunn, B., H. Kamath, and J.-M. Tarascon, *Electrical Energy Storage for the Grid: A Battery of Choices.* Science, 2011. **334**(6058): p. 928.

9.   Beauregard, G., *HYBRIDS PLUS PLUG IN HYBRID ELECTRIC VEHICLE.* 2008, eTec.

10.   Smith, B., *Chevrolet volt battery incident overview report 1, U.S. Department of Transportation, National Highway Traffic Safety Administration.* 2012.

11.   *Aircraft incident report: auxiliary power unit battery fire, Japan airlines Boeing 787, JA 829 J, Boston, Massachusetts, January 7, 2013.* 2014.

12.   Goto, N., *Aircraft serious incident investigation report: all Nippon airways Co. Ltd. JA804A. .* 2014.

13.   *Failure Analysis of Samsung Note 7.* 2017, Underwriters Laboratory.

14.   *Crash and Post-crash Fire of Electric-powered Passenger Vehicle.* 2018, National Transport Safety Board: Mounain View, CA.

15.   Bandhauer, T.M., S. Garimella, and T.F. Fuller, *A Critical Review of Thermal Issues in Lithium-Ion Batteries.* Journal of The Electrochemical Society, 2011. **158**(3): p. R1-R25.

16.   Leising, R.A., et al., *Abuse Testing of Lithium-Ion Batteries: Characterization of the Overcharge Reaction of LiCoO2/Graphite Cells.* Journal of The Electrochemical Society, 2001. **148**(8): p. A838-A844.

17.   Spotnitz, R. and J. Franklin, *Abuse behavior of high-power, lithium-ion cells.* Journal of Power Sources, 2003. **113**(1): p. 81-100.

18.   Zhang, L., et al., *Capacity fading mechanism during long-term cycling of over-discharged LiCoO2/mesocarbon microbeads battery.* Journal of Power Sources, 2015. **293**: p. 1006-1015.

19.   Guo, R., et al., *Mechanism of the entire overdischarge process and overdischarge-induced internal short circuit in lithium-ion batteries.* Scientific Reports, 2016. **6**: p. 30248.

20. LI, H.-F., J.-K. GAO, and S.-L. ZHANG, *Effect of Overdischarge on Swelling and Recharge Performance of Lithium Ion Cells.* Chinese Journal of Chemistry, 2008. **26**(9): p. 1585-1588.

21. Erol, S., M.E. Orazem, and R.P. Muller, *Influence of overcharge and over-discharge on the impedance response of LiCoO2/C batteries.* Journal of Power Sources, 2014. **270**: p. 92-100.

22. Fear, C., et al., *Elucidating Copper Dissolution Phenomenon in Li-Ion Cells under Overdischarge Extremes.* Journal of The Electrochemical Society, 2018. **165**(9): p. A1639-A1647.

23. Maleki, H. and J. N. Howard, *Effects of overdischarge on performance and thermal stability of a Li-ion cell.* Vol. 160. 2006. 1395-1402.

24. Scrosati, B. and J. Garche, *Lithium batteries: Status, prospects and future.* Journal of Power Sources, 2010. **195**(9): p. 2419-2430.

25. Burns, J.C., et al., *Predicting and Extending the Lifetime of Li-Ion Batteries.* Journal of The Electrochemical Society, 2013. **160**(9): p. A1451-A1456.

26. Smith, K., et al. *Comparison of Plug-In Hybrid Electric Vehicle Battery Life Across Geographies and Drive-Cycles.* in *SAE World Congress and Exhibition 2012.* 2012. United States.

27. de Hoog, J., et al., *Combined cycling and calendar capacity fade modeling of a Nickel-Manganese-Cobalt Oxide Cell with real-life profile validation.* Applied Energy, 2017. **200**: p. 47-61.

28. Rahn, C.D. and C.-Y. Wang, *Battery systems engineering.* 2013, Hoboken: John Wiley & Sons Inc.

29. Erdinc, O., B. Vural, and M. Uzunoglu. *A dynamic lithium-ion battery model considering the effects of temperature and capacity fading.* in *2009 International Conference on Clean Electrical Power.* 2009.

30. Sarre, G., P. Blanchard, and M. Broussely, *Aging of lithium-ion batteries.* Journal of Power Sources, 2004. **127**(1): p. 65-71.

31. Bögel, W., J.P. Büchel, and H. Katz, *Real-life EV battery cycling on the test bench.* Journal of Power Sources, 1998. **72**(1): p. 37-42.

32. Ohue, K., et al., *Self-discharge behavior of polyacenic semiconductor and graphite negative electrodes for lithium-ion batteries.* Journal of Power Sources, 2011. **196**(7): p. 3604-3610.

33. Kassem, M., et al., *Calendar aging of a graphite/LiFePO4 cell.* Journal of Power Sources, 2012. **208**: p. 296-305.

34. Zhang, S.S., *The effect of the charging protocol on the cycle life of a Li-ion battery.* Journal of Power Sources, 2006. **161**(2): p. 1385-1391.

35. Asakura, K., M. Shimomura, and T. Shodai, *Study of life evaluation methods for Li-ion batteries for backup applications.* Journal of Power Sources, 2003. **119-121**: p. 902-905.

36.   Vetter, J., et al., *Ageing mechanisms in lithium-ion batteries.* Journal of Power Sources, 2005. **147**(1): p. 269-281.

37.   Aurbach, D., et al., *On the correlation between surface chemistry and performance of graphite negative electrodes for Li ion batteries.* Electrochimica Acta, 1999. **45**(1): p. 67-86.

38.   Novák, P., et al., *The complex electrochemistry of graphite electrodes in lithium-ion batteries.* Journal of Power Sources, 2001. **97-98**: p. 39-46.

39.   Agubra, V. and J. Fergus, *Lithium Ion Battery Anode Aging Mechanisms.* Materials (Basel, Switzerland), 2013. **6**(4): p. 1310-1325.

40.   Verma, P., P. Maire, and P. Novák, *A review of the features and analyses of the solid electrolyte interphase in Li-ion batteries.* Electrochimica Acta, 2010. **55**(22): p. 6332-6341.

41.   Jung, S.-K., et al., *Understanding the Degradation Mechanisms of LiNi0.5Co0.2Mn0.3O2 Cathode Material in Lithium Ion Batteries.* Advanced Energy Materials, 2014. **4**(1): p. 1300787.

42.   Jannesari, H., M.D. Emami, and C. Ziegler, *Effect of electrolyte transport properties and variations in the morphological parameters on the variation of side reaction rate across the anode electrode and the aging of lithium ion batteries.* Journal of Power Sources, 2011. **196**(22): p. 9654-9664.

43.   Birkl, C.R., et al., *Degradation diagnostics for lithium ion cells.* Journal of Power Sources, 2017. **341**: p. 373-386.

44.   Schuster, S.F., et al., *Nonlinear aging characteristics of lithium-ion cells under different operational conditions.* Journal of Energy Storage, 2015. **1**: p. 44-53.

45.   Arora, P., R.E. White, and M. Doyle, *Capacity Fade Mechanisms and Side Reactions in Lithium‐Ion Batteries.* Journal of The Electrochemical Society, 1998. **145**(10): p. 3647-3667.

46.   Buqa, H., et al., *SEI film formation on highly crystalline graphitic materials in lithium-ion batteries.* Journal of Power Sources, 2006. **153**(2): p. 385-390.

47.   Goers, D., et al., *The influence of the local current density on the electrochemical exfoliation of graphite in lithium-ion battery negative electrodes.* Electrochimica Acta, 2011. **56**(11): p. 3799-3808.

48.   Fernández Lisbona, D. and T. Snee, *A review of hazards associated with primary lithium and lithium-ion batteries.* Vol. 89. 2011.

49.   Ji, Y., Y. Zhang, and C.-Y. Wang, *Li-Ion Cell Operation at Low Temperatures.* Journal of The Electrochemical Society, 2013. **160**(4): p. A636-A649.

50.   Zinth, V., et al., *Lithium plating in lithium-ion batteries at sub-ambient temperatures investigated by in situ neutron diffraction.* Journal of Power Sources, 2014. **271**: p. 152-159.

51.   Petzl, M. and M.A. Danzer, *Nondestructive detection, characterization, and quantification of lithium plating in commercial lithium-ion batteries.* Journal of Power Sources, 2014. **254**: p. 80-87.

52. Waldmann, T., et al., *Temperature dependent ageing mechanisms in Lithium-ion batteries – A Post-Mortem study.* Journal of Power Sources, 2014. **262**: p. 129-135.

53. Bitzer, B. and A. Gruhle, *A new method for detecting lithium plating by measuring the cell thickness.* Journal of Power Sources, 2014. **262**: p. 297-302.

54. Petzl, M., M. Kasper, and M.A. Danzer, *Lithium plating in a commercial lithium-ion battery – A low-temperature aging study.* Journal of Power Sources, 2015. **275**: p. 799-807.

55. Dubarry, M. and B.Y. Liaw, *Identify capacity fading mechanism in a commercial LiFePO4 cell.* Journal of Power Sources, 2009. **194**(1): p. 541-549.

56. Liu, P., et al., *Aging Mechanisms of LiFePO4 Batteries Deduced by Electrochemical and Structural Analyses.* Journal of The Electrochemical Society, 2010. **157**(4): p. A499-A507.

57. Dubarry, M., C. Truchot, and B.Y. Liaw, *Cell degradation in commercial LiFePO4 cells with high-power and high-energy designs.* Journal of Power Sources, 2014. **258**: p. 408-419.

58. Wang, J., et al., *Degradation of lithium ion batteries employing graphite negatives and nickel–cobalt–manganese oxide + spinel manganese oxide positives: Part 1, aging mechanisms and life estimation.* Journal of Power Sources, 2014. **269**: p. 937-948.

59. Ecker, M., et al., *Calendar and cycle life study of Li(NiMnCo)O2-based 18650 lithium-ion batteries.* Journal of Power Sources, 2014. **248**: p. 839-851.

60. Schmalstieg, J., et al., *A holistic aging model for Li(NiMnCo)O2 based 18650 lithium-ion batteries.* Journal of Power Sources, 2014. **257**: p. 325-334.

61. Broussely, M., et al., *Main aging mechanisms in Li ion batteries.* Journal of Power Sources, 2005. **146**(1): p. 90-96.

62. Zier, M., et al., *Lithium dendrite and solid electrolyte interphase investigation using OsO4.* Journal of Power Sources, 2014. **266**: p. 198-207.

63. Yang, X.-G., et al., *Modeling of lithium plating induced aging of lithium-ion batteries: Transition from linear to nonlinear aging.* Journal of Power Sources, 2017. **360**: p. 28-40.

64. Zheng, Y., et al., *Investigating the error sources of the online state of charge estimation methods for lithium-ion batteries in electric vehicles.* Journal of Power Sources, 2018. **377**: p. 161-188.

65. Zhang, L., et al., *Molecular engineering towards safer lithium-ion batteries: a highly stable and compatible redox shuttle for overcharge protection.* Energy & Environmental Science, 2012. **5**(8): p. 8204-8207.

66. Ouyang, M., et al., *Overcharge-induced capacity fading analysis for large format lithium-ion batteries with LiyNi1/3Co1/3Mn1/3O2+LiyMn2O4 composite cathode.* Journal of Power Sources, 2015. **279**: p. 626-635.

67. Ren, D., et al., *Overcharge behaviors and failure mechanism of lithium-ion batteries under different test conditions.* Applied Energy, 2019. **250**: p. 323-332.

68. Lu, W., et al., *Overcharge Effect on Morphology and Structure of Carbon Electrodes for Lithium-Ion Batteries.* Journal of The Electrochemical Society, 2012. **159**(5): p. A566-A570.

69. Ohsaki, T., et al., *Overcharge reaction of lithium-ion batteries.* Journal of Power Sources, 2005. **146**(1): p. 97-100.

70. Devie, A., M. Dubarry, and B.Y. Liaw, *Overcharge Study in Li4Ti5O12 Based Lithium-Ion Pouch Cell: I. Quantitative Diagnosis of Degradation Modes.* Journal of The Electrochemical Society, 2015. **162**(6): p. A1033-A1040.

71. Perkins, R.D., et al., *Controls oriented reduced order modeling of lithium deposition on overcharge.* Journal of Power Sources, 2012. **209**: p. 318-325.

72. Arora, P., M. Doyle, and R.E. White, *Mathematical Modeling of the Lithium Deposition Overcharge Reaction in Lithium-Ion Batteries Using Carbon-Based Negative Electrodes.* Journal of The Electrochemical Society, 1999. **146**(10): p. 3543-3553.

73. Feng, X., et al., *Thermal runaway mechanism of lithium ion battery for electric vehicles: A review.* Energy Storage Materials, 2018. **10**: p. 246-267.

74. Lin, C.-K., et al., *In situ high-energy X-ray diffraction to study overcharge abuse of 18650-size lithium-ion battery.* Journal of Power Sources, 2013. **230**: p. 32-37.

75. Lopez, C.F., J.A. Jeevarajan, and P.P. Mukherjee, *Experimental Analysis of Thermal Runaway and Propagation in Lithium-Ion Battery Modules.* Journal of The Electrochemical Society, 2015. **162**(9): p. A1905-A1915.

76. Lopez, C.F., J.A. Jeevarajan, and P.P. Mukherjee, *Characterization of Lithium-Ion Battery Thermal Abuse Behavior Using Experimental and Computational Analysis.* Journal of The Electrochemical Society, 2015. **162**(10): p. A2163-A2173.

77. Leising, R.A., et al., *A study of the overcharge reaction of lithium-ion batteries.* Journal of Power Sources, 2001. **97-98**: p. 681-683.

78. Zhang, Z., D. Fouchard, and J.R. Rea, *Differential scanning calorimetry material studies: implications for the safety of lithium-ion cells.* Journal of Power Sources, 1998. **70**(1): p. 16-20.

79. Mendoza-Hernandez, O.S., et al., *Cathode material comparison of thermal runaway behavior of Li-ion cells at different state of charges including over charge.* Journal of Power Sources, 2015. **280**: p. 499-504.

80. Larsson, F. and B.-E. Mellander, *Abuse by External Heating, Overcharge and Short Circuiting of Commercial Lithium-Ion Battery Cells.* Journal of The Electrochemical Society, 2014. **161**(10): p. A1611-A1617.

81. Takahashi, M., K. Komatsu, and K. Maeda, *The Safety Evaluation Test of Lithium-Ion Batteries in Vehicles - Investigation of Overcharge Test Method.* ECS Transactions, 2012. **41**(39): p. 27-41.

82. Zhao, Y., et al., *Preventing lithium ion battery failure during high temperatures by externally applied compression.* Journal of Energy Storage, 2017. **13**: p. 296-303.

83. Hofmann, A., et al., *Preventing Li-ion cell explosion during thermal runaway with reduced pressure.* Applied Thermal Engineering, 2017. **124**: p. 539-544.

84. Kong, W., et al., *Gas evolution behaviors for several cathode materials in lithium-ion batteries.* Journal of Power Sources, 2005. **142**(1): p. 285-291.

85. Kumai, K., et al., *Gas generation mechanism due to electrolyte decomposition in commercial lithium-ion cell.* Journal of Power Sources, 1999. **81-82**: p. 715-719.

86. Metzger, M., et al., *Origin of H2 Evolution in LIBs: H2O Reduction vs. Electrolyte Oxidation.* Journal of The Electrochemical Society, 2016. **163**(5): p. A798-A809.

87. Jung, R., et al., *Oxygen Release and Its Effect on the Cycling Stability of LiNixMnyCozO2 (NMC) Cathode Materials for Li-Ion Batteries.* Journal of The Electrochemical Society, 2017. **164**(7): p. A1361-A1377.

88. Buchberger, I., et al., *Aging Analysis of Graphite/LiNi1/3Mn1/3Co1/3O2 Cells Using XRD, PGAA, and AC Impedance.* Journal of The Electrochemical Society, 2015. **162**(14): p. A2737-A2746.

89. Gallus, D.R., et al., *The influence of different conducting salts on the metal dissolution and capacity fading of NCM cathode material.* Electrochimica Acta, 2014. **134**: p. 393-398.

90. Wandt, J., et al., *Transition metal dissolution and deposition in Li-ion batteries investigated by operando X-ray absorption spectroscopy.* Journal of Materials Chemistry A, 2016. **4**(47): p. 18300-18305.

91. Andersson, A.M., et al., *Surface Characterization of Electrodes from High Power Lithium-Ion Batteries.* Journal of The Electrochemical Society, 2002. **149**(10): p. A1358-A1369.

92. Zheng, H., et al., *Correlation between dissolution behavior and electrochemical cycling performance for LiNi1/3Co1/3Mn1/3O2-based cells.* Journal of Power Sources, 2012. **207**: p. 134-140.

93. Lu, Y.-C., et al., *Probing the Origin of Enhanced Stability of "AlPO4" Nanoparticle Coated LiCoO2 during Cycling to High Voltages: Combined XRD and XPS Studies.* Chemistry of Materials, 2009. **21**(19): p. 4408-4424.

94. Galushkin, N.E., N.N. Yazvinskaya, and D.N. Galushkin, *Mechanism of Gases Generation during Lithium-Ion Batteries Cycling.* Journal of The Electrochemical Society, 2019. **166**(6): p. A897-A908.

95. Luo, J.-Y., et al., *Raising the cycling stability of aqueous lithium-ion batteries by eliminating oxygen in the electrolyte.* Nature Chemistry, 2010. **2**: p. 760.

96. Winter, M. and J.O. Besenhard, *Wiederaufladbare Batterien.* Chemie in unserer Zeit, 1999. **33**(6): p. 320-332.

97. Xu, K., *Nonaqueous Liquid Electrolytes for Lithium-Based Rechargeable Batteries.* Chemical Reviews, 2004. **104**(10): p. 4303-4418.

98. Ue, M. and S. Mori, *Mobility and Ionic Association of Lithium Salts in a Propylene Carbonate‐Ethyl Methyl Carbonate Mixed Solvent.* Journal of The Electrochemical Society, 1995. **142**(8): p. 2577-2581.

99. Sloop, S.E., et al., *Chemical Reactivity of PF 5 and LiPF6 in Ethylene Carbonate/Dimethyl Carbonate Solutions.* Electrochemical and Solid-State Letters, 2001. **4**(4): p. A42-A44.

100. Campion, C.L., et al., *Suppression of Toxic Compounds Produced in the Decomposition of Lithium-Ion Battery Electrolytes.* Electrochemical and Solid-State Letters, 2004. **7**(7): p. A194-A197.

101.   Eom, J.-Y., I.-H. Jung, and J.-H. Lee, *Effects of vinylene carbonate on high temperature storage of high voltage Li-ion batteries.* Journal of Power Sources, 2011. **196**(22): p. 9810-9814.

102.   Gireaud, L., et al., *Mass Spectrometry Investigations on Electrolyte Degradation Products for the Development of Nanocomposite Electrodes in Lithium Ion Batteries.* Analytical Chemistry, 2006. **78**(11): p. 3688-3698.

103.   Johnson, B.A. and R.E. White, *Characterization of commercially available lithium-ion batteries.* Journal of Power Sources, 1998. **70**(1): p. 48-54.

104.   Gachot, G., et al., *Gas Chromatography/Mass Spectrometry As a Suitable Tool for the Li-Ion Battery Electrolyte Degradation Mechanisms Study.* Analytical Chemistry, 2011. **83**(2): p. 478-485.

105.   Horsthemke, F., et al., *Fast screening method to characterize lithium ion battery electrolytes by means of solid phase microextraction – gas chromatography – mass spectrometry.* RSC Advances, 2017. **7**(74): p. 46989-46998.

106.   Gachot, G., et al., *Thermal behaviour of the lithiated-graphite/electrolyte interface through GC/MS analysis.* Electrochimica Acta, 2012. **83**: p. 402-409.

107.   Roth, E.P. and C.J. Orendorff, *How Electrolytes Influence Battery Safety.* The Electrochemical Society Interface, 2012. **21**(2): p. 45-49.

108.   Liu, L. and M. Zhu, *Modeling of SEI Layer Growth and Electrochemical Impedance Spectroscopy Response using a Thermal-Electrochemical Model of Li-ion Batteries.* ECS Transactions, 2014. **61**(27): p. 43-61.

109.   Remmlinger, J., et al., *State-of-health monitoring of lithium-ion batteries in electric vehicles by on-board internal resistance estimation.* Journal of Power Sources, 2011. **196**(12): p. 5357-5363.

110.   Bloom, I., et al., *Differential voltage analyses of high-power, lithium-ion cells: 1. Technique and application.* Journal of Power Sources, 2005. **139**(1): p. 295-303.

111.   Honbo, H., et al., *Electrochemical properties and Li deposition morphologies of surface modified graphite after grinding.* Journal of Power Sources, 2009. **189**(1): p. 337-343.

112.   Kanamura, K., S. Shiraishi, and Z.i. Takehara, *Electrochemical Deposition of Uniform Lithium on an Ni Substrate in a Nonaqueous Electrolyte.* Journal of The Electrochemical Society, 1994. **141**(9): p. L108-L110.

113.   Orsini, F., et al., *In situ Scanning Electron Microscopy (SEM) observation of interfaces within plastic lithium batteries.* Journal of Power Sources, 1998. **76**(1): p. 19-29.

114.   Yoshimatsu, I., T. Hirai, and J.i. Yamaki, *Lithium Electrode Morphology during Cycling in Lithium Cells.* Journal of The Electrochemical Society, 1988. **135**(10): p. 2422-2427.

115.   Liu, R., et al., *Achieving Low Overpotential Lithium−Oxygen Batteries by Exploiting a New Electrolyte Based on N,N´-Dimethylpropyleneurea.* ACS Energy Letters, 2017. **2**(2): p. 313-318.

PUBLICATIONS

IN PREPARATION

Anjul Arun Vyas, Daniel Juarez-Robles, Judith Jeevarajan, Partha P. Mukherjee, "Long-term aging-overcharge interplay of Li-ion pouch cells", *In preparation to be submitted to Journal of Electrochemical, June 2019*.

Daniel Juarez-Robles, **Anjul Arun Vyas**, Timothy Transue, Judith Jeevarajan, Partha P. Mukherjee, "Long-term aging-overdischarge interplay of Li-ion pouch cells", *In preparation to be submitted to Journal of Elcetrochemical Society, June 2019*.